Article

Clinical functional proteomics of intercellular signalling in pancreatic cancer

https://doi.org/10.1038/s41586-024-08225-y

Received: 21 July 2023

Accepted: 15 October 2024

Published online: 13 November 2024

Check for updates

Peiwu Huang[1,7], Weina Gao[1,7], Changying Fu[1,7], Min Wang[2,7], Yunguang Li[3,7], Bizhu Chu[1], An He[1], Yuan Li[1], Xiaomei Deng[1], Yehan Zhang[3], Qian Kong[1], Jingxiong Yuan[2], Hebin Wang[2], Yu Shi[4,6]✉, Dong Gao[3,5]✉, Renyi Qin[2]✉, Tony Hunter[4] & Ruijun Tian[1]✉

Pancreatic ductal adenocarcinoma (PDAC) has an atypical, highly stromal tumour microenvironment (TME) that profoundly contributes to its poor prognosis[1]. Here, to better understand the intercellular signalling between cancer and stromal cells directly in PDAC tumours, we developed a multidimensional proteomic strategy called TMEPro. We applied TMEPro to profile the glycosylated secreted and plasma membrane proteome of 100 human pancreatic tissue samples to a great depth, define cell type origins and identify potential paracrine cross-talk, especially that mediated through tyrosine phosphorylation. Temporal dynamics during pancreatic tumour progression were investigated in a genetically engineered PDAC mouse model. Functionally, we revealed reciprocal signalling between stromal cells and cancer cells mediated by the stromal PDGFR–PTPN11–FOS signalling axis. Furthermore, we examined the generic shedding mechanism of plasma membrane proteins in PDAC tumours and revealed that matrix-metalloprotease-mediated shedding of the AXL receptor tyrosine kinase ectodomain provides an additional dimension of intercellular signalling regulation in the PDAC TME. Importantly, the level of shed AXL has a potential correlation with lymph node metastasis, and inhibition of AXL shedding and its kinase activity showed a substantial synergistic effect in inhibiting cancer cell growth. In summary, we provide TMEPro, a generically applicable clinical functional proteomic strategy, and a comprehensive resource for better understanding the PDAC TME and facilitating the discovery of new diagnostic and therapeutic targets.

PDAC is one of the most lethal cancers, with a 5 year survival rate of below 10% and a median survival time of less than 6 months[2]. PDAC has become the third leading cause of cancer-related mortality by 2024[3]. The lack of reliable early diagnostic biomarkers and tenacious resistance to almost all existing therapies are major causes of poor prognosis[4]. Comprehensive proteomic and genomic characterization of PDAC has revealed correlations of protein expression, post-translational modifications and genomic alterations with clinical information, and identified molecular subtypes[5,6]. However, a common limitation of these studies is that global profiling of bulk tissues cannot fully elucidate the impact of the cellular complexity and heterogeneity of PDAC.

The TME is a key hallmark of cancer[7]. The PDAC TME is atypically enriched with many non-malignant stromal cells and extensive extracellular matrix (ECM) components, which promote cancer proliferation, metastasis and drug resistance[1]. Many therapeutic strategies targeting the dense stroma have been tested but, to date, no clinical trial has led to approved PDAC therapies. Increasing efforts have been made to explore the diversity of TME, and its cross-talk with cancer cells. For example, laser-capture microdissection (LCM)-based proteome profiling has revealed molecular subtypes of cancer and stromal cells that may contribute to different patient outcomes[8]. However, proteome-level functional information on reciprocal signalling between stromal and cancer cells is largely missing.

Cell–cell communication is initiated mainly by secreted and plasma membrane (S–PM) proteins[9], which are a rich source of biomarkers and therapeutic targets[10]. The paracrine binding of secreted ligands to PM receptors elicits the activation of many types of intracellular signalling in target cells, including critical phosphotyrosine (pTyr)-mediated signalling cascades[11]. Mass spectrometry (MS)-based proteomics has gained increasing popularity for studying signal transduction with spatial and temporal resolution in pancreatic cancer[12]. It was previously demonstrated that oncogenic KRAS drives reciprocal signalling between pancreatic stellate cells (PSCs) and pancreatic cancer cells (PCCs) through signalling axes such as GAS6–AXL and IGF1–IGF1R to regulate the proliferation and apoptosis of PCCs in a coculture system[13]. We investigated paracrine signalling from PCCs to PSCs by global profiling of the secretome, pTyr proteome and STAT3 interactome and revealed that PSC-derived LIF is a key paracrine mediator that acts on

[1]State Key Laboratory of Medical Proteomics and Shenzhen Key Laboratory of Functional Proteomics, Department of Chemistry and Research Center for Chemical Biology and Omics Analysis, School of Science and Guangming Advanced Research Institute, Southern University of Science and Technology, Shenzhen, China. [2]Department of Biliary-Pancreatic Surgery, Tongji Hospital, Tongji Medical College, Huazhong University of Science and Technology, Wuhan, China. [3]Key Laboratory of Multi-Cell Systems, Center for Excellence in Molecular Cell Science, Shanghai Institute of Biochemistry and Cell Biology, Chinese Academy of Sciences, Shanghai, China. [4]Molecular and Cell Biology Laboratory, Salk Institute for Biological Studies, La Jolla, CA, USA. [5]Institute of Cancer Research, Shenzhen Bay Laboratory, Shenzhen, China. [6]Present address: Bristol Myers Squibb, San Diego, CA, USA. [7]These authors contributed equally: Peiwu Huang, Weina Gao, Changying Fu, Min Wang, Yunguang Li. ✉e-mail: shiyu.xy@gmail.com; dong.gao@sibcb.ac.cn; ryqin@tjh.tjmu.edu.cn; tianrj@sustech.edu.cn

PCCs to affect progression and drug response[14]. However, these functional proteomic investigations were performed on a cell-line-based system and might not faithfully recapitulate the physiological intercellular signalling events in PDAC.

Here we describe a generically applicable clinical functional proteomic strategy, called TMEPro, for comprehensive exploration of the PDAC TME at the proteome scale. TMEPro integrates multidimensional proteome information with spatial and temporal resolution to comprehensively delineate the functional interplay between PCCs and stromal cells in PDAC tissues from patients and a genetically engineered mouse PDAC model, and provide a valuable resource for functional and translational research on PDAC. Importantly, we revealed a reciprocal signalling link between stromal and cancer cells mediated by the stromal PDGFR–PTPN11–FOS signalling axis, and an additional dimension of intercellular signalling regulation mediated by AXL ectodomain shedding.

Landscape of the intercellular S–PM proteome

As S–PM proteins are usually low in abundance but represent the majority of heavily glycosylated proteins in the human proteome[15], we optimized a hydrazide-chemistry-based technique in the first step of the TMEPro strategy to selectively enrich and comprehensively profile the glycosylated S–PM proteome (Fig. 1a, Extended Data Fig. 1 and Supplementary Discussion). We then used the TMEPro strategy to assess a cohort of human pancreatic tissue samples including 29 tumours, 27 paired non-cancerous adjacent tissues (NT), 28 chronic pancreatitis (CP) and 16 normal pancreatic tissues (Supplementary Table 1). Negligible variation in label-free quantification (LFQ) intensity of glycoprotein standard fetuin and high correlation coefficient between biological replicates demonstrate the high-quality nature of the dataset (Fig. 1b and Extended Data Fig. 2a). In total, 2,741 S–PM proteins, 6,181 non-redundant *N*-glycosites and 80 new *N*-glycoproteins were identified, covering more than half of the predicted S–PM proteome (Fig. 1b and Supplementary Table 1). As we analysed all possible predicted S–PM proteins in the public database, the coverage should be much higher when considering only the S–PM proteins expressed in a single pancreatic tissue sample. Notably, annotation of our S–PM proteome revealed that 76% of these proteins had intercellular communication roles[16], including the top two classes, transmembrane receptors and secreted ligands, which are critical for intercellular signalling (Extended Data Fig. 2b).

We next examined the S–PM proteome features of the PDAC TME by performing a quantitative comparison between tumour and normal tissues, and identified more than 1,000 differentially expressed proteins. These proteins spanned four orders of magnitude and included 31 well-characterized cancer biomarkers and 91 protein targets with FDA-approved drugs (Fig. 1c and Supplementary Table 1). Overall, the majority of differentially expressed proteins gradually trended from normal to tumour samples (Fig. 1c). Considerable similarity was found between tumour and CP samples, which is expected because CP is a progressive inflammatory disease with a high level of fibrosis that shares many common pathological features with PDAC[17]. Gene Ontology molecular function (GOMF) analysis revealed that the S–PM proteins differentially expressed between tumour and normal tissues could be classified into five major clusters, which overlapped with the differentially expressed proteins between tumour and CP tissues, although to a lesser extent (Fig. 1d, Extended Data Fig. 2c,d and Supplementary Table 1). To our knowledge, this dataset represents the most comprehensive coverage of the S–PM proteome and *N*-glycoproteome in human PDAC tissues and provides an untapped resource for investigating intercellular signalling in the PDAC TME.

Spatial and cell-type-specific proteome

To examine the cell-type origin of the S–PM proteome and its potential intercellular signalling role, we first deconvoluted the cell types of the S–PM proteome in 29 bulk tumour tissues (Fig. 1b) using a published single-cell RNA-sequencing dataset of PDAC[18], and found that cancer cells and cancer-associated fibroblasts (CAFs) were the two major cell populations (Extended Data Fig. 3a and Supplementary Table 2). Thus, we performed spatially resolved proteome profiling of PCCs and stroma from 13 PDAC tumour samples (Methods, Fig. 2a, Extended Data Fig. 3b and Supplementary Table 1). A total of 7,000–8,000 proteins, including approximately 1,400 S–PM proteins, per stromal or PCC region were identified with a high quantification reproducibility between biological samples (Extended Data Fig. 3c,d and Supplementary Table 2), representing one of the largest spatial proteome landscapes of PDAC achieved to date. As a complementary approach to confirm the cellular origin of these spatially defined S–PM proteins, secretome and hydrazide-chemistry-based transmembrane proteome profiling was performed on six representative human PCC lines as well as two CAF lines (Fig. 2a). By combining tumour and cell line datasets, 2,331 S–PM proteins were identified, among which 787 and 584 were enriched in PCC and stromal cells, respectively, with the well-known markers listed (Fig. 2b and Supplementary Table 2). In comparison, more S–PM proteins were covered by our spatial proteomic dataset than the recent spatial and cell-type-specific proteomic and transcriptomic datasets (Extended Data Fig. 3e,f).

Notably, the spatially resolved and cell-type-specific proteome dataset covered more than 76% of the S–PM proteome identified in bulk tumour tissues (Extended Data Fig. 3g). These data therefore experimentally defined the cell type origin of the identified S–PM proteins in the bulk tissues and accordingly correlate with clinical significance when comparing tumour and normal tissues (Extended Data Fig. 3g). Unbiased GOMF analysis revealed that the spatially resolved and cell-type-specific S–PM proteome has molecular functions similar to the significantly changed S–PM proteome in bulk tissue profiling (Fig. 2c and Supplementary Table 2). Notably, the majority of proteins associated with the ECM and protease activity were stroma specific, while approximately 90% of the transporters were PCC specific, which could be explained by metabolic pathway reprogramming to meet the increased energy and biosynthetic needs of cancer cells surrounded by dense and poorly vascularized stroma[19]. Importantly, six PCC-specific PM proteins with upregulated expression in tumours were validated by tyramide signal amplification (TSA) staining (Fig. 2c and Extended Data Fig. 3h). These PCC-specific membrane proteins might therefore be used as surface markers for targeted PDAC therapy.

To systematically examine the intercellular signalling flow between tumour and stromal cells, we first annotated pairwise relationships in the S–PM proteome identified from bulk tissues (Methods and Extended Data Fig. 2b). In total, 1,724 pairs consisting of 427 ligands and 424 receptors were identified, covering the majority of identified ligands or receptors included in our pair database (Extended Data Fig. 3i,j and Supplementary Table 2). Growth factor-, cytokine- and integrin-related pairs were among the GOMF terms that were most enriched in the receptor–ligand pairs (Extended Data Fig. 3k and Supplementary Table 2). Importantly, ligands and receptors of 54% of the pairs were consistently upregulated in tumours, indicating their potential functional importance in the PDAC TME (Extended Data Fig. 3l). Among these pairs, 524 had defined cell type origins for both ligands and receptors, including 262 paracrine signalling pairs. As more ligands were stroma specific and more receptors were PCC specific, a higher number of pairs could be defined as being involved in intercellular signalling from stromal cells to PCCs ($n = 190$) than from PCCs to stromal cells ($n = 72$) (Fig. 2d, Extended Data Fig. 3m and Supplementary Table 2). Functionally, many signalling proteins were included in these paracrine signalling pairs. For example, the ECM and integrin families were more enriched in the stoma, whereas the receptor tyrosine kinase (RTK) and transporter families were more enriched in the PCCs (Fig. 2d).

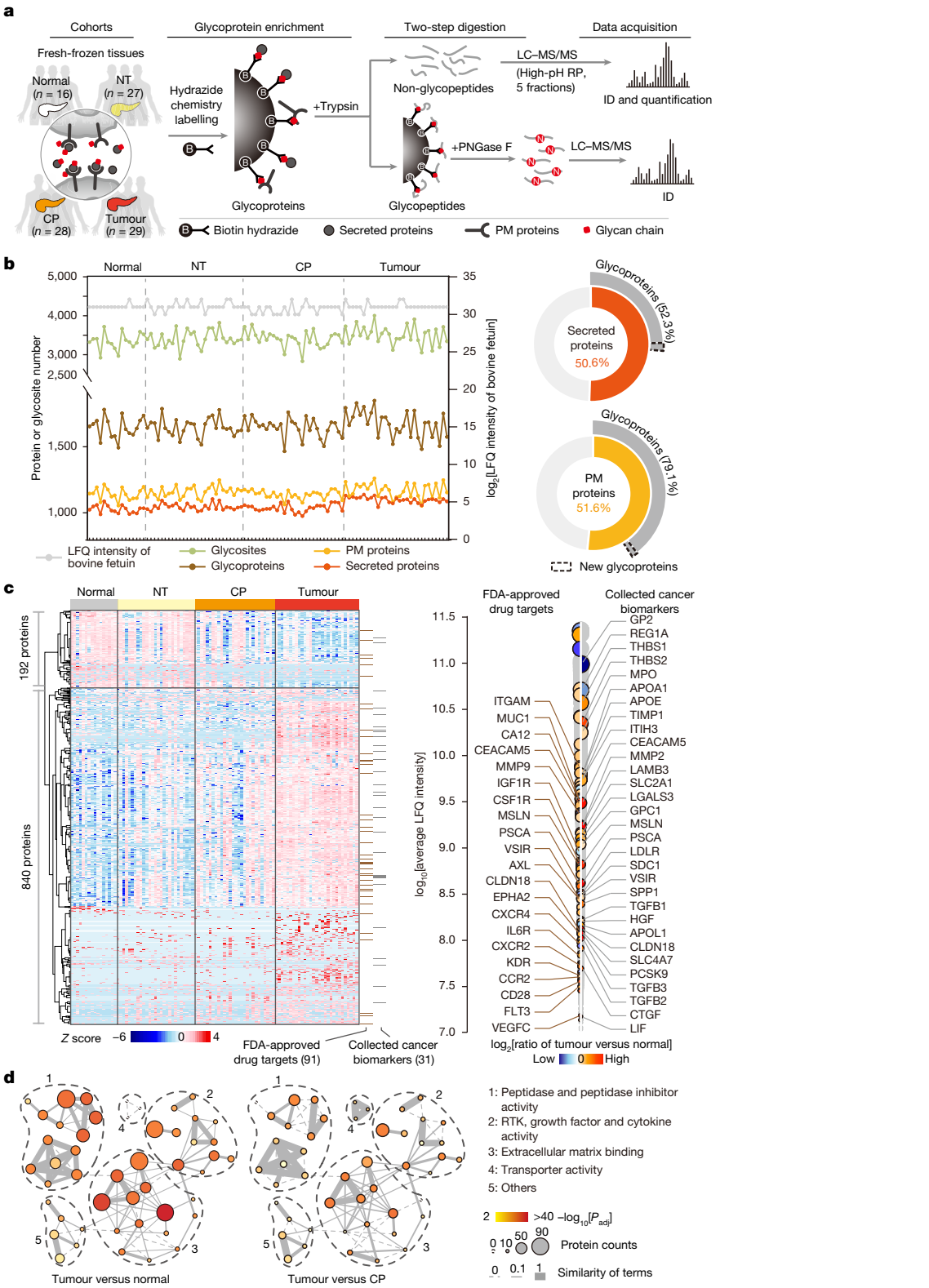

Fig. 1 | Deep profiling of the S–PM proteome in PDAC. a, The sample cohort and the workflow for simultaneous profiling of S–PM proteins in bulk tissues. LC, liquid chromatography; RP, reversed-phase. **b**, S–PM proteome profiling of 100 pancreatic tissues (left) and coverage of the total identified S–PM proteins in human secreted and PM protein databases (right; Methods). Glycoproteins were the proteins identified with *N*-glycosites. New glycoproteins were the proteins that were not annotated in UniProt as *N*-linked glycoproteins but were identified with *N*-glycosites in our dataset. Bovine fetuin was spiked in after tissue lysis as a quality control for the experimental procedures. **c**, Consensus clustering of S–PM proteins significantly changed between tumour and normal samples, and the dynamic range of their LFQ intensities; FDA-approved drug targets implicated in PDAC mechanism or therapy and well-established cancer biomarkers among all the significantly changed S–PM proteins shown in grey are annotated with gene names. **d**, Clustering of the top 50 GOMF terms of significantly changed S–PM proteins. The top 50 GOMF term network was generated using all of the significant proteins between tumour samples and the other three sample groups (tumour versus NT is shown in Extended Data Fig. 2c). Similarity of terms indicates the overlap of proteins between terms. *P* values were calculated by hypergeometric distribution.

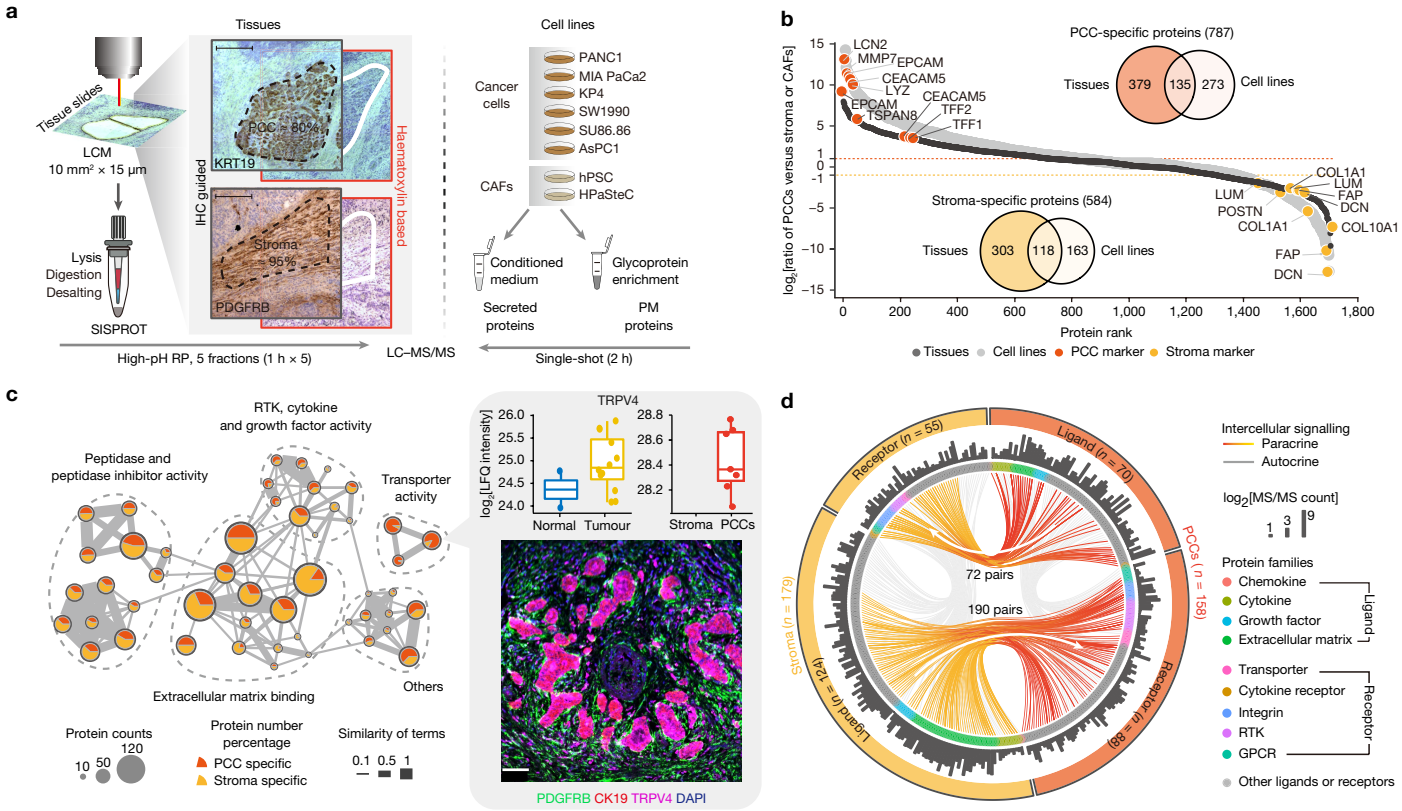

Fig. 2 | Spatially resolved and cell-type-specific proteome profiling reveals intercellular signalling in PDAC. a, The workflow of spatially resolved and cell-type-specific proteome profiling in PDAC. Scale bars, 200 µm. The centrifuge tube images were adapted from ref. 28, copyright 2016 American Chemical Society. **b**, The distribution of LFQ intensity ratios of S–PM proteins identified in tissue and cell line samples. PCC- or stroma-enriched proteins identified using two strategies were combined for downstream analysis. **c**, The top 50 GOMF terms of PCC- or stroma-specific S–PM proteins overlapped with those identified in bulk tumour tissues in Fig. 1d. The pie charts represent the percentage of stroma and PCC-specific proteins within each GO term. For the box plots, the box limits show the interquartile range, the centre line shows the median, and the upper and lower whiskers show 1.5× the interquartile range above and below the third and first quartiles, respectively. Six novel PCC-specific proteins were validated by TSA staining, with TRPV4 presented as an example. Scale bar, 50 µm. **d**, Potential autocrine and paracrine signalling between PCCs and/or stroma. The bars in the circos plot show the relative abundances of proteins in the spatially resolved or cell-type-specific proteome dataset.

Time-resolved profiling of S–PM proteome

We next examined the S–PM proteome during PDAC tumour development using the genetically engineered KPC (*Kras*$^{LSL\text{-}G12D/+}$;*Trp53*$^{flox/flox}$;*Pdx1-cre*) mouse model[14]. Given that late-stage PDAC is surgically unresectable due to metastasis and that very early-stage PDAC is difficult to diagnose, we chose this model because it best represents the progression of the PDAC TME from early stage to late stage adenocarcinoma[20]. On this basis, we collected tumour tissues from the KPC mice at different ages, corresponding to various tumour progression stages, and normal mouse pancreas tissue (NT), to characterize temporal alterations in the S–PM proteome during tumour progression (Fig. 3a). As we reported previously, inflammation, pancreatic intraepithelial neoplasia lesions and a few small solid tumour nodules were evident in the pancreas at 3 weeks of age; there was evidence of advanced PDAC at 5 weeks of age; and almost all observed masses were advanced invasive tumours at 7 weeks of age[14]. Using our glycoprotein enrichment method of the TMEPro strategy with single-shot proteomic analysis, we identified approximately 1,500 S–PM proteins by non-glycopeptides and 3,000 *N*-glycosites in each sample, with high reproducibility between biological replicates (Fig. 3b, Extended Data Fig. 4a and Supplementary Table 3). Quantitative analysis of the temporal S–PM proteome showed that the pancreatic tissues of KPC mice at 3 weeks had a pattern most similar to that of NTs and was quite distinct from those at 5 and 7 weeks (Extended Data Fig. 4b,c and Supplementary Table 3). Encouragingly, almost 90% of the significant S–PM proteins that overlapped between humans and mice exhibited consistent expression trends in the two species (Extended Data Fig. 4d and Supplementary Table 3). These results demonstrate the feasibility of using KPC mice for studying early pancreatic cancer development.

Next, we performed expression-level-based clustering of S–PM proteins that were consistently altered between humans and mice, and found that these proteins were grouped into three clusters (Fig. 3c and Supplementary Table 3). Based on a membership value of >0.45, 529 S–PM proteins were defined as tumour-progression-related proteins, including 25 reported PDAC markers and 57 FDA-approved drug targets, such as LIF, THBS2, TIMP1, GPC1, MSLN and LGALS3 (Fig. 3d and Extended Data Fig. 4e). Importantly, cell-adhesion- and ECM-related proteins were highly enriched in cluster 3, as expected due to the dense stroma of the late-stage PDAC (Extended Data Fig. 4f and Supplementary Table 3). In comparison, cluster 2, which shows upregulation beginning at 3 weeks, contains various functional proteins that are expected to be critical for early PDAC TME development and intercellular signal transduction; thus, this cluster is potentially a valuable resource for the validation of biomarkers for the early detection of PDAC. We chose TNFRSF11B (cluster 2) and NPTX1 (cluster 3) for enzyme-linked immunosorbent assay (ELISA) validation, and found that their levels were significantly increased in the plasma samples of patients with PDAC compared with the healthy control individuals (Extended Data Fig. 4g and Supplementary Table 3).

Finally, we annotated the human ligand–receptor pairs by cross-referencing the tumour progression trends in the KPC model. Among

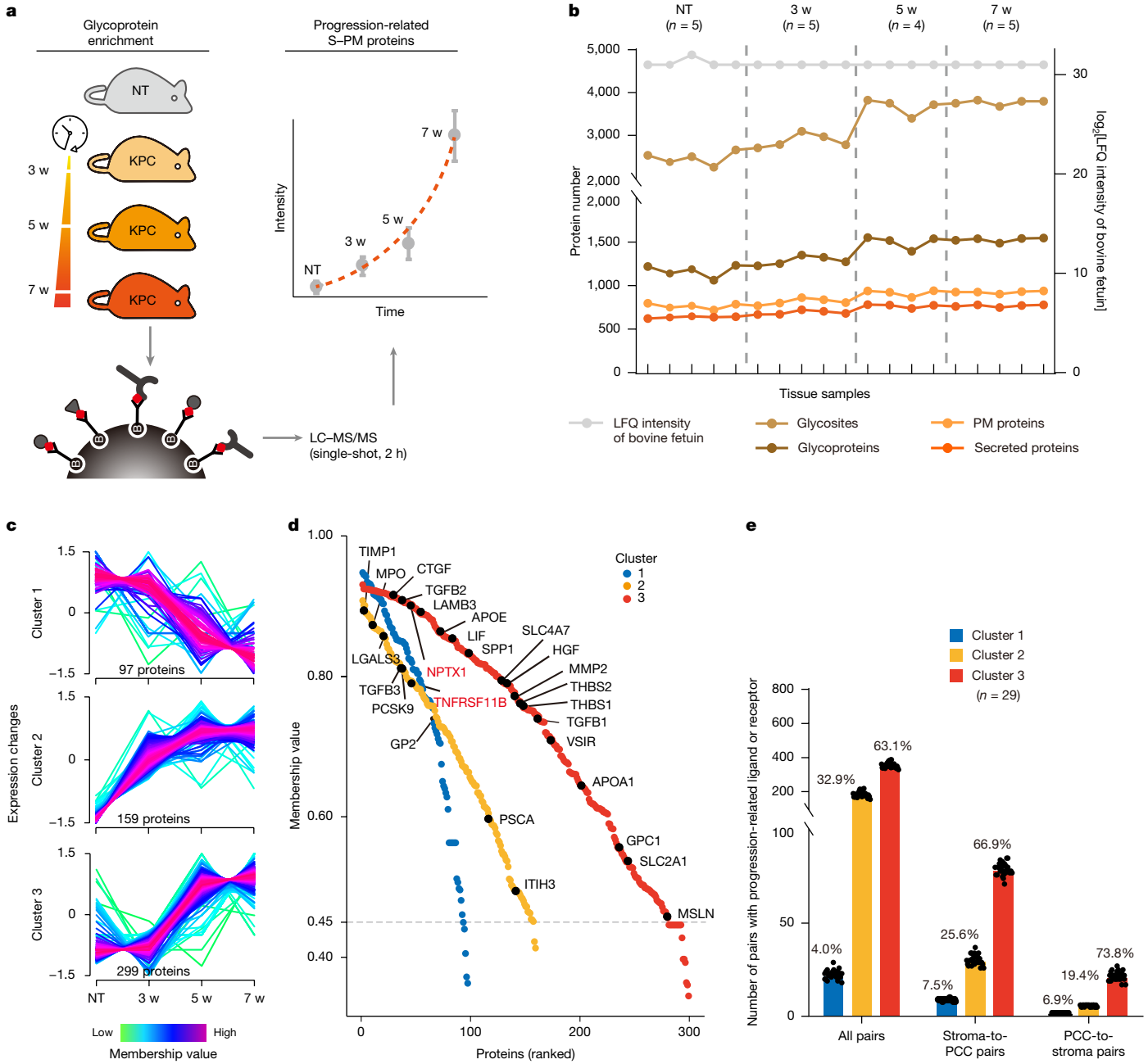

Fig. 3 | Time-resolved profiling of the intercellular signalling proteome during tumour progression in a PDAC mouse model. a, Workflow for S–PM proteome profiling in mouse models. Mouse pancreatic tissues were collected from the KPC model at different tumour stages and from normal mouse pancreas (NT). w, week. **b**, S–PM proteomic events in each mouse sample. **c**,**d**, Expression trend-based clustering of significant S–PM proteins with consistent trends between mouse and human tissue samples. The proteins were grouped into three major expression trends (**c**) and ranked according to membership score, with previously reported cancer markers in Fig. 1f highlighted (**d**). TNFRSF11B and NPTX1 are two unreported proteins that were chosen for ELISA validation. **e**, Annotation of ligand–receptor pairs in 29 bulk human tumour tissues according to the number of pairs with tumour progression trends in three clusters. Data are mean ± s.d. All pairs refer to the pairs shown in Extended Data Fig. 3j in which the expression of at least the ligand or receptor was significantly changed in human tumour versus normal tissues in *N*-glycoproteomic dataset.

the 1,724 pairs with both the ligand and receptor identified in bulk human tissues (Extended Data Fig. 3j), approximately 600 pairs with at least the ligand or receptor significantly changed in tumour versus normal in each human bulk tumour tissue sample. In KPC mice, 81% of the ligand–receptor pairs exhibited progression trends for the ligand or receptor, while 15% exhibited progression trends for both the ligand and receptor (Extended Data Fig. 4h). These percentages were similar for both stroma-to-PCC pairs and PCC-to-stroma pairs, suggesting that paracrine communication has an important role in intercellular interactions in both directions. Notably, the majority of the pairs was assigned to cluster 3, demonstrating more active intercellular signalling and the importance of the TME in late-stage tumour progression (Fig. 3e). The identification of these paracrine signalling pairs associated with tumour progression could therefore provide a rich resource for exploring tumour progression in the context of tumour–stroma interactions.

Signalling activation mediated by pTyr

As the pTyr machinery is well known to activate the first wave of intercellular signalling, we went on to investigate the activation status of

ligand–receptor downstream signalling axes mediated by pTyr in PDAC. As pTyr accounts for less than 1% of the phosphoproteome[21], we integrated both our photoreactive pTyr protein complex profiling probe (Photo-pTyr-scaffold) approach and SH2-superbinder-based pTyr peptide enrichment approach into the TMEPro strategy for simultaneously enriching and profiling pTyr-mediated protein complexes and pTyr sites (Fig. 4a, Extended Data Fig. 5a and Supplementary Table 1). With this step of the TMEPro strategy, we aimed to identify key pTyr machinery proteins and their pTyr sites, including pTyr writers (kinases), readers (proteins containing an SH2 or PTB domain) and erasers (phosphatases), which often form protein complexes through pTyr sites and indicate the activation of the signalling pathways[22].

Taking advantage of the Photo-pTyr-scaffold approach with high-affinity pTyr protein recognition and photocrosslinking to capture transient pTyr protein complexes, we identified 464 PM proteins, 51 pTyr writers, 94 pTyr readers and 46 pTyr erasers, many of which were identified with corresponding pTyr sites (Fig. 4b, Extended Data Fig. 5b and Supplementary Table 4). After normalizing the LFQ intensities based on the bait protein (Src SH2 superbinder), we quantitatively analysed pTyr proteins identified using the Photo-pTyr-scaffold approach to avoid pTyr site-specific alteration. Heat maps of the three classes of significantly changed proteins revealed that most were more highly activated in tumour tissues than in normal tissues, and that the majority were identified with pTyr sites, including 16 FDA-approved drug targets (Fig. 4c, Extended Data Fig. 5c and Supplementary Table 4). PDGFRB, PTPN11 and TLN1 were among the most significantly altered pTyr machinery proteins with identified pTyr sites and merit further investigation (Fig. 4c and Extended Data Fig. 5d).

Signalling network assembly and validation

To systematically assemble the multidimensional proteomic datasets acquired by the TMEPro strategy (Figs. 1–4), we performed systematic bioinformatic analyses to examine the ligand–receptor–pTyr-machinery-mediated intercellular signalling network between PCCs and stromal cells. First, Gene Ontology biological process (GOBP) analysis of the S–PM proteome showed high coverage of cancer signalling pathways (Extended Data Fig. 5e and Supplementary Table 4). In total, 9,299 signalling axes were predicted, which were classified into 16 categories on the basis of their significance in the comparison of tumour and normal human tissues at each node (Supplementary Table 4). We were particularly interested in the 'activated' signalling axes filtered based on significant changes in both receptor and downstream signalling proteins in the pTyr-mediated protein complex dataset, in which we focused on 148 ligand–receptor pairs and 1,672 signalling axes containing at least a significantly changed ligand or receptor in the *N*-glycoproteomic dataset (Extended Data Fig. 5f and Supplementary Table 4). Among these pairs, 18 were paracrine signalling pairs that exhibited tumour progression trends (Extended Data Fig. 5g). These 18 pairs are involved in 291 signalling axes closely related to RTKs, such as the insulin receptor axis in PCCs and PDGFR-related axes in stromal cells (Fig. 4d and Extended Data Fig. 5h). By systematically integrating the multidimensional proteome, we therefore delineated the first wave of intercellular signalling in PDAC tumour after ligand–receptor interactions.

We went on to validate the paracrine PDGFR RTK signalling mediated by stromal PDGFRA and PDGFRB, which were both significantly upregulated and had high levels of pTyr in tumours (Extended Data Fig. 6a). Moreover, their ligand, PDGFC, was significantly upregulated in tumours and preferentially derived from PCCs. Global pTyr profiling revealed that stimulating PSCs with conditioned medium (CM) from PCCs activated the PDGFR signalling cascades, especially for PDGFRA and PTPN11 (Fig. 4e and Supplementary Table 5). The pTyr activation of PDGFRA was validated by western blotting with the signals being attenuated by the PDGFR inhibitor crenolanib (PDGFRi; Extended Data Fig. 6b). We further validated the attenuation of pTyr activation of PTPN11 in PSCs after *PDGFR* knockdown or crenolanib treatment; by contrast, PTPN11 inhibition by SHP099 (PTPN11i) did not affect AKT activation, but abrogated ERK1/2 activation (Extended Data Fig. 6c,d). These results suggest that PDGF–PDGFR–PTPN11–ERK signalling is critical for the paracrine signalling activation from PCCs to PSCs.

To further examine the downstream effect of the PDGFR–PTPN11 signalling axis in PSCs, we profiled the PSC secretome after PDGFR or PTPN11 inhibition (Extended Data Fig. 6e and Supplementary Table 5). Notably, LIF was one of the most substantially changed proteins. Inhibition of the PDGFR–PTPN11–ERK signalling axis had the most profound effect on abolishing PDGFB-induced LIF protein secretion and mRNA expression (Fig. 4f and Extended Data Fig. 6f,g). Finally, we validated that FOS was a key downstream transcription factor that regulates LIF transcription (Fig. 4g and Extended Data Fig. 6h,i). Taken together, these findings confirmed the intercellular signalling pathway in which PCC-derived PDGFs activate a PDGFR–PTPN11–ERK–FOS signalling axis to enhance LIF expression and secretion in PSCs (Fig. 4h), while PSC-derived LIF activates the LIFR–GP130–STAT3 signalling axis in PCCs[14], suggesting a potential clinical application in PDAC by targeting this paracrine signalling pathway.

Generic shedding mechanism of PM proteins

In contrast to tyrosine-phosphorylation-mediated signal transduction, ectodomain shedding of PM proteins can initiate additional dimensions of intercellular signalling, such as termination of receptor-mediated signal transduction[23]. We developed a bioinformatic analysis pipeline to examine the ectodomain-shedding process directly in tumour tissues (Methods, Fig. 5a and Extended Data Fig. 7a). In principle, the PM proteome of the eight cell lines profiled after glycoprotein enrichment (Fig. 2b) represents the full-length PM proteins, while the secretome contains shed extracellular domains (ECDs) of PM proteins. Accordingly, the S–PM proteome of tissue samples contains both shed ECDs (if any) and full-length PM proteins. The amino acid sequences of PM proteins were divided in silico into ECDs and intracellular domains (ICDs) for database searching, leading to identification of ECDs and ICDs in different datasets (Extended Data Fig. 7a and Supplementary Table 6). Given that the sequence lengths of the ECD and ICD of each PM protein varies considerably, we developed $Index_{training}$ and $Index_{test}$ values to predict shed PM proteins. By filtering the $Index_{training}$ value generated from the unique peptide ratio of ECD/ICD in the secretome dataset to that in the PM proteome dataset, 45 PM proteins were identified as shed proteins (Extended Data Fig. 7a). Encouragingly, using the same filtering criteria for the $Index_{test}$ value by comparing the tumour S–PM dataset and the PM proteome dataset, 22 out of the 45 PM proteins were identified as shed proteins in tumour tissues including AXL, which was determined to be the most significantly shed PM protein (Fig. 5a,b). Of the 22 proteins, 70% were previously reported to be shed (Supplementary Table 6), indicating the high fidelity of the data processing strategy. Notably, 13 of the 22 shed proteins were PCC specific, among which four proteins (AXL, MET, EPHA4 and EFNB2) were RTK related, and six proteins, including NECTIN2 and CDH3, were related to cell adhesion (Extended Data Fig. 7b), indicating that shedding of these PM protein families might have important roles in regulating intercellular signalling in the PDAC TME.

Ectodomain shedding is regulated by proteases known as sheddases. In total, we identified 118 significantly changed proteases in our S–PM proteome dataset (Fig. 5c and Supplementary Table 6), of which 23 are from the canonical ADAM and matrix metalloprotease (MMP) families[24]. MMP family proteases were more upregulated in tumour samples, suggesting that MMP family members are likely to be more important regulators of ectodomain shedding in PDAC than ADAM family proteases (Fig. 5d). To examine the potential proteases that are responsible for shedding of the 22 shed proteins identified in tumours,

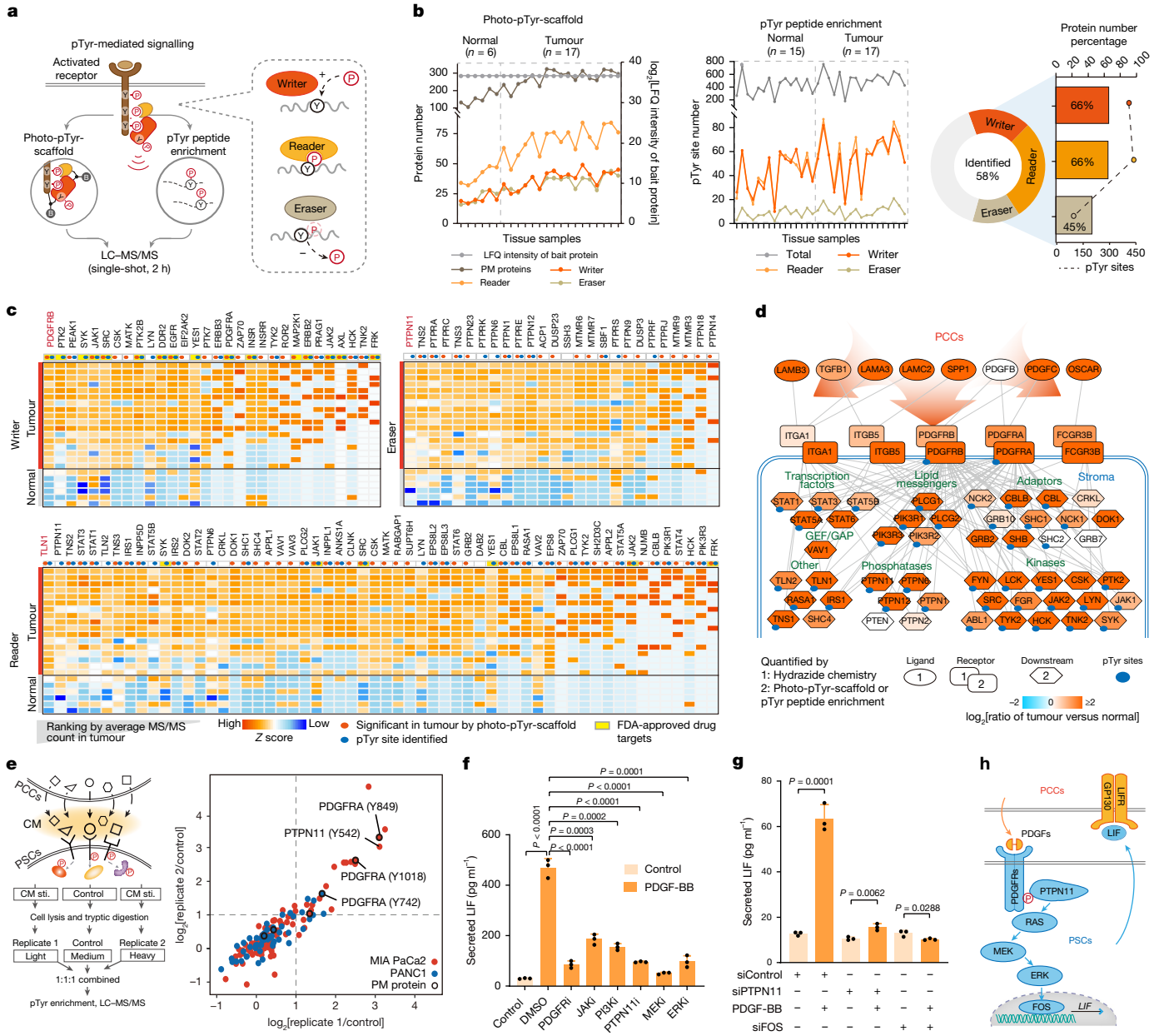

Fig. 4 | Functional profiling of tyrosine-phosphorylation-mediated intercellular signalling in PDAC. a, The combined strategy of the Photo-pTyr-scaffold approach and pTyr peptide enrichment approach for examining pTyr-mediated protein complexes and pTyr sites in PDAC. **b**, The number of pTyr writers, readers and erasers identified by the Photo-pTyr scaffold, the number of pTyr sites identified by pTyr peptide enrichment and the coverage of corresponding databases by combining two approaches. **c**, The relative expression levels of pTyr writers, erasers and readers in the Photo-pTyr-scaffold dataset. Top-ranked proteins (according to average MS/MS counts in tumour) are highlighted in red. **d**, The activated paracrine signalling pairs from PCCs to stromal cells in tumour and their downstream proteins screened out from Extended Data Fig. 5g. **e**, pTyr site profiling of PSCs after stimulation (sti.) with CM collected from PANC1 ($n = 2$) or MIA PaCa2 ($n = 2$) cells. Dimethyl labelling was used for pTyr peptide quantification. **f**,**g**, Investigation of LIF secretion after inhibitor treatment in PDGF-activated PSCs (**f**) and *FOS* or *PTPN11* small interfering RNA (siRNA) knockdown (**g**). Data are mean ± s.d. of $n = 3$ biological replicates. *P* values were calculated using two-tailed unpaired Student's *t*-tests. **h**, Schematic of the characterized stromal PDGFR–PTPN11–ERK–FOS signalling axis.

4 MMPs were examined on the basis of their significant upregulation in tumour tissues, especially in comparison to ADAM10 and ADAM17, which are known sheddases for AXL (Fig. 5d and Extended Data Fig. 7c). Encouragingly, global secretome profiling revealed that knocking down *MMP1* and *MMP11* in PCCs substantially reduced the ectodomain shedding of many of the 22 PM proteins, while knocking down *MMP9* and, especially, *MMP15* had a minor effect (Fig. 5e, Extended Data Fig. 7d–g and Supplementary Table 6). We performed further western blot analysis to validate the participation of MMP1 and MMP11 in AXL shedding (Fig. 5f and Extended Data Fig. 7e,h). Taken together, these findings suggest that MMP-mediated membrane receptor shedding might function as an additional dimension of intercellular signalling regulation.

Additional dimension of AXL signalling

AXL is a member of the TAM family of RTKs, along with TYRO3 and MERTK, that is aberrantly expressed in various cancer types and promotes chemoresistance and metastasis[25]. In our dataset, AXL was more

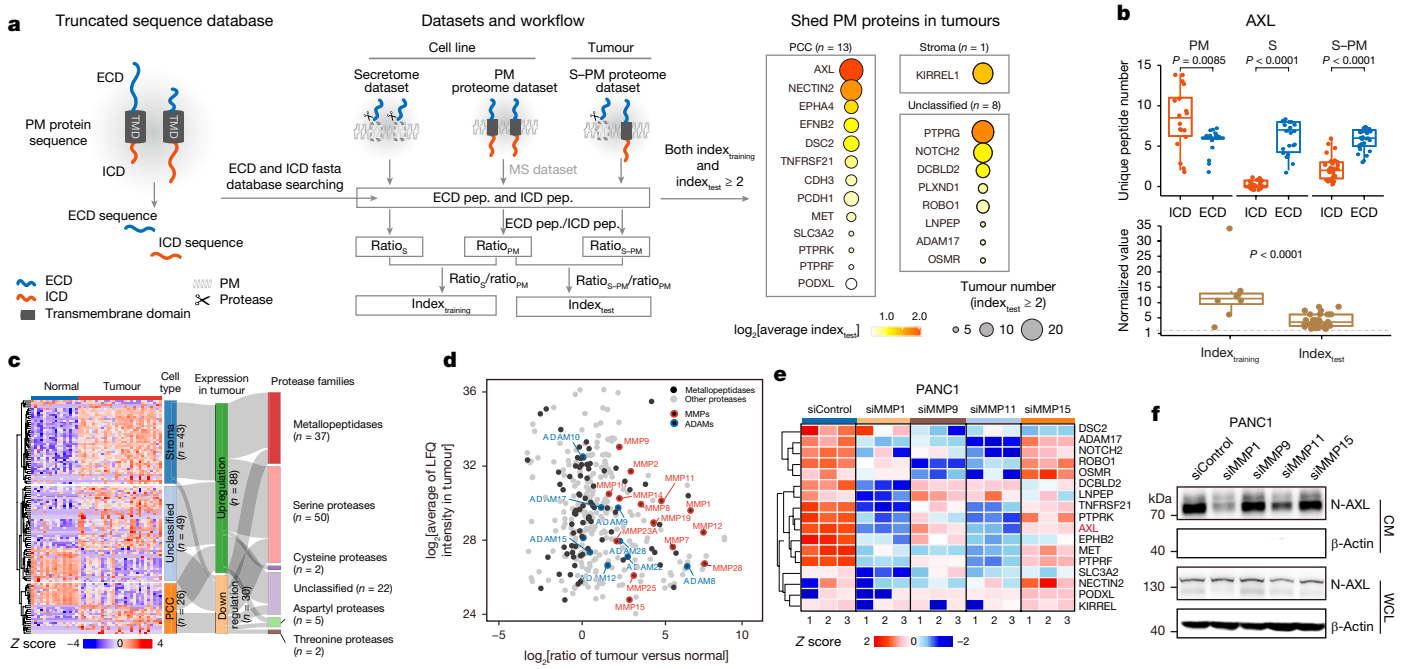

Fig. 5 | Exploration of generic shedding mechanism of PM proteins in PDAC. **a**, The bioinformatics workflow for the identification of shed PM proteins in tumours by using the secretome and PM proteome datasets of eight pancreatic cell lines as the training set. The 22 shed proteins were classified according to cell type specificity and ranked by $Index_{test}$. pep., unique peptides; TMD, transmembrane domain. **b**, AXL is shown as an example in the identification of shed PM proteins in 29 tumour samples. Box plots are as defined in Fig. 2c. *P* values were calculated using two-tailed unpaired Student's *t*-tests. **c**, Heat map of the 118 proteases significantly changed in tumour versus normal by *N*-glycoproteomic analysis and subtyping of them on the basis of cell type specificity, expression trend and protease family. **d**, Expression levels and ratios (against normal tissues) of the ADAM and MMP metalloproteinase families in tumour tissues. **e**, Secretome profiling for identification of shedding substrates of MMPs in PANC1 cells. $n = 3$ biological replicates. Replicates 1–3 are indicated on the *x* axis. Selected MMPs were knocked down by siRNAs. The heat map shows the shedding levels of the 17 out of 22 shed PM proteins identified in tumours. **f**, Validation of AXL shedding after *MMP* knockdown by siRNAs in PANC1 cells. sAXL in PANC1 CM and full-length AXL in whole-cell lysates (WCLs) were detected by western blotting. β-Actin was run on the same gel as the loading control. Quantification is shown in Extended Data Fig. 7e. N-AXL, AXL extracellular domain.

significantly and actively regulated than the other two TAM members (Extended Data Fig. 8a), suggesting that AXL signalling has an important role in PDAC.

To determine the extent to which AXL was shed in tumours, we performed parallel reaction monitoring (PRM)-based targeted MS analysis to absolutely quantify the in situ levels of full-length (represented by the ICD) and the ECD of AXL and its ligand GAS6 in PCC and stroma regions of 50 tumour tissues (Fig. 6a,b). To increase the sensitivity and remove any ICDs derived from shedding, glycoproteins in LCM-collected tissue slices were enriched and processed using FISGlyco technology. Heavy-isotope-labelled standard peptides were spiked into each sample for absolute quantification. Clear PRM transition peaks covering six orders of magnitude indicated high sensitivity for quantitative analysis of peptides derived from the AXL ICD, the AXL ECD and GAS6 (Extended Data Fig. 8b–e). Our PRM results revealed that AXL and its ligand GAS6 were expressed at similar levels in PCCs and the stroma region (Fig. 6b and Supplementary Table 7). Notably, the level of AXL ECD was 3.5-fold higher than the full-length AXL level, suggesting that approximately 70% of AXL was shed in both PCC and stromal regions of PDAC tumours.

Notably, when we classified 41 tumour samples from patients with or without lymph node metastasis according to the relative levels of shed AXL (sAXL) and GAS6 that were consistent in stroma and PCC regions, we found a significant positive correlation between relative sAXL and GAS6 levels and lymph node metastasis (Fig. 6c, Extended Data Fig. 8f–i and Supplementary Table 7). Specifically, the absolute level of sAXL was calculated by subtracting full-length AXL from ECD of AXL. Considering that sAXL and GAS6 probably enter the bloodstream, we examined their potential as disease-specific biomarkers. Encouragingly, ELISA analysis of sAXL and GAS6 showed that they were significantly upregulated in the plasma samples from 36 patients with PDAC in the training cohort and 123 patients in the validation cohort compared with those in normal plasma samples (Extended Data Fig. 8j). Combined analysis of sAXL and GAS6 increased the area under the curve (AUC) of CA19-9, the only clinically used biomarker for pancreatic cancer, indicating the potential of this panel as a PDAC biomarker (Fig. 6d).

To validate the potential roles of MMP-family protease-mediated shedding in AXL signalling regulation, we treated PANC1 cells and primary cancer cells derived from KPC mouse tumours (KPCP) with 10 μM BB-94, a broad-spectrum MMP inhibitor, which nearly abrogated shedding of AXL into the CM (Extended Data Fig. 9a,b). Given the extremely high binding affinity (K_d of 33 pM) between AXL and GAS6[26], sAXL might function as a high-affinity decoy receptor to neutralize GAS6 and attenuate AXL signalling. Western blot and PRM analyses confirmed that GAS6 pre-incubation with PANC1 CM containing sAXL almost completely abrogated the GAS6-mediated activation of three pTyr sites on AXL and its key signalling node AKT, and this change was reversed when the cells from which the CM was collected were also treated with BB-94 (Fig. 6e and Extended Data Fig. 9c,d).

Finally, we examined the phenotypic effects of MMP-mediated AXL signalling on PDAC tumour growth. We used the R428 AXL kinase inhibitor that entered into a phase II clinical trial for PDAC treatment (ClinicalTrials.gov: NCT03649321). We first evaluated the synergistic effect of BB-94 and R428 on the patient-derived organoids (PDO) biobank (Methods), from which 66 PDOs derived from PDAC patients were enrolled in this study (Extended Data Fig. 9e). PDOs and PDO-derived xenografts displayed the histological and immunohistological patterns present in the original patient tumour samples (Extended Data Fig. 9f).

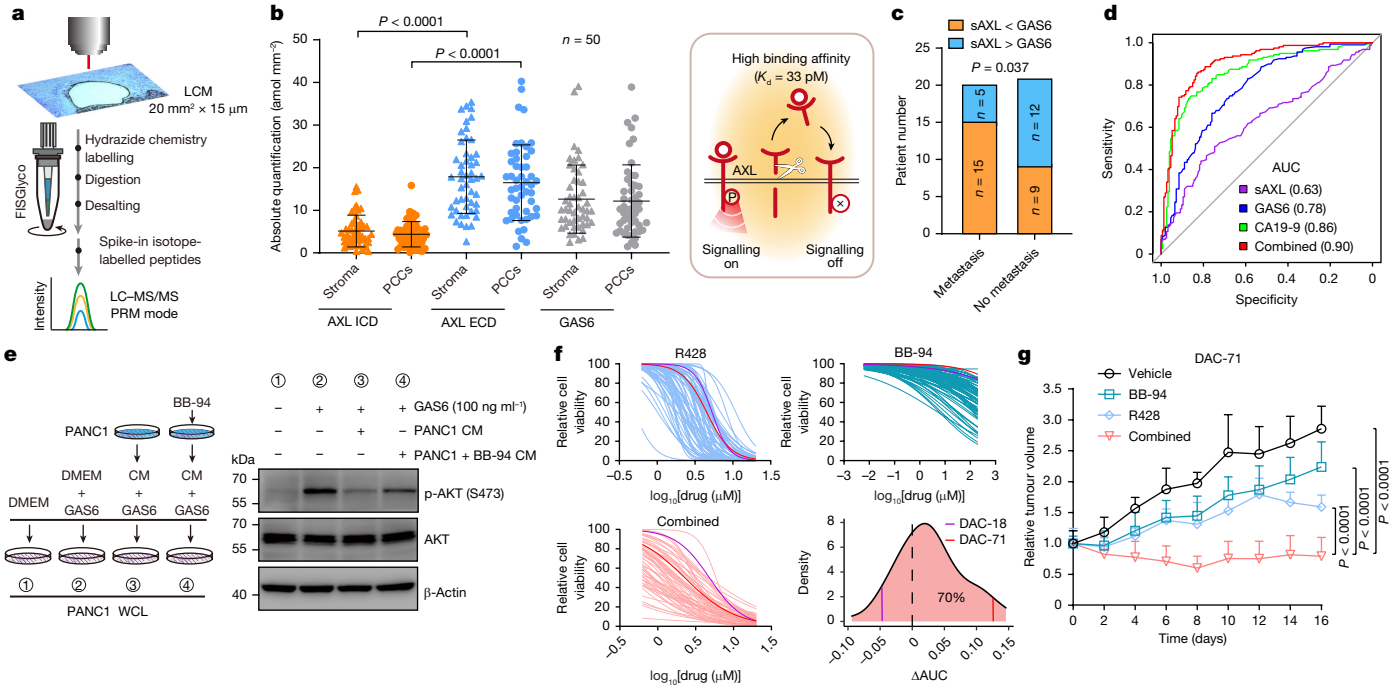

Fig. 6 | Additional dimension of signalling regulation by MMP-mediated AXL shedding. a, Schematic of absolute quantification of full-length AXL (ICD), ECD of AXL, sAXL (sAXL = ECD − ICD) and the ligand GAS6 with spatial resolution in tumour tissues. The centrifuge tube images were adapted from ref. 28, copyright 2016 American Chemical Society. **b**, Absolute quantification of the ECD and ICD of AXL, and the ligand GAS6 with spatial resolution in 50 tumour tissues. Data are mean + s.d. of $n = 50$ tumours. The schematic demonstrates the potential activation status of the AXL signalling pathway in relation to sAXL shedding level and GAS6 level. **c**, The correlation of relative sAXL and GAS6 levels with lymph node metastasis. One-sided χ^2 tests were performed on the relative trend numbers of 41 samples, in which sAXL and GAS6 have consistent relative trends in PCC and stromal regions. **d**, Diagnostic performance of individual targets and a biomarker panel by combining sAXL and GAS6 with CA19-9. **e**, Neutralization of GAS6 signalling by sAXL. The CM of PANC1 cells with or without BB-94 treatment was collected and incubated with GAS6 for 30 min before stimulation of PANC1 for 5 min at 37 °C; whole-cell lysates were collected for western blot analysis. Owing to similar molecular masses of proteins, the samples were run on separate gels, with β-actin as the sample processing control. Quantifications are shown in Extended Data Fig. 9c. **f**, Synergistic efficiency between BB-94 and R428 on 66 PDOs. **g**, Validation of the synergistic effect between BB-94 and R428 on the organoid-derived xenograft model. The PDO with a notably synergistic effect was chosen on the basis of the result shown in **f**, and inoculated subcutaneously into SCID mice for the drug treatment assay. Data are mean + s.d. of $n = 8$ xenograft tumours per condition. *P* values were calculated using two-tailed paired Student's *t*-tests (**b**) and two-tailed unpaired Student's *t*-tests (**g**).

As expected, R428 treatment alone markedly reduced the proliferation of PDOs in a dose-dependent manner, whereas BB-94 treatment alone exhibited a minimal effect, even at concentrations of up to 100 µM. Notably, when combined, the treatment remarkably enhanced the sensitivity of the majority of PDOs to R428 in the presence of BB-94, with a notable synergistic effect observed in 70% of the PDOs (Fig. 6f). This synergistic effect was further confirmed in vivo using PDO-derived xenograft models, including one with (DAC-71) and one without (DAC-18) observed synergistic response, aligning closely with the in vitro results of PDOs (Fig. 6g and Extended Data Fig. 9g–k). Consistently, the combined administration of R428 and BB-94 significantly reduced tumour growth in an orthotopic mouse model compared with R428 or BB-94 treatment alone (Extended Data Fig. 9l). Moreover, we observed that elevated mRNA expression levels of *MMP1* and *MMP11* correlated positively with stronger synergistic response in PDOs (Extended Data Fig. 9m), consistent with the expected regulation by AXL shedding. The stable knockdown of *MMP1* or *MMP11* significantly enhanced the efficiency of inhibition of cancer cell proliferation in a colony-formation assay (Extended Data Fig. 9n,o). Moreover, blocking AXL shedding (where the AXL signalling pathway was more active) promoted cell migration and induced an epithelial–mesenchymal transition, as indicated by the increased Snail and ZEB1 expression and decreased E-cadherin expression[27] (Extended Data Fig. 9p,q). Collectively, these data demonstrate that sAXL may act as a decoy receptor for GAS6 to attenuate intercellular AXL signalling and potentially regulate PDAC tumour growth and metastasis. Quantifying AXL shedding and GAS6 levels might help to stratify patients who would be expected to receive more therapeutic benefit from an AXL kinase inhibitor treatment.

Discussion

PDAC creates an atypical, highly stromal TME that actively interacts with tumour cells to affect their proliferation, migration and drug resistance[1]. To address the limitation of current proteomic studies of PDAC based on global proteome profiling of bulk tissues or functional proteomic profiling in cultured cell lines, we developed and applied TMEPro—a clinical functional proteomic strategy—to investigate the dynamic intercellular signalling events in the PDAC TME directly from clinical tissue samples. By seamlessly integrating spatially and temporally resolved S–PM functional proteomes through multidimensional bioinformatic analysis, we constructed a comprehensive signalling map mediated by ligand–receptor interactions between cancer cells and stromal cells in the PDAC TME. The functional proteomic resource led to the identification of a reciprocal signalling axis in stromal cells and an additional dimension of intercellular signalling regulation by AXL shedding in cancer cells. Overall, this study provides a comprehensive landscape of the intercellular signalling network between PCCs and stromal cells in PDAC mediated by secreted ligands and PM receptors. We believe that the TMEPro is widely applicable for studying other cancer types, and the proteomic resources are of broad interest to the community, especially when testable biomarkers and clinical vulnerabilities are not identifiable through genomic assessment alone (Supplementary Discussion).

Online content

Any methods, additional references, Nature Portfolio reporting summaries, source data, extended data, supplementary information, acknowledgements, peer review information; details of author contributions and competing interests; and statements of data and code availability are available at https://doi.org/10.1038/s41586-024-08225-y.

1. Ho, W. J., Jaffee, E. M. & Zheng, L. The tumour microenvironment in pancreatic cancer—clinical challenges and opportunities. *Nat. Rev. Clin. Oncol.* **17**, 527–540 (2020).
2. Siegel, R. L., Miller, K. D., Fuchs, H. E. & Jemal, A. Cancer statistics, 2021. *CA Cancer J. Clin.* **71**, 7–33 (2021).
3. Siegel, R. L., Giaquinto, A. N. & Jemal, A. Cancer statistics, 2024. *CA Cancer J. Clin.* **74**, 12–49 (2024).
4. Kleeff, J. et al. Pancreatic cancer. *Nat. Rev. Dis. Primers* **2**, 16022 (2016).
5. Cao, L. et al. Proteogenomic characterization of pancreatic ductal adenocarcinoma. *Cell* **184**, 5031–5052 (2021).
6. Jiang, L. et al. Prospective observational study on biomarkers of response in pancreatic ductal adenocarcinoma. *Nat. Med.* **30**, 749–761 (2024).
7. Hanahan, D. & Weinberg, R. A. Hallmarks of cancer: the next generation. *Cell* **144**, 646–674 (2011).
8. Grünwald, B. T. et al. Spatially confined sub-tumor microenvironments in pancreatic cancer. *Cell* **184**, 5577–5592 (2021).
9. Scott, J. D. & Pawson, T. Cell signaling in space and time: where proteins come together and when they're apart. *Science* **326**, 1220–1224 (2009).
10. Uhlén, M. et al. Tissue-based map of the human proteome. *Science* **347**, 1260419 (2015).
11. Hunter, T. Tyrosine phosphorylation: thirty years and counting. *Curr. Opin. Cell Biol.* **21**, 140–146 (2009).
12. Huang, P., Gao, W., Fu, C. & Tian, R. Functional and clinical proteomic exploration of pancreatic cancer. *Mol. Cell. Proteom.* **22**, 100575 (2023).
13. Tape, C. J. et al. Oncogenic KRAS regulates tumor cell signaling via stromal reciprocation. *Cell* **165**, 910–920 (2016).
14. Shi, Y. et al. Targeting LIF-mediated paracrine interaction for pancreatic cancer therapy and monitoring. *Nature* **569**, 131–135 (2019).
15. Pan, S., Chen, R., Aebersold, R. & Brentnall, T. A. Mass spectrometry based glycoproteomics—from a proteomics perspective. *Mol. Cell. Proteom.* **10**, R110.003251 (2011).
16. Türei, D. et al. Integrated intra- and intercellular signaling knowledge for multicellular omics analysis. *Mol. Syst. Biol.* **17**, e9923 (2021).
17. Gukovsky, I., Li, N., Todoric, J., Gukovskaya, A. & Karin, M. Inflammation, autophagy, and obesity: common features in the pathogenesis of pancreatitis and pancreatic cancer. *Gastroenterology* **144**, 1199–1209 (2013).
18. Peng, J. et al. Single-cell RNA-seq highlights intra-tumoral heterogeneity and malignant progression in pancreatic ductal adenocarcinoma. *Cell Res.* **29**, 725–738 (2019).
19. DeBerardinis, R. J., Lum, J. J., Hatzivassiliou, G. & Thompson, C. B. The biology of cancer: metabolic reprogramming fuels cell growth and proliferation. *Cell Metab.* **7**, 11–20 (2008).
20. Olive, K. P. et al. Inhibition of Hedgehog signaling enhances delivery of chemotherapy in a mouse model of pancreatic cancer. *Science* **324**, 1457–1461 (2009).
21. Del Rosario, A. M. & White, F. M. Quantifying oncogenic phosphotyrosine signaling networks through systems biology. *Curr. Opin. Genet. Dev.* **20**, 23–30 (2010).
22. Lim, W. A. & Pawson, T. Phosphotyrosine signaling: evolving a new cellular communication system. *Cell* **142**, 661–667 (2010).
23. Merilahti, J. A. M. & Elenius, K. Gamma-secretase-dependent signaling of receptor tyrosine kinases. *Oncogene* **38**, 151–163 (2019).
24. Klein, T., Eckhard, U., Dufour, A., Solis, N. & Overall, C. M. Proteolytic cleavage-mechanisms, function, and "omic" approaches for a near-ubiquitous posttranslational modification. *Chem. Rev.* **118**, 1137–1168 (2018).
25. Graham, D. K., DeRyckere, D., Davies, K. D. & Earp, H. S. The TAM family: phosphatidylserine sensing receptor tyrosine kinases gone awry in cancer. *Nat. Rev. Cancer* **14**, 769–785 (2014).
26. Kariolis, M. S. et al. An engineered Axl 'decoy receptor' effectively silences the Gas6-Axl signaling axis. *Nat. Chem. Biol.* **10**, 977–983 (2014).
27. Nieto, M. A., Huang, R. Y., Jackson, R. A. & Thiery, J. P. EMT: 2016. *Cell* **166**, 21–45 (2016).
28. Chen, W. et al. Simple and integrated spintip-based technology applied for deep proteome profiling. *Anal. Chem.* **88**, 4864–4871 (2016).

Methods

Cell Lines

The sources of human pancreatic cancer cell lines PANC1 (CRL-1469), AsPC1 (CRL-1682), MIA PaCa2 (CRL-1420), KP4 (JCRB0182) and human PSCs were described previously[14]. The human pancreatic cancer cell lines SU.86.86 (CRL-1837) and SW 1990 (CRL-2172), and the human embryonic kidney cell line HER293T were purchased from ATCC. The human PSC line HPaSteC was purchased from ScienCell. Note that PSCs are the precursor cells of PDAC CAFs and transition into the major form of PDAC CAFs after in vitro culture[29]. Cells were cultured according to the supplier's instructions. All the cell lines from ATCC were authenticated by short tandem repeat profiling by ATCC. Other cell lines were not authenticated. Cell lines were tested for mycoplasma contamination every month; the test results were negative.

Mice

The KPC (*Kras*$^{LSL\text{-}G12D/+}$;*Trp53*$^{flox/flox}$;*Pdx1-cre*) mouse model was described previously[14]. NSG mice (aged 5 weeks) were purchased from Shanghai Model Organisms Center. SCID mice (aged 6 weeks) were purchased from Biocytogen Pharmaceuticals. Mice were housed in standard closed plastic cages supplied with bedding, food and water. The specific-pathogen-free room is maintained at a temperature of 20–26 °C, humidity of 40–70% and under a 12 h–12 h light–dark cycle (on from 07:00 to 19:00). All of the animal studies were performed in accordance with the guidelines and regulations, and ethical approval was received from the Institutional Animal Care and Use Committee (IACUC) at Southern University of Science and Technology (experiments using orthotopic mouse models) or from IACUC at Center for Excellence in Molecular Cell Science (experiments using xenograft mouse models).

Human samples

Human pancreatic tissue samples and plasma samples were obtained from Affiliated Tongji Hospital, Tongji Medical College, Huazhong University of Science and Technology, with approval by the Medical Ethics Committee of Tongji Medical Hospital (TJDBPS02). In total, 122 patients were enrolled in this study for collection of frozen tissue samples, including 78 patients with PDAC, 16 patients with other cancer diagnosed with tumour sites close (within 5 cm) to the pancreas and some part of normal pancreas necessarily resected and 28 patients with CP. Plasma samples from 159 patients with PDAC and 154 normal control individuals were collected for measurement of TNFRSF11B, NPTX1, CA19-9, sAXL and GAS6 levels. Tissue and plasma samples were collected from the patients with informed consent. The clinical parameters were summarized in Supplementary Tables 1 and 3, respectively.

Glycoprotein enrichment and on-bead digestion

Protein extraction. Tissue was ground to a powder in liquid nitrogen and lysed by vortex in lysis and labelling buffer containing 1% (v/v) Triton X-100, 2% (w/v) SDS, 200 mM sodium chloride and 100 mM sodium acetate, pH 5.5. The sample was further disrupted by sonication (Scientz JY 96-IIN, Ningbo scientz, 20% energy) on ice for a total of 2 min with cycles of 3 s on and then 3 s off. Tissue debris was removed by centrifugation. Cultured cells were directly lysed in lysis and labelling buffer after washing with PBS, and then sonicated for 30 s with the same setting. The protein concentration was measured using the BCA method. To mitigate the potential variation resulting from the technical challenge in preparing pancreatic tissue samples due to the dense stroma and abundant proteases, 25 ng of bovine fetuin (New England Biolabs) was spiked into 500 μg of lysate as a glycoprotein standard for experimental quality control before glycoprotein enrichment to monitor the entire workflow.

Glycoprotein labelling and enrichment. Glycoproteins were covalently labelled by the hydrazide group of the synthesized biotin-hydrazide probe directly after tissue protein extraction and oxidation, and then enriched by Streptavidin beads (Supplementary information). First, oxidation of glycans on glycoproteins was performed by adding sodium periodate to a final concentration of 2 mM and incubated at 4 °C for 30 min, and the residual sodium periodate was quenched by reacting with 4 mM sodium thiosulfate for 10 min at room temperature. Oxidized glycans were labelled with biotin-hydrazide probe at 2 mM final concentration at room temperature for 30 min. Excess probe was removed by methanol and chloroform precipitation. Protein pellets were redissolved in lysis buffer containing 8 M urea and 100 mM Tris-HCl, pH 7.8, followed by protein reduction with 10 mM dithiothreitol (DTT) at 50 °C for 20 min, and alkylation with 30 mM iodoacetamide (IAA) at room temperature for 30 min. The urea concentration was diluted to 2 M before pull-down of labelled proteins by 25 μl of Streptavidin beads at room temperature for 1 h with gentle rotation.

On-bead digestion. The Streptavidin beads were washed three times with 6 M urea buffer containing 0.1% (v/w) SDS and 100 mM Tris-HCl, pH 7.8, once with 1 M NaCl, once with 80% (v/v) acetonitrile (ACN) in 50 mM ammonium bicarbonate (ABC), and finally twice with 50 mM ABC. Under this harsh washing condition, only a few dozen proteins were non-specifically absorbed onto the Streptavidin beads, accounting for less than 1% of totally identified proteins (Extended Data Fig. 1f). First, protein digestion was performed at 37 °C overnight in 50 μl of 50 mM ABC containing 1 μg trypsin. After digestion, non-glycopeptides were collected. The beads were washed as described above except that 6 M urea was removed from the first wash buffer. Glycopeptides were released by treatment with 250 U of PNGase F (New England Biolabs) in 30 μl of 50 mM ABC and incubation at 37 °C for 1 h. Glycopeptides and non-glycopeptides obtained from cell lines and mouse tissues were desalted on C18 StageTip as described elsewhere[30]. The non-glycopeptides from human tissue samples were loaded onto the C18 StageTip, desalted and fractionated into five fractions by sequential elution with ACN serial dilutions (3%, 6%, 9%, 15% and 80% (v/v)) in 5 mM ammonium formate, pH 10. The collected eluents were dried using Speed-Vac and stored at −20 °C before nano-liquid chromatography (nano-LC)–MS/MS analysis.

Immunohistochemistry-guided LCM and sample preparation by SISPROT

For spatially resolved proteome analysis, 13 frozen tumour tissues as indicated in Supplementary Table 1 were embedded in OCT medium (Sakura Finetek) and sliced on a CM 1900 Cryostat platform (Leica). Immunohistochemistry (IHC) staining was performed as previously described[31]. In brief, frozen sections (thickness, 8 μm) were fixed in formaldehyde (4% in water, w/v) and incubated with hydrogen peroxide (3% in water, w/v) for 15 min. The sections were then blocked with 10% (v/v) goat serum (Boster Biological Technology) before incubation with KRT19 (a marker of epithelial cells, and commonly used target to stain cancer cells) or PDGFRB (a marker of CAFs) primary antibody (KRT19, Abcam, 1:1,000; PDGERB, Cell Signaling Technology, 1:1,000) for 1 h at 37 °C. After washing with PBS, the sections were incubated with HRP-conjugated goat anti-rabbit IgG for 30 min at room temperature, and signals were detected using the Dako REAL EnVision Detection kit. Finally, nuclei were visualized by haematoxylin staining. LCM was performed using the LMD7000 system (Leica) using frozen sections adjacent to IHC staining sections. Tissue sections (15 μm thickness) stuck to PEN-membrane coated slides (Leica) were moderately stained by haematoxylin and dehydrated through a graded series of ethanol solutions. LCM of PCC and stromal regions was guided by the IHC staining images targeting KRT19 and PDGFRB, respectively, with a sum area of 10 mm^2.

Proteins were extracted and reduced from LCM samples by heating at 95 °C for 10 min in lysis buffer containing 600 mM guanidine HCl, 1% (w/v) *n*-dodecyl β-D-maltoside, 150 mM NaCl, 15 mM TCEP and 10 mM

HEPES, pH 7.4, then sonicated for 20 min in a water bath sonicator (AutoScience). Proteins were digested using the SISPROT technology, with slight modifications[28,31,32]. In brief, the sample pH was adjusted to around 3 before loading into the SISPROT spintip fabricated by packing C18 plugs and then a strong cation exchange resin into a 200 µl pipette tip. The spintips were washed with 80% (v/v) ACN buffered by 8 mM potassium citrate, pH 3, and then with water. Proteins were digested and alkylated by 1 µg trypsin in 50 mM ABC containing 10 mM IAA. After digestion, peptides were eluted onto the C18 plugs and then desalted and fractionated into five fractions as described above.

CM preparation for secretome profiling

Cells cultured in 6-well plates at approximately 80% confluence were washed three times with PBS and starved in culture medium without fetal bovine serum (FBS) for 24–36 h. CM was centrifuged and then filtered through a 0.22 µm syringe filter unit (Millipore) to remove any cell debris. CM was centrifuged in a 3 kDa cut-off filter (Millipore), and the medium was exchanged to PBS in the same filter, and then dried using a Speed-Vac. For western blot analysis, proteins were redissolved in western blot loading buffer and boiled at 100 °C for 5 min. For secretome profiling, proteins were redissolved in 8 M urea lysis buffer containing 50 mM ABC, reduced, alkylated and then digested overnight with trypsin after the urea concentration was diluted to 1 M with 50 mM ABC. Peptides were desalted using HLB cartridges (Waters, 10 mg sorbent) before nano-LC–MS/MS analysis.

Enrichment of pTyr peptides

Tissue and cell line protein extractions were performed as described in the 'Glycoprotein enrichment and on-bead digestion' section, except that the lysis buffer, contained 1% (v/v) Triton X-100, 8 M urea, 50 mM Tris-HCl (pH 8.5), protease and phosphatase inhibitor cocktails. Then, 2 mg of protein was reduced, alkylated and then precipitated by methanol and chloroform. The protein pellet was resolved in 8 M urea buffer containing 50 mM ABC, and the urea concentration was diluted to 1 M before overnight trypsin digestion. Peptides were desalted using C18 cartridges (50 mg sorbent) and dried using the Speed-Vac.

pTyr enrichment related to Fig. 4 and Extended Data Fig. 9d was performed as described previously[33,34]. In brief, his-tagged Src homology 2 (SH2) superbinder was expressed in *E. coli* BL21 and purified using Ni beads (GE Healthcare). The peptide samples were redissolved in immunoaffinity purification (IAP) buffer (10 mM Na_2HPO_4, 50 mM Tris-HCl and 50 mM NaCl, pH 7.8) and incubated overnight with Src SH2 superbinder-conjugated Ni beads at 4 °C under gentle rotation. The beads were washed three times with IAP buffer, and pTyr peptides were eluted by 500 mM imidazole in PBS. The samples were desalted using C18 cartridges (50 mg sorbent) and eluted by immobilized titanium ion-affinity chromatography (Ti^{4+}-IMAC) loading buffer (6% (v/v) TFA, 80% (v/v) ACN) and further purified by Ti^{4+}-IMAC beads in a spintip-based manner as previously described[35]. In brief, one plug of C8 SPE disk (3M, Empore) was packed into the bottom of a 200 µl pipette tip as a sieve, and 4 mg Ti^{4+}-IMAC beads were loaded into the tip. After equilibrating with Ti^{4+}-IMAC loading buffer, peptides were loaded onto the spintip under mild centrifugation. The spintip was washed twice with buffer containing 6% (v/v) TFA, 50% (v/v) ACN and 200 mM NaCl, and twice with buffer containing 0.1% (v/v) TFA and 50% (v/v) ACN. The enriched pTyr peptides were eluted by 10% (v/v) $NH_3{\cdot}H_2O$ and 50% (v/v) ACN. The two eluants were combined, desalted and stored at −20 °C before nano-LC–MS/MS analysis.

pTyr profiling related to Fig. 4e was done as described previously[14,36]. In brief, hPSCs were incubated with CM from PANC1 ($n = 2$) or MIA PaCa2 ($n = 2$) cells for 5 min at 37 °C before lysis in 1% (v/v) Nonidet P-40, 0.1% (w/v) sodium deoxycholate, 150 mM NaCl, 1 mM sodium orthovanadate, 50 mM Tris·HCl, pH 7.4, protease and phosphatase inhibitor cocktails. Cell lysate was reduced with DTT, alkylated with IAA and digested to peptides with trypsin. Peptides from replicate experiments were labelled with light and heavy dimethyl while pTyr peptides from non-stimulated PSCs were labelled with medium dimethyl as control, and differently labelled peptides were equally mixed and desalted. For pTyr peptide enrichment, mixed peptides were dissolved in 0.3% (v/v) Nonidet P-40, 100 mM NaCl, 100 mM Tris·HCl, pH 7.4, and then enriched by anti-phosphotyrosine antibody 4G10-conjugated beads (Merck, 16-199).

Enrichment of pTyr-mediated protein complexes

The Photo-pTyr scaffold approach was used to enrich pTyr-mediated protein complexes as described previously[34]. In brief, Src SH2 superbinder protein was conjugated to the NHS group of a custom-synthesized trifunctional probe TM2 (containing a biotin and a benzophenone photoreactive group) to assemble the Photo-pTyr scaffold. Tissue homogenization was performed as described above in a Nonidet P-40 buffer containing 1% (v/v) Nonidet P-40, 150 mM NaCl, 50 mM Tris-HCl pH 7.4, and phosphatase and protease inhibitors. A total of 1.5 mg proteins was incubated with 50 µg Photo-pTyr scaffold for 2 h at 4 °C with gentle rotation. Cross-linking was performed by ultraviolet irradiation in a quartz colorimetric cuvette on ice for 30 min using a CL-1000L UV Crosslinker (UVP). The labelled proteins were then pulled down by 30 µl of Streptavidin beads, followed by a harsh wash using a modified RIPA buffer containing 1% (w/v) SDS, 1% (v/v) Triton X-100, 1% (w/v) sodium deoxycholate, 1 M NaCl and 50 mM Tris-HCl, pH 7.4. After reduction and alkylation, proteins were on-bead digested with trypsin at 37 °C for 16 h. The peptides were collected, desalted and stored at −20 °C for nano-LC–MS/MS analysis.

Nano-LC–MS/MS analysis

Glycoproteome profiling of human tissue samples was performed on the Orbitrap Fusion mass spectrometer (Thermo Fisher Scientific) coupled with an Easy-nLC 1000 liquid chromatography system (Thermo Fisher Scientific). Peptides were dissolved in mobile phase A (0.1% (v/v) formic acid in water) and separated by a home-made 100 µm inner diameter capillary tip column packed with 20 cm of 1.9 µm/120 Å C18 resin (Dr Maisch). Using a 250 nl min^{-1} flow rate, the effective linear gradient went from 7% mobile phase B (0.1% (v/v) formic acid in ACN) to 22% over 100 min, and then linearly increased to 35% over 20 min. Full MS spectra (m/z of 350–1,550) were acquired in the Orbitrap analyzer using resolution of 120,000 (at m/z 200), an AGC target of 2×10^5 and a maximum injection time (MIT) of 100 ms. MS/MS scans were performed in data-dependent mode with a cycle time of 3 s for precursor selection, followed by quadrupole isolation through a 1.6 Da window. Precursors were fragmented by high-energy collisional dissociation (HCD) using normalized collision energy (NCE) of 30%. Spectra of product ions were acquired in the ion-trap mass analyzer using rapid scan rate, an AGC target of 1×10^4 and an MIT of 40 ms. The dynamic exclusion time was 30 s for m/z of scanned precursors.

Nano-LC–MS/MS analysis of other samples was performed on the Q Exactive HF-X mass spectrometer coupled with the Easy-nLC 1200 liquid chromatograph system (Thermo Fisher Scientific). The analytical column was the same as described above. The effective gradient increased linearly from 8% mobile phase B (0.1% (v/v) formic acid in 90% (v/v) ACN) to 25% over 50 min (LCM samples and phosphopeptides) or over 100 min (cell line, mouse and Photo-pTyr-scaffold samples), and then increased to 40% over 10 min or 20 min, respectively, at a constant flow rate of 250 nl min^{-1}. Full MS scans covering m/z of 350–1,550 were acquired using an Orbitrap resolution of 120,000, an AGC target of 3×10^6 and an MIT of 60 ms. The top 50 (15 for phosphopeptides) most abundant precursors from each full MS1 scan were selected and isolated through a 1.2 Da window (0.7 Da for phosphopeptides), and fragmented by HCD at NCE of 27% (32% for phosphopeptides). MS/MS spectra were scanned with a resolution of 7,500 (45,000 for phosphopeptides), an AGC target of 1×10^5 and an MIT of 25 ms (86 ms for phosphopeptides). Nano-LC–MS/MS analysis of dimethyl-labelled pTyr

peptides was performed on the LTQ-Orbitrap Elite mass spectrometer system as described previously[14].

PRM-MS assay

Absolute quantification of AXL and GAS6 in PCC and stromal regions of 50 tumour tissues was performed by PRM using stable-isotope-labelled heavy peptides as internal standards. PCC and stromal regions were collected from frozen tumour tissue sections (thickness, 15 µm) by LCM with collected area of 20 mm^2. Glycoproteins were enriched using the FISGlyco method[37]. Non-glycopeptides were released from the FISGlyco device by trypsin digestion. Stable-isotope-labelled heavy peptides (600 attomoles per peptide) were spiked into each sample, and one third of each sample was injected for absolute quantification by PRM[38].

PRM-MS assays were performed on the Orbitrap Exploris 480 mass spectrometer (Thermo Fisher Scientific) coupled with an UltiMate 3000 RSLCnano chromatography system (Thermo Fisher Scientific). Peptides were separated using a custom-made analytical column as described above at flow rate of 500 nl min^{-1}. The effective gradient linearly increased from 8% solvent B (0.1% (v/v) formic acid in 80% (v/v) ACN) to 28% over 50 min, and then linearly increased to 42% over 10 min. MS spectra were acquired using 445.12 as the internal mass calibration. The full MS scans (m/z of 400 to 900) were acquired at an Orbitrap resolution of 120,000, normalized AGC target of 3×10^6 and MIT of 50 ms. Targeted peptides were scheduled within a ±2 min window of the retention time detected by heavy peptides. Precursors were isolated through a 1 Da window, and fragmented by HCD at NCE of 30%. The fragment ions were scanned at Orbitrap resolution of 45,000, AGC target of 1×10^6 and MIT of 150 ms.

MS data processing

MS database searching. Raw files were searched against the UniProt human proteome database (version 2019-06-22, 74,416 entries), an in-house generated human PM protein database with sequences divided into ECDs and ICDs, or a mouse proteome database (version 2017-02-12, 50,306 entries) using MaxQuant software (v.1.5.5.1). Carbamidomethylation of cysteine was set as static modification. Deamidation (N/Q) and oxidation (M) were set as dynamic modifications for all datasets, and phospho-S/T/Y was also added as a dynamic modification for the pTyr peptide enrichment dataset. Two missed cleavages were permitted. Label-free quantification was enabled for global normalization. Match between runs was selected to reduce missing values. The raw files of dimethyl-labelling-based pTyr quantification were analysed using MaxQuant software (v.1.1.1.36) for database searching targeting the IPI human database (v.3.79) containing 91,464 entries, with phospho-S/T/Y set as variable modification. A minimum ratio count of 2 was required for protein quantification of dimethyl-labelled pTyr peptides. Unless specified otherwise, at least two unique peptides identified across all samples were required for protein/domain identification in each dataset of this study.

Database generation. Generation of S–PM protein databases. The human PM protein database containing 2,829 PM proteins was referenced from reported work[39]. The transmembrane domains were confirmed by TMHMM (v.2.0)[40] and the UniProtKB/Swiss-Prot database (version 2018_01). A secreted protein database was generated according to the following steps. First, canonical secreted proteins were screened out from three available online sources: proteins containing signal peptides in UniProtKB/Swiss-Prot database, proteins containing signal peptides predicted by SignalP (v.4.1)[41] or predicted by Phobius[42]. Then, proteins included in at least two sources were kept in the database. Finally, proteins included in the PM protein database were removed, generating the final secreted protein database with 2,534 secreted proteins.

Generation of cancer biomarker database. The cancer biomarkers were selected from an initial pool of over a hundred scientific articles. After a stringent curation process focusing on the credibility of the journals and the relevance of the content, we narrowed down to approximately 50 high-quality studies. From these selected studies, we curated a list of 65 reported pancreatic cancer markers, comprising 52 S–PM proteins. Among them, 48 S–PM proteins were identified in our dataset, with 31 showing significant differences between pancreatic cancer tissues and normal counterparts. The PubMed article IDs of the literature sources for the markers are annotated in Supplementary Table 1.

Generation of ligand–receptor database. The ligand–receptor pair database was established as previously described with minor modifications[43]. First, reported ligand–receptor pairs were downloaded from the following databases: DLRP[44], IUPHAR[45] and HPMR[46] on 30 August 2018, 29 May 2018 and 28 May 2018, respectively. By combining the three databases, 1,179 ligand–receptor pairs were obtained. Then, in silico ligand–receptor pairs were generated between putative ligands and putative receptors of our S–PM databases on the basis of experimentally validated protein–protein interactions (PPIs) in HPRD[47] and STRING (v.10.5)[48]. From HPRD, we obtained binary PPIs evidenced by one of the three sources (in vivo, in vitro and yeast 2-hybrid). From STRING, we obtained PPIs based on physical-binding interactions in *Homo sapiens* with confidence score ≥ 700, and experimentally supported interactions with confidence score ≥700. Moreover, the pair database was extended by PPIs in the OmniPath database[16]. Finally, by integrating these six online available databases and references, we built up an in-house ligand–receptor database containing 788 ligands, 766 receptors and 3,919 pairs.

Generation of pTyr writer, reader and eraser databases. pTyr writer, reader and eraser databases were generated from references, including 98 pTyr writers[49,50]; 157 pTyr readers, of which 112 contain an SH2 domain[9,51] and 53 contain a PTB domain[52,53]; and 108 pTyr erasers[54,55].

Identification of *N*-glycosites and phosphosites. *N*-glycosites were determined with canonical sequence motifs N-!P-S/T or N-X-C, whereas N is deamidated asparagine, !P represents any amino acid except proline and X represents any amino acid[56]. Under these criteria, 6,181 *N*-glycosites were identified from 100 tissue samples, in which 98.7% were class I sites with a score difference of higher than 5 and a localization probability of higher than 0.75. A total of 1,360 pTyr sites was identified by pTyr peptide enrichment from 32 tissue samples (Extended Data Fig. 5a) with phosphorylation on tyrosine, in which 90.9% were class I sites satisfying a score difference higher than 5 and localization probability higher than 0.75 (ref. 57).

Identification and quantification of S–PM proteins. The protein group tables generated by non-glycopeptides and glycopeptides were combined, and a total of 2,741 S–PM proteins was identified with at least two unique peptides required for non-glycopeptides and one unique peptide required for glycopeptides. LFQ intensities were $\log_2$-transformed and normalized by using the R package (v.3.38.3). A total of 2,658 S–PM proteins was quantified with at least one value across 100 pancreatic samples. Statistical significance was calculated between tumour and normal samples with $P < 0.05$ and fold change > 2, or normalized ratio of quantified sample count > 2 and at least 5 samples quantified in at least one group. S–PM proteins in the mouse dataset were processed using the same workflow and criteria as human tissue samples. After combining protein group tables generated by non-glycopeptides and glycopeptides, a total of 1,684 S–PM proteins was quantified across all of the mouse samples. Statistical significance was calculated between tumour samples of different ages and NT samples, with $P < 0.05$ and fold change > 2, or normalized ratio of quantified sample count > 2, and at least half of samples quantified in at least one group. Moreover, as approximately one-third of S–PM proteins quantified with intensities were without LFQ intensities in mouse samples, to increase S–PM proteome coverage, those S–PM proteins filtered out due to less quantified samples by LFQ intensities, but met the above criteria for calculating

significance when using raw intensities, were also included in the final list of significantly changed S–PM proteins.

Quantification of spatially resolved and cell-type-specific proteins. For quantification, LFQ intensities were $\log_2$-transformed and normalized by Limma for removing batch effects. The PCC- or stroma-specific proteins were defined according to the statistical criteria as mentioned above. Furthermore, proteins were retained based on at least five samples quantified in at least one group for LCM samples, or at least two replicates quantified in at least one PCC or PSC line for cell line samples. Significant proteins quantified using two strategies were combined for downstream analysis. For contradictory results between tissues and cell lines, tissue quantification results were used for deciding cell type specificity of these proteins.

Quantification of pTyr protein complexes and pTyr peptides. LFQ intensities were $\log_2$-transformed and normalized to the LFQ intensity of the bait protein (SH2 superbinder) in each sample. Statistical significance was calculated between tumour and normal samples with $P < 0.05$ and fold change > 2, or normalized ratio of quantified sample count > 2. Moreover, proteins were retained when satisfying more than 20% (at least three samples) quantified in at least one group for the Photo-pTyr-scaffold dataset and at least five samples quantified in at least one group for pTyr-peptide enrichment dataset.

Identification of shed PM proteins. Shed PM proteins in PDAC tumours were identified using the secretomes and PM proteomes of eight pancreatic cell lines as a training set according to the following cut-offs, as also depicted in Extended Data Fig. 7a. Step 1: calculation of the ECD-to-ICD ratio under three different conditions: (1) full-length PM proteins were quantified in the PM proteome of 8 cell lines: 1,012 ECDs or ICDs were identified from 773 PM proteins. Both ECDs and ICDs were strictly required with at least 2 unique peptides for both replicates of any PM protein. The strict requirement ensured the calculation accuracy of ECD-to-ICD ratio based on unique peptide number for full-length PM proteins. Under this stringent filtering criterion, the Ratio_{PM} of 136 PM proteins were retained. (2) Shed PM proteins were quantified in the secretome (S) of 8 cell lines: 806 ECDs or ICDs were identified from 667 PM proteins. To ensure reproducible quantification of ECDs of PM proteins in the secretome, ECDs were required with at least 2 unique peptides for both replicates of any PM protein. For those shed PM proteins for which an ECD was quantified, but a paired ICD was not identified in the secretome, the missing value of unique peptide number was imputed by 1 for ratio calculation. The Ratio_{S} was calculated for 377 PM proteins that met the cut-off criteria. (3) Entire and shed PM proteins were quantified in tumours: 1,387 ECDs or ICDs were quantified from 1,044 proteins. ECD or ICD were required with at least 2 unique peptides. (4) Real shed proteins were identified in both secretome and PM proteome. This analysis yielded $\text{Ratio}_{\text{S–PM}}$ for 1,088 S–PM proteins.

Step 2: Identification of shed PM proteins through a filtering process that calculates two index values. Given that the lengths of the ECDs and ICDs vary considerably among PM proteins, the index value serves as a parameter for identifying real shed proteins and measuring the degree of shedding. The index value was calculated by normalizing the ratio of ECD/ICD under shedding conditions (such as the secretome of cell lines or S–PM proteome of tissue samples) to that ratio under full-length condition (PM proteome of cell lines). The above calculation method can exclude a large number of false-positive shedding proteins, and screen out more credible shedding proteins. (1) Real shed proteins in the cell line dataset are those PM proteins that meet the cut-off criteria for both the PM proteome and the secretome. ECD/ICD ratios of 107 PM proteins were both quantified in secretome and PM proteome. To determine real shed proteins in the secretome but not contamination by full-length PM proteins from cell debris, the shedding levels in the secretome were re-evaluated by normalizing the ratio of ECD/ICD in the secretome to that in the PM proteome of each cell line, generating the value named $\text{Index}_{\text{training}}$. The larger value of $\text{Index}_{\text{training}}$, the higher shedding level of PM protein. In total, 45 shed PM proteins were identified with $\text{Index}_{\text{training}} \geqq 2$ in at least 2 cell lines. (2) The shedding levels of PM proteins in tumours were also re-evaluated using the same criteria, generating the value named $\text{Index}_{\text{test}}$. Collectively, 22 out of the 45 shed PM proteins in the secretome were identified with $\text{Index}_{\text{test}} \geqq 2$ in at least 6 tumours and were defined as shed PM proteins in tumour.

PRM quantification. Extraction of peptide transition peak areas from PRM raw files were performed using Skyline (v.20.2.0.286). Data satisfying the following criteria were accepted for further analysis: the same retention time for endogenous light peptide and stable isotope-labelled heavy peptide; variation of retention time across all samples within ±2 min; and mass difference within ±5 ppm. The peak area of each peptide was calculated by summing the peak area of all its transitions manually checked with clear peaks. The absolute amount of light peptide was calculated by dividing the peak area of light peptide to that of its corresponding heavy peptide, and then by multiplying the absolute amount of heavy peptide. The absolute amount of light peptide per square millimetre of tissue section was calculated by dividing by 20 and multiplying by 3, as 20 mm^2 of the tissue section was processed, and one-third of the sample was injected for nano-LC–MS/MS analysis. For protein quantified by two peptides, averages were calculated to represent the protein/domain level.

Bioinformatics and statistical analysis

Except where otherwise stated, bioinformatics and statistical analyses were performed using R (v.3.6.1). R packages for data visualization and plotting included: ggplot2 (v.3.3.5), ggpubr (v.0.4.0), pheatmap (v.1.0.12), igraph (v.1.2.6), RColorBrewer (v.1.1-2), reshape2 (v.1.4.4), ggrepel (v.0.9.1), circlize (v.0.4.12), dplyr (v.1.0.5), networkD3 (v.0.4), voronoiTreemap (v.0.2.1) and cytoscape software (v.3.8.2). Correlation coefficients of $\log_2$-transformed LFQ intensities between biological replicates were determined by the Pearson correlation. Cell type deconvolution of tumour samples was performed using our bulk tumour S–PM proteome and published single-cell RNA-sequencing dataset of PDAC[18], and the deconvolution method CIBERSORTx[58]. Gene Ontology enrichments were computed using the enrichGO function of the R package clusterProfiler (v.3.10.1). Module connectivity was computed using the Jaccard index with a threshold of more than 0.08. Protein entry was mapped by annotation R package org.Hs.eg.db (v.3.7.0). The tumour-progression-related S–PM proteins in the time-resolved proteomic dataset were clustered using the fuzzy *c*-means method from R package Mfuzz (v.2.50.0), which calculates membership values for quantification data based on existing cluster centroids and the fuzzification parameter[59]. The membership value ranges from 0 (indicating no association) to 1 (indicating full association). Each cluster is designated by the function of prominent members. Proteins with a membership score of higher than 0.45 were defined as tumour-progression-related proteins, including MSLN and ITIH3, two important PDAC markers[60,61]. The pathway enrichment of ligands, receptors and pTyr-mediated complexes was analysed using the STRING web-based platform (interaction sources including databases and experiments with interaction score ≥ 0.4).

siRNA knockdown

siRNAs targeting the mRNAs of 8 genes (*PDGFRA*, *PDGFRB*, *PTPN11*, *FOS*, *MMP1*, *MMP9*, *MMP11* and *MMP15*) were self-designed (Supplementary Tables 5 and 6), chemically synthesized (RiboBio) and then transfected into target cells using the Lipofectamine RNAiMax kit according to the supplier's instructions.

RT–qPCR analysis

Total RNA was extracted using the TRIzol reagent as indicated in the kit's instructions. The first-strand cDNA was synthesized using the

High-Capacity cDNA Reverse Transcription Kit. The mRNA levels of targeted genes were quantified by quantitative PCR with reverse transcription (RT–qPCR) using the TB Green Premix Ex Taq II reagent (Takara) on the CFX96 system (Bio-Rad). The sequences of primers for RT–qPCR are summarized in Supplementary Table 6. Data were analysed using GraphPad Prism (v.7.0). The $2^{-\Delta\Delta C_t}$ method was used to calculate mRNA levels of targeted genes. Actin was used as an internal control for normalization.

Western blots

For validation of PDGFR signalling, PDGFB was chosen instead of PDGFC for cell stimulation because the PDGF-BB (Peprotech, 100-14B) homodimer can activate both homodimers or heterodimers of PDGFRA and PDGFRB, while PDGF-CC cannot activate the PDGFRB homodimer[62]. Cells or lyophilized CM were lysed in RIPA buffer containing 1% (w/v) SDS, 1% (v/v) Triton X-100, 1% (w/v) sodium deoxycholate, 1 M NaCl, 50 mM Tris-HCl, pH 7.4, and protease and phosphatase inhibitor cocktail, and sonicated to further disrupt cells. Lysates were centrifuged, and the protein concentration was measured using the BCA method. Sample loading buffer containing 10 mM DTT was added to protein extracts and heated at 95 °C for 5 min. Proteins were separated through a 10% SDS–PAGE gel and transferred onto PVDF membranes. The membranes were blocked with 5% (w/v) non-fat milk resolved in TBS containing 0.1% Tween-20 (TBST) for 1 h at room temperature, followed by incubation with primary antibodies at 4 °C overnight. The primary antibodies against the following proteins were used: β-actin (Cell Signaling Technology, 3700S, 1:5,000), PDGFRA (Cell Signaling Technology, 3174S, 1:1,000), phospho-PDGFRA-Y742 (Abcam, ab5452, 1:1,000), AXL-ectodomain (Abcam, ab219651, 1:1,000), PDGFRB (Cell Signaling Technology, 3169S, 1:1,000), PTPN11 (Abcam, ab32083, 1:2,000), phospho-PTPN11-Y542 (Abcam, ab62322, 1:5,000), AKT (Cell Signaling Technology, 4685S, 1:2,000), phospho-AKT-S473 (Cell Signaling Technology, 4060S, 1:2,000), ERK (Cell Signaling Technology, 4695S, 1:2,000), phospho-ERK-T202/Y204 (Cell Signaling Technology, 4370S, 1:2,000), E-cadherin (Cell Signaling Technology, 3195, 1:1,000), N-cadherin (Cell Signaling Technology, 13116, 1:1,000), Snail (Cell Signaling Technology, 3879, 1:1,000) and ZEB1 (Cell Signaling Technology, 3396, 1:1,000). After washing three times with TBST, the membranes were incubated with HRP-conjugated goat anti-rabbit IgG (Beyotime, A0208, 1:2,000) or goat anti-mouse IgG (Beyotime, A0216, 1:2,000) at room temperature for 1 h. After washing three times with TBST, Clarity Western ECL substrate (Bio-Rad, 1705061) was added to the membranes, and the signal was detected using a Tanon 6100C gel imaging system.

Chromatin immunoprecipitation assay

Binding of FOS to the *LIF* promoter region after PDGFB stimulation was tested using the SimpleChIP enzymatic chromatin IP kit (Cell Signaling Technology, 9003S) according to the kit's instructions, with minor modifications as previously described[63]. In brief, PANC1 cells were stimulated with 100 ng ml^{-1} PDGF-BB (Peprotech, 100-14B) in culture medium for 24 h. Control cells were cultured in normal medium without PDGF-BB. Cells were fixed with 1% (w/v) formaldehyde for 10 min at room temperature, and cross-linking was quenched by the 10× glycine buffer. Cells were lysed in lysis buffer, and then digested with micrococcal nuclease. After sonication and centrifugation, the supernatant was collected and incubated overnight with anti-FOS antibody (Cell Signaling Technology, 2250) or IgG as a negative control. The DNA fragment–antibody complexes were pulled-down by incubating with protein-G-conjugated magnetic beads for 2 h. The beads were thoroughly washed, immunocomplexes were eluted and cross-linking was reversed by adding 5 M NaCl, proteinase K and incubating at 65 °C for 2 h. DNA was purified using spin columns and four LIF promoter sequence regions were detected by PCR using primers described previously[64].

Promoter luciferase assay

The LIF promoter luciferase reporter plasmid, pRL-TK *Renilla* luciferase plasmid and pGL4.1-basic empty vector were provided by J. Chen. The transfection efficiency was measured using the pRL-TK *Renilla* luciferase plasmid as the internal standard. Cells at a density of around 1×10^5 cells per well in 24-well plates were co-transfected with 0.05 μg pRL-TK and 500 ng luciferase reporter plasmid or an empty vector using the lipo3000 transfection kit (Thermo Fisher Scientific, L3000001). Cells with or without PDGF-BB (Peprotech, 100-14B) stimulation were collected and *LIF* promoter luciferase activity was measured using the dual-luciferase reporter assay kit (Promega, E1910) using *Renilla* luciferase activity as internal standard for normalization. Signal was detected on a SpectraMax i3x multi-mode microplate reader (Molecular Devices).

Luminex and Simoa ELISA assay

Plasma levels of TNFRSF11B, NPTX1, CA19-9, sAXL and GAS6 were measured using the commercial Luminex ELISA assay from Merck or R&D Systems, respectively, according to the manufacturer's instructions. The main steps include adding of protein standard or samples to a 96-well plate, incubating with magnetic beads coated with capture antibodies, incubating with biotinylated detection antibodies, incubating with substrate-conjugated Streptavidin and finally the signal was read using the Luminex MAGPIX System. The LIF protein level in CM was measured by single-molecule array (Simoa) ELISA as described previously[14]. HPaSteCs cells were treated with inhibitors targeting PDGFRB (Crenolanib, Selleck, S2730), PTPN11 (SHP099, Selleck, S6388), JAK1/2 (Ruxolitinib, MedChemExpress, HY-50856), MEKs (mirdametinib, MedChemExpress, HY-10254), ERKs (ravoxertinib, MedChemExpress, HY-15947), or PI3K (LY294002, MedChemExpress, HY-10108), respectively, before CM was collected. The Simoa ELISA assay was developed using a Simoa homebrew assay starter kit (Quanterix, 101351). In brief, a homemade LIF antibody was used as capture antibody and conjugated to magnetic beads, while a commercial anti-LIF (R&D Systems, AF-250-NA) was used as the detection antibody and biotinylated with an NHS-PEG_4-biotin probe. LIF standard (Symansis, 3014D) or CM was first incubated with capture beads in a 96-well plate. After washing to remove non-specific proteins, biotinylated detection antibody was added for incubation. Finally, SBG substrate was added and signal was read on the Quanterix SR-X machine.

Multiplex TSA staining

Multiplex TSA staining was performed according to the supplier's instructions. In brief, FFPE tissues were sliced at 4 μm thickness and stuck onto glass slides. Tissue sections were deparaffinized by xylene and rehydrated through ethanol gradients. For antigen retrieval, the sections were boiled in 10 mM sodium citrate buffer, pH 6.0, or citrate-EDTA buffer (10 mM citric acid, 1 mM EDTA, pH 8) for 3 min in a pressure cooker (step 1). After cooling down, the tissue sections were incubated with hydrogen peroxide (3% in water, w/v) for 20 min to inactivate endogenous peroxidase (step 2). The sections were then blocked with 10% (v/v) goat serum before incubating with primary antibodies for 2 h at room temperature (step 3). The following primary antibodies against the indicated proteins were used for TSA staining: KRT19 (Abcam, ab52625, 1:1,000), PDGERB (Cell Signaling Technology, 3169S, 1:1,000), TRPV4 (Abcam, ab191580, 1:500), SLC1A3 (Abcam, ab416, 1:200), PKD1 (Abcam, ab74115, 1:200), TMPRSS4 (Abcam, ab150595, 1:200), CDON (Abcam, ab227056, 1:200) and LRIG2 (Abcam, ab157492, 1:100). The sections were incubated with HRP-conjugated secondary antibody for 1 h at room temperature (step 4). TSA fluorophore labelling was performed by adding Fluor NEON-TSA reagent (step 5). TBST washing was performed following each step. Next, steps 1 to 5 were repeated until all of the target proteins from the concerning panel were labelled with different fluorophore dyes. DAPI was used to stain

genomic DNA. Colocalization analysis between targeted proteins and KRT19 or PDGFRB was performed using Colocalization Finder plugin (v.1.8) in FIJI to calculate their Pearson's correlation coefficients[65].

Lentiviral shRNA cloning, production and infection

To generate MIA PaCa2 cell lines with stable knockdown of *MMP1* and *MMP11*, two pairs of shRNAs were synthesized for each protease. The shRNA sequences are summarized in Supplementary Table 6. The related oligonucleotides were cloned into pLKO.1, and then the acquired plasmid was co-transfected into HEK293T cells with lentiviral packaging plasmids psPAX2 and pMD2.G for lentivirus production. After infection, MIA PaCa2 cells were selected with 5 μg ml^{-1} puromycin in culture medium.

Colony-formation assay

MIA PaCa2 cells with stable knockdown of *MMP1* or *MMP11* were seeded as 500 cells per well and cultured in DMEM medium containing 10% (v/v) FBS with DMSO or 1.5 μM R428. After 14 days, cell colonies were washed with 1× PBS, fixed with 4% (v/v) paraformaldehyde for 30 min and washed once again with PBS; then, 1 ml 0.1% (v/v) crystal violet staining solution was added to each well and stained for 20–30 min. Finally, the cells were washed once more with PBS and air-dried for imaging. The cells were then eluted in 500 μl 10% acetic acid (v/v) for 10 min, and the absorbance was measured at 570 nm. In a single experiment, assays were conducted in triplicate and then as three independent experiments.

Cell migration assay

The cell migration assay was performed using Transwell chambers with 8 μm pores (Falcon) and a 24-well plate as the lower chamber. A cell suspension containing 1×10^5 MIA PaCa2 cells per ml in serum-free medium was added to the upper chamber and then placed in the lower chamber containing serum-free CM collected from MIA PaCa2 cells under different treatments. MIA PaCa2 cells were incubated for 48 h at 37 °C in cell incubator supplied with 5% CO_2. After incubation, cells remaining on the top surface of the upper chambers were removed. Migrated cells were fixed with methanol, stained with crystal violet (Sigma-Aldrich) and photographed using a light microscope at ×100 magnification.

Immunohistochemistry

Immunohistochemistry staining of organoids and organoid-related tumour tissues was performed as described in our previous study[66]. The following primary antibodies were used: anti-KRT19 (Cell Signaling Technology, 12434, 1:500), anti-SOX9 (Cell Signaling Technology, 82630, 1:500), anti-Ki-67 (Abcam, ab16667, 1:500).

Drug treatment assay on organoids

The patients cohort and organoid culture were described previously[66]. For the drug treatment assay, the organoids were digested with Tryp-LE (Gibco), which was subsequently inactivated with 1640 basic medium containing 10% (v/v) FBS. The cells were washed with PBS and then resuspended in medium and dispensed into 384-well plates (3,000 cells per well). Then, R428 and BB-94 with six different concentration gradients (R428, 20 μM, twofold dilution; BB-94, 200 μM, eightfold dilution) were added the next day using the Mosquito workstation. After 5 days of drug treatment, cell viability was detected by adding 25 μl of CellCounting-Lite 2.0 (Vazyme), gently shaking for 10 min at room temperature before luminescence signal detection using the Envision plate reader. The average inhibition rates were calculated from two independent experiments. The viability was set to 100 if it was higher than the baseline, and each drug concentration (μM) was $\log_{10}$-transformed. The AUC was calculated using the sintegral function in R, and the normalized AUC was obtained by dividing one AUC by the maximum AUC for each drug. To detect synergistic effect, observed combination responses were compared to expected combination responses. For the latter, we used Bliss independence of the response to BB-94 and R428 alone. Conceptually, every point on the Bliss dose response curve is defined as the product between the BB-94 viability and the corresponding point on the R428 dose response curve[67]. Shifts in potency (ΔAUC) were calculated as the difference between the observed combination response and the expected Bliss (ΔAUC = Bliss AUC − combination AUC). ΔAUC > 0 represents synergy.

Animal studies

For generation and drug treatment of the orthotopic model, primary murine tumour cells (KPCP) were isolated from tumours of 7–9-week-old KPC mice as reported previously[68], and an orthotopic PDAC model was constructed using NSG mice aged 6–7 weeks and weighing 20–25 g. A mixture of 1×10^5 KPCP cells in 50 μl of PBS was implanted into the pancreata. Then, 7 days after implantation, two mice were randomly euthanized and dissected to confirm tumour formation and the mice were allowed to establish for 7 days before beginning treatment. The mice were randomized to four groups, and treated with delivery vehicle (5% (v/v) DMSO, 40% (v/v) PEG300 and 5% (v/v) Tween-80 in water), BB-94 (30 mg kg^{-1}, intraperitoneal), R428 (30 mg kg^{-1}, oral) or combined administration of BB-94 (30 mg kg^{-1}, intraperitoneal) and R428 (30 mg kg^{-1}, oral). After daily administration for 14 days, the mice were euthanized according to IACUC guidelines and tumour wet weights were measured immediately after resection. For generation and drug treatment of the xenograft model, the indicated organoids were subcutaneously inoculated into both flanks of the eight-week-old female SCID mice ($n = 4$ per group, 2×10^6 cells per injection). After the xenografts became palpable (~200 mm^3), mice were randomized to four groups, and treated the same as for the orthotopic model. Tumour sizes were measured every 2 days and the tumour volume was calculated according to the equation V (in mm^3) = 0.5 × length × width (ref. 67). Mice were euthanized according to the experimental protocols or when they met limits designated by our IACUC (10% of body weight and 20 mm in any direction).

Reporting summary

Further information on research design is available in the Nature Portfolio Reporting Summary linked to this article.

Data availability

The MS proteomics data have been deposited to the ProteomeXchange Consortium via the PRIDE[69] partner repository under dataset identifier PXD048644. The UniProt human and mouse proteome databases are available online (https://www.uniprot.org/). All other data supporting the findings of this study are available within the Article and its Supplementary Information. Source data are provided with this paper.

Code availability

No new algorithms were developed for this Article. Scripts to reproduce the figures are available from the corresponding authors on reasonable request.

29. Erkan, M. et al. StellaTUM: current consensus and discussion on pancreatic stellate cell research. *Gut* **61**, 172–178 (2012).
30. Rappsilber, J., Mann, M. & Ishihama, Y. Protocol for micro-purification, enrichment, pre-fractionation and storage of peptides for proteomics using StageTips. *Nat. Protoc.* **2**, 1896–1906 (2007).
31. Huang, P. et al. Spatial proteome profiling by immunohistochemistry-based laser capture microdissection and data-independent acquisition proteomics. *Anal. Chim. Acta* **1127**, 140–148 (2020).
32. Xu, R. et al. Spatial-resolution cell type proteome profiling of cancer tissue by fully integrated proteomics technology. *Anal. Chem.* **90**, 5879–5886 (2018).
33. Bian, Y. et al. Ultra-deep tyrosine phosphoproteomics enabled by a phosphotyrosine superbinder. *Nat. Chem. Biol.* **12**, 959–966 (2016).

34. Chu, B. et al. Photoaffinity-engineered protein scaffold for systematically exploring native phosphotyrosine signaling complexes in tumor samples. *Proc. Natl Acad. Sci. USA* **115**, E8863–E8872 (2018).
35. Zhou, H. et al. Robust phosphoproteome enrichment using monodisperse microsphere-based immobilized titanium (IV) ion affinity chromatography. *Nat. Protoc.* **8**, 461–480 (2013).
36. Tian, R. et al. Combinatorial proteomic analysis of intercellular signaling applied to the CD28 T-cell costimulatory receptor. *Proc. Natl Acad. Sci. USA* **112**, E1594–E1603 (2015).
37. Huang, P., Li, H., Gao, W., Cai, Z. & Tian, R. A fully integrated spintip-based approach for sensitive and quantitative profiling of region-resolved in vivo brain glycoproteome. *Anal. Chem.* **91**, 9181–9189 (2019).
38. Jedrychowski, M. P. et al. Detection and quantitation of circulating human irisin by tandem mass spectrometry. *Cell Metab.* **22**, 734–740 (2015).
39. Bausch-Fluck, D. et al. The in silico human surfaceome. *Proc. Natl Acad. Sci. USA* **115**, E10988–E10997 (2018).
40. Möller, S., Croning, M. D. & Apweiler, R. Evaluation of methods for the prediction of membrane spanning regions. *Bioinformatics* **17**, 646–653 (2001).
41. Nielsen, H. Predicting secretory proteins with SignalP. *Methods Mol. Biol.* **1611**, 59–73 (2017).
42. Käll, L., Krogh, A. & Sonnhammer, E. L. A combined transmembrane topology and signal peptide prediction method. *J. Mol. Biol.* **338**, 1027–1036 (2004).
43. Ramilowski, J. A. et al. A draft network of ligand-receptor-mediated multicellular signalling in human. *Nat. Commun.* **6**, 7866 (2015).
44. Graeber, T. G. & Eisenberg, D. Bioinformatic identification of potential autocrine signaling loops in cancers from gene expression profiles. *Nat. Genet.* **29**, 295–300 (2001).
45. Sharman, J. L. et al. IUPHAR-DB: updated database content and new features. *Nucleic Acids Res.* **41**, D1083–D1088 (2013).
46. Ben-Shlomo, I., Yu Hsu, S., Rauch, R., Kowalski, H. W. & Hsueh, A. J. Signaling receptome: a genomic and evolutionary perspective of plasma membrane receptors involved in signal transduction. *Sci. STKE* **2003**, RE9 (2003).
47. Keshava Prasad, T. S. et al. Human Protein Reference Database—2009 update. *Nucleic Acids Res.* **37**, D767–D772 (2009).
48. Szklarczyk, D. et al. The STRING database in 2021: customizable protein-protein networks, and functional characterization of user-uploaded gene/measurement sets. *Nucleic Acids Res.* **49**, D605–D612 (2021).
49. Manning, G., Whyte, D. B., Martinez, R., Hunter, T. & Sudarsanam, S. The protein kinase complement of the human genome. *Science* **298**, 1912–1934 (2002).
50. Lemmon, M. A. & Schlessinger, J. Cell signaling by receptor tyrosine kinases. *Cell* **141**, 1117–1134 (2010).
51. Liu, B. A. et al. The human and mouse complement of SH2 domain proteins-establishing the boundaries of phosphotyrosine signaling. *Mol. Cell* **22**, 851–868 (2006).
52. Wagner, M. J., Stacey, M. M., Liu, B. A. & Pawson, T. Molecular mechanisms of SH2- and PTB-domain-containing proteins in receptor tyrosine kinase signaling. *Cold Spring Harb. Perspect. Biol.* **5**, a008987 (2013).
53. Uhlik, M. T. et al. Structural and evolutionary division of phosphotyrosine binding (PTB) domains. *J. Mol. Biol.* **345**, 1–20 (2005).
54. Alonso, A. et al. Protein tyrosine phosphatases in the human genome. *Cell* **117**, 699–711 (2004).
55. Pao, L. I., Badour, K., Siminovitch, K. A. & Neel, B. G. Nonreceptor protein-tyrosine phosphatases in immune cell signaling. *Annu. Rev. Immunol.* **25**, 473–523 (2007).
56. Zielinska, D. F., Gnad, F., Wisniewski, J. R. & Mann, M. Precision mapping of an in vivo *N*-glycoproteome reveals rigid topological and sequence constraints. *Cell* **141**, 897–907 (2010).
57. Tyanova, S., Temu, T. & Cox, J. The MaxQuant computational platform for mass spectrometry-based shotgun proteomics. *Nat. Protoc.* **11**, 2301–2319 (2016).
58. Newman, A. M. et al. Determining cell type abundance and expression from bulk tissues with digital cytometry. *Nat. Biotechnol.* **37**, 773–782 (2019).
59. Futschik, M. E. & Carlisle, B. Noise-robust soft clustering of gene expression time-course data. *J. Bioinform. Comput. Biol.* **3**, 965–988 (2005).
60. Morello, A., Sadelain, M. & Adusumilli, P. S. Mesothelin-targeted CARs: driving T cells to solid tumors. *Cancer Discov.* **6**, 133–146 (2016).
61. Liu, X. et al. A new panel of pancreatic cancer biomarkers discovered using a mass spectrometry-based pipeline. *Br. J. Cancer* **117**, 1846–1854 (2017).
62. Fredriksson, L., Li, H. & Eriksson, U. The PDGF family: four gene products form five dimeric isoforms. *Cytokine Growth Factor Rev.* **15**, 197–204 (2004).
63. Fu, C. et al. The transcription factor ZFHX3 is crucial for the angiogenic function of hypoxia-inducible factor 1α in liver cancer cells. *J. Biol. Chem.* **295**, 7060–7074 (2020).
64. Zhu, S. et al. GDF15 promotes glioma stem cell-like phenotype via regulation of ERK1/2-c-Fos-LIF signaling. *Cell Death Discov.* **7**, 3 (2021).
65. Bolte, S. & Cordelières, F. P. A guided tour into subcellular colocalization analysis in light microscopy. *J. Microsc.* **224**, 213–232 (2006).
66. Shi, X. et al. Integrated profiling of human pancreatic cancer organoids reveals chromatin accessibility features associated with drug sensitivity. *Nat. Commun.* **13**, 2169 (2022).
67. Jaaks, P. et al. Effective drug combinations in breast, colon and pancreatic cancer cells. *Nature* **603**, 166–173 (2022).
68. Liu, C. et al. Kindlin-2 enhances c-Myc translation through association with DDX3X to promote pancreatic ductal adenocarcinoma progression. *Theranostics* **13**, 4333–4355 (2023).
69. Perez-Riverol, Y. et al. The PRIDE database resources in 2022: a hub for mass spectrometry-based proteomics evidences. *Nucleic Acids Res.* **50**, D543–d552 (2022).
70. Matthews, M. L. et al. Chemoproteomic profiling and discovery of protein electrophiles in human cells. *Nat. Chem.* **9**, 234–243 (2017).
71. Maurer, C. et al. Experimental microdissection enables functional harmonisation of pancreatic cancer subtypes. *Gut* **68**, 1034–1043 (2019).
72. Elyada, E. et al. Cross-species single-cell analysis of pancreatic ductal adenocarcinoma reveals antigen-presenting cancer-associated fibroblasts. *Cancer Discov.* **9**, 1102–1123 (2019).
73. Kim, J. et al. Detection of early pancreatic ductal adenocarcinoma with thrombospondin-2 and CA19-9 blood markers. *Sci. Transl. Med.* **9**, eaah5583 (2017).
74. Cohen, J. D. et al. Detection and localization of surgically resectable cancers with a multi-analyte blood test. *Science* **359**, 926–930 (2018).
75. Melo, S. A. et al. Glypican-1 identifies cancer exosomes and detects early pancreatic cancer. *Nature* **523**, 177–182 (2015).
76. Seguin, L. et al. Galectin-3, a druggable vulnerability for KRAS-addicted cancers. *Cancer Discov.* **7**, 1464–1479 (2017).
77. Jones, S. et al. Core signaling pathways in human pancreatic cancers revealed by global genomic analyses. *Science* **321**, 1801–1806 (2008).
78. Makohon-Moore, A. & Iacobuzio-Donahue, C. A. Pancreatic cancer biology and genetics from an evolutionary perspective. *Nat. Rev. Cancer* **16**, 553–565 (2016).

Acknowledgements This study was supported by grants from the China State Key Basic Research Program Grants (2020YFE0202200, 2021YFA1301601, 2021YFA1301602, 2021YFA1302603, 2023YFC2506401, 2022YFC3401104, 2022YFA1105300-03 and 2020YFA0509002); the National Natural Science Foundation of China (22125403, 92253304, 91953118, 92359302, 32201218, 82341074, 32171433, 22104047, 22004056, 82273438 and 32125013); the Shenzhen Innovation of Science and Technology Commission (ZDSYS20230626090803004, JSGGZD20220822095200001, KJZD20230923114220041, JCYJ20200109141212325, JCYJ20210324120210029 and JCYJ20200109140814408); Guangdong province (2019B151502050); the Basic Frontier Science Research Program of Chinese Academy of Sciences (ZDBS-LY-SM015); the Shanghai Municipal Science and Technology Major Project; and the Innovative Research Team of High-level Local Universities in Shanghai (SHSMUZDCX20211800). Work in the T.H. group was supported by grants from the NCI (CA080100 and CA082683), NIH NCI 1 P01 (CA265762-01A1), Lustgarten Foundation Awards (388246 and 552873) and core services funded through an NCI Cancer Center Support Grant (CA014195). T.H. is a Frank and Elsa Schilling American Cancer Society Professor, and the Renato Dulbecco Chain in Cancer Research.

Author contributions R.T. conceived and designed the study. P.H. performed most MS-based experiments, ELISA and initial data analysis. W.G. performed analysis of proteomic data, with assistance from Yuan Li. C.F. performed the majority of the in vitro and part of the in vivo validation experiments and analysed the data with assistance from X.D. Yunguang Li performed organoid-related experiments and analysed the data with assistance from Y.Z. B.C. performed profiling of pTyr protein complexes and in vitro validation of AXL shedding. M.W., J.Y., H.W. and R.Q. collected and analysed clinical samples. Y.S. provided the genetically engineered mouse model of pancreatic cancer and analysed the data. A.H. synthesized the biotin-hydrazide probe. Q.K. assisted with phosphoproteomic-related experiments. P.H., W.G., C.F., Y.S., T.H. and R.T. wrote the manuscript with input from all of the authors. R.T., T.H., R.Q., D.G. and Y.S. supervised the study.

Competing interests R.T. is a founder of BayOmics.

Additional information

Supplementary information The online version contains supplementary material available at https://doi.org/10.1038/s41586-024-08225-y.

Correspondence and requests for materials should be addressed to Yu Shi, Dong Gao, Renyi Qin or Ruijun Tian.

Peer review information *Nature* thanks the anonymous reviewers for their contribution to the peer review of this work. Peer reviewer reports are available.

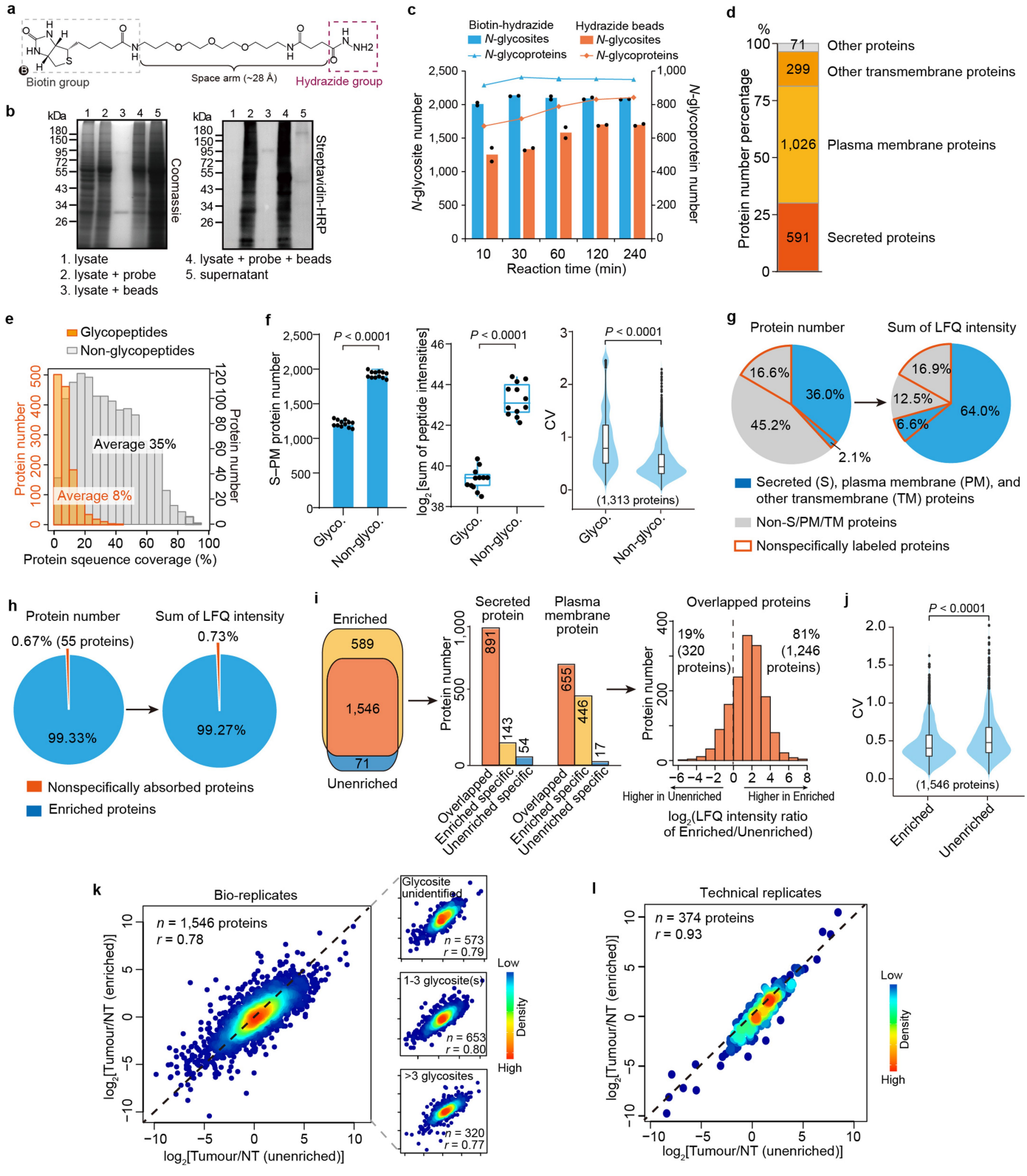

Extended Data Fig. 1 | See next page for caption.

Extended Data Fig. 1 | Optimization of *N*-glycoproteomic method using the synthesized long chain biotin-hydrazide probe. a, Chemical structure of in-house synthesized biotin-hydrazide for glycoprotein labelling and enrichment. **b**, Labelling and enrichment efficiency of the biotin-hydrazide probe. Mouse pancreas proteins were extracted and labelled with 2 mM probe for 1 h (lane 2). Lysate without biotin-hydrazide labelling was subjected for streptavidin pull down as control (lane 3). Labelled proteins were pulled down by streptavidin beads (lane 4). Supernatant was collected from the streptavidin pull down (lane 5). **c**, Comparison of biotin-hydrazide probe-based method with conventional hydrazide bead-based method. Either biotin-hydrazide probe or hydrazide beads were incubated with 500 μg lysate for different times. After on-bead trypsin digestion to remove non-glycopeptides, glycopeptides were released from the streptavidin beads or hydrazide beads by PNGase F for LC–MS/MS analysis. Data are mean of two technical replicates. **d**,**e**, Subcellular location of proteins identified by glycopeptides (**d**) and sequence coverage comparison of 1,313 S–PM proteins commonly identified by glycopeptides and non-glycopeptides (**e**) using 6 pairs of tumour and NT samples. **f**, The comparison of analysis by non-glycopeptides and glycopeptides in terms of identification and quantification performance of S–PM proteins. The left panel is the number of S–PM proteins identified by glycopeptides and non-glycopeptides. Data are mean ± s.d. of 6 pairs of tumour and NT samples. The middle panel is the sum peptide intensities of all identified S–PM proteins from these 12 tissue samples. The right panel is the CV of 1,313 overlapped S–PM proteins quantified with LFQ intensities by glycopeptides and non-glycopeptides. **g**, The percentage of secreted (S), plasma membrane (PM), and other transmembrane (TM) proteins, non-S/PM/TM proteins, and nonspecifically labelled proteins reported by Matthews et al.[70] to total proteins in terms of protein number (left panel) and sum LFQ intensity (right panel) as identified by glycopeptides and non-glycopeptides. **h**, The percentage of proteins nonspecifically absorbed on streptavidin beads to total proteins identified by glycoprotein enrichment. The experimental procedure for identification of nonspecifically absorbed proteins was the same as glycoprotein enrichment, except that no biotin-hydrazide probe was added. Proteins identified only in the streptavidin pull down sample without biotin-hydrazide probe or having 2-fold higher LFQ intensity as compared with glycoprotein enrichment were defined as nonspecifically absorbed proteins. **i**,**j**, Comparison of quantification performance of S–PM proteins by global proteomic method (Unenriched) and *N*-glycoproteomic method (Enriched) using 6 pairs of tumour and NT samples. S–PM proteins quantified by Unenriched and Enriched were compared in terms of protein number and intensities (**i**), and CV of 1,546 S–PM proteins commonly quantified by Unenriched and Enrich (**j**). **k**,**l**, Correlation of the average tumour/NT ratios of commonly quantified S–PM proteins between the two methods. Bio-replicates denote correlation of the 6 pairs of tumour and NT samples; correlations of glycoproteins identified with different number of *N*-glycosites are independently displayed (**k**); technical replicates denote correlation of 1 pair of tumour and NT samples for three technical replicates (**l**).

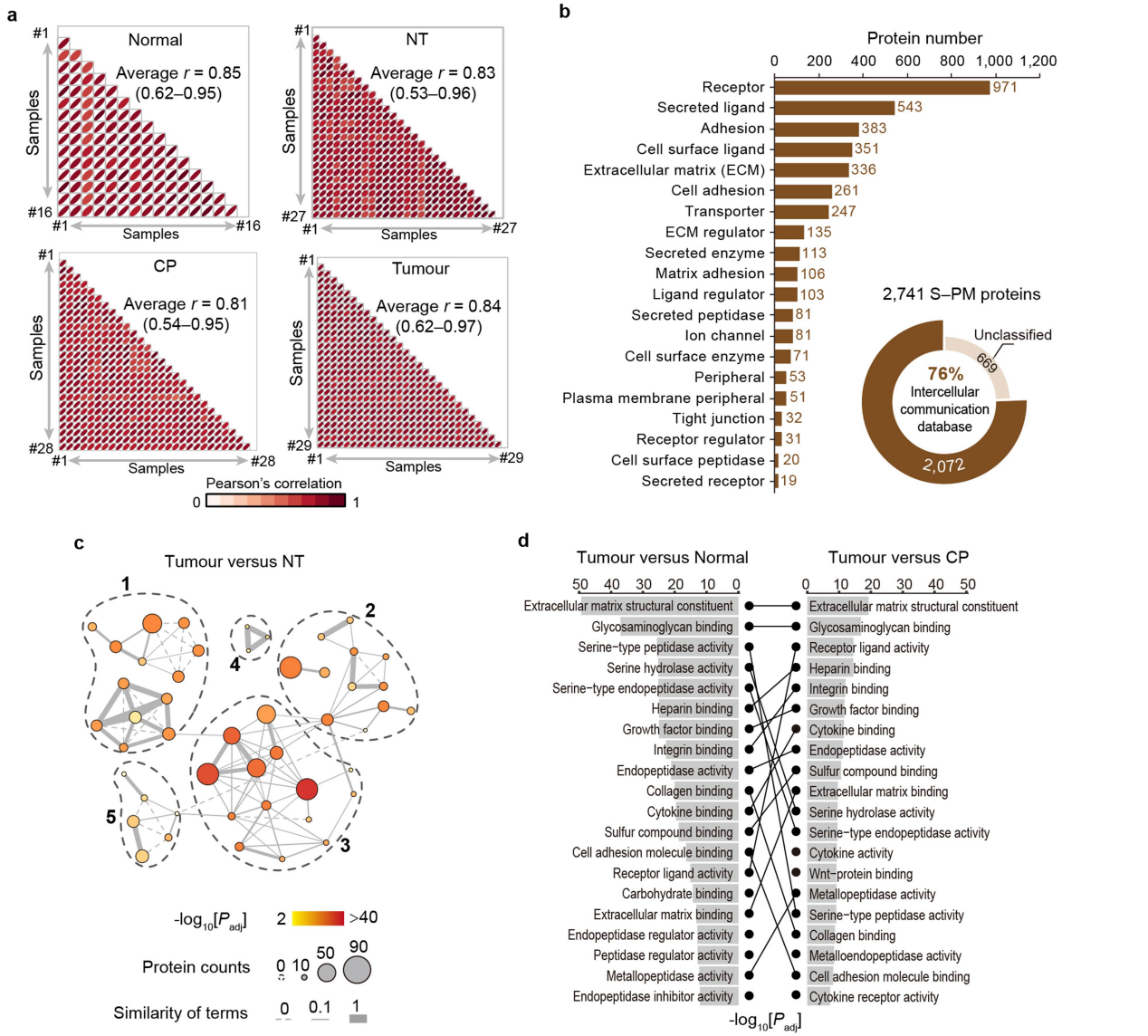

Extended Data Fig. 2 | Sample quality control and functional annotation of S–PM proteome in PDAC. a, Pearson's correlation coefficients of LFQ intensities between any two samples from the same group of normal, NT, CP, or tumour tissues, respectively. **b**, Classification of S–PM proteins according to their roles in intercellular communications. The bar graph shows the top 20 intercellular communication roles. **c**, Clustering of top 50 GOMF terms of significantly changed S–PM proteins between Tumour and NT, related to Fig. 1g. **d**, Comparison of top 20 GOMF terms of significantly altered S–PM proteins between Tumour versus Normal and Tumour versus CP. *P* values are from hypergeometric distribution (**c**, **d**).

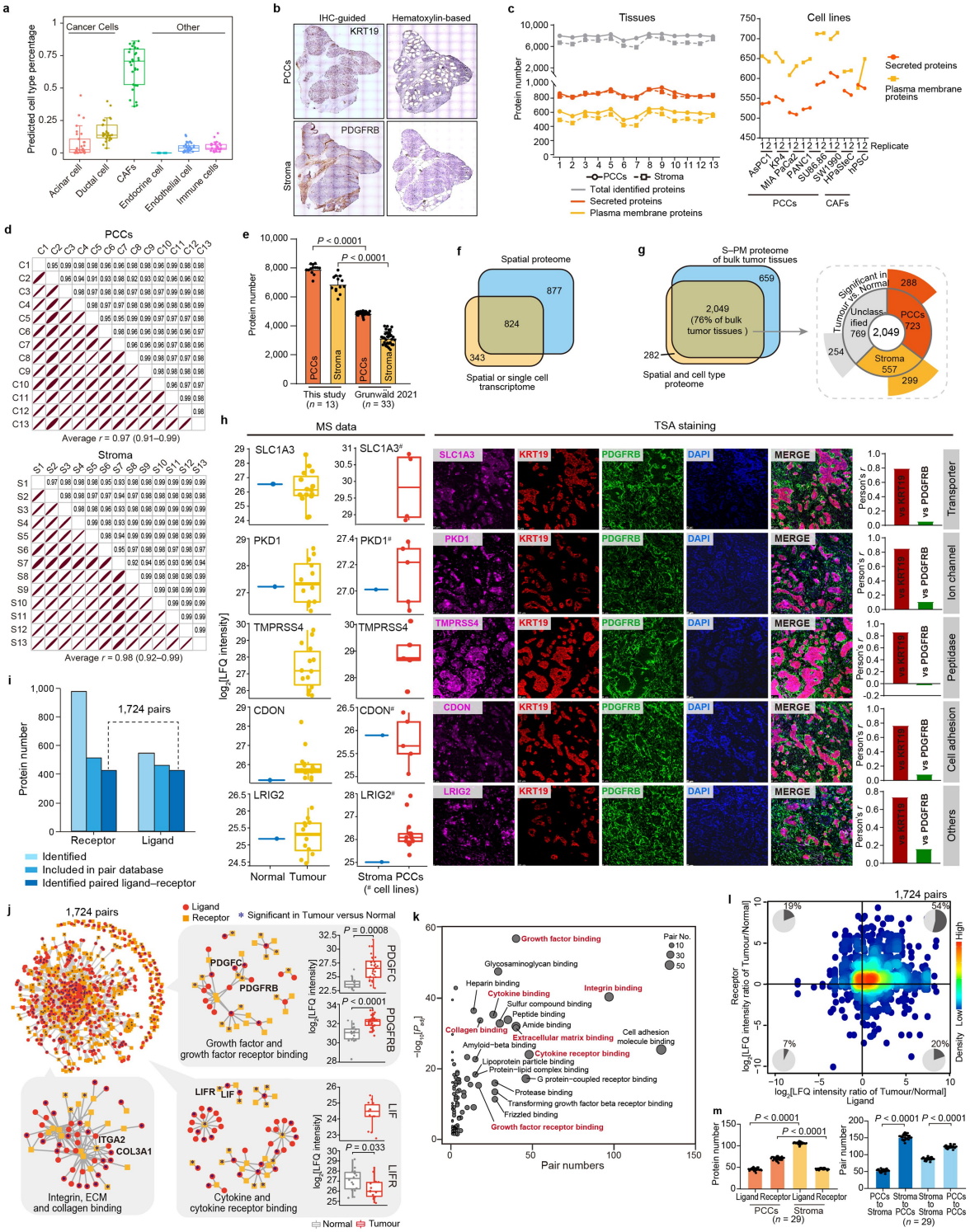

Extended Data Fig. 3 | See next page for caption.

Extended Data Fig. 3 | Extended analysis of spatially resolved and cell type-specific proteomic data and validation of PCC specific proteins. a, Cell type deconvolution of 29 tumour samples using our bulk S–PM proteome in Fig. 1b and published scRNA-seq dataset of PDAC (Methods). Box plots are as defined in Fig. 2c. **b**, Representative images of IHC-guided and hematoxylin staining-based LCM of PCC and stromal regions from tumour tissue section. The stroma region was stained by IHC targeting PDGFRB, a marker of stroma cells. The PCC region was stained by IHC targeting KRT19, a marker of epithelial cells. **c**, The number of S–PM proteins identified in each of the tissue and cell line samples. **d**, Pearson's correlation coefficients of LFQ intensities between any two biological replicates from the same region of PCCs or stroma. **e**, Comparison of proteome depth of our LCM-based proteomic dataset with a recently published LCM-based proteomic dataset of PDAC[8]. The raw files of the published dataset were downloaded and processed using the same workflow and criteria as our dataset. **f**, Comparison of the S–PM proteins identified in spatial proteomic dataset with genes of S–PM proteins from the transcriptomic dataset summarized from spatial or scRNA-seq analysis of PDAC[18,71,72]. All the identified genes of S–PM proteins from the three references were combined as the transcriptome dataset. **g**, Cell-type annotation of the S–PM proteins identified from *N*-glycoproteomic profiling of 29 bulk tumour tissues. **h**, TSA staining of 5 PCC-specific and tumour-upregulated PM proteins, including the aspartate/glutamate transporter SLC1A3, the PKD1 calcium channels, the TMPRSS4 protease, the CDON Hedgehog signalling regulator, and the LRIG2 protease regulator. KRT19 and PDGFRB were marker of PCCs and stroma, respectively. Box plots are as defined in Fig. 2c. The pearson's *r* values indicates the colocalization potential of target proteins with KRT19 or PDGFRB (Methods). **i**,**j**, The number of ligands, receptors, and ligand–receptor pairs annotated from secreted ligands and plasma membrane receptors of Extended Data Fig. 2b by an in-house ligand–receptor database (see Methods) (**h**), and display of the 1,724 ligand–receptor pairs (j). The pairs of three classes of most enriched GOMF terms are shown as examples, with representative proteins displayed. **k**, Dot plot showing GOMF terms of the 1,724 ligand–receptor pairs. Top 20 GOMF terms according to pair number were annotated and terms in red were presented in **j**. **l**, Protein expression trend of the 1,724 pairs according to LFQ intensity ratio distribution of tumour and normal tissues. One dot represents one pair. The X and Y axes are the $\log_2$ transformed LFQ ratio between Tumour and Normal of ligand and receptor, respectively. The pie chart shows the percentage of pairs in each section to total pairs. **m**, The number of spatially resolved and cell type-specific ligands and receptors (top panel) and their predicated signalling flow (bottom panel) in 29 tumours. Data are mean ± s.d. *P* values are from two-tailed unpaired Student's *t*-test (**e**,**m**), or hypergeometric distribution (**k**).

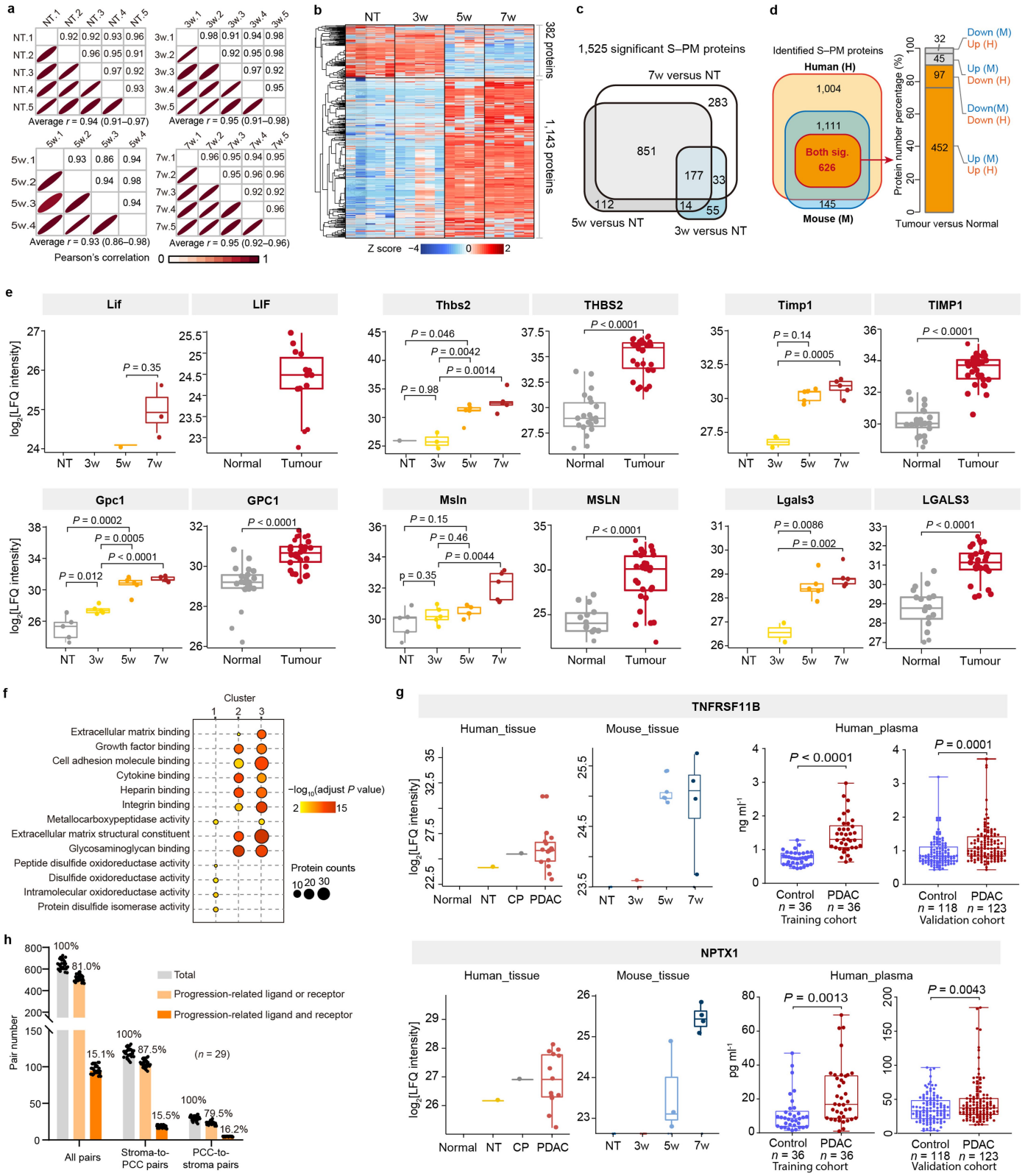

Extended Data Fig. 4 | See next page for caption.

Extended Data Fig. 4 | Extended analysis for time-resolved *N*-glycoproteomic profiling of KPC mouse model. a, Pearson's correlation coefficients of LFQ intensities between any two samples from the same group of NT, 3 weeks, 5 weeks, or 7 weeks of KPC mice, respectively. **b**, Consensus-clustering analysis of S–PM proteins differentially expressed between NT and different tumour stages of the KPC mouse model. **c**, The number of differentially expressed S–PM proteins in each stage of tumour tissues as compared with NT, respectively. **d**, Overlap and expression trend consistency of differentially expressed proteins between human PDAC and KPC mouse model. **e**, Relative expression levels of representative PDAC biomarkers, including Lif[14], Thbs2[73], Timp1[74], Gpc1[75], Msln[60], and Lgals3[76], in different stage tumour tissues of KPC mice and in human pancreatic tissues. The number of human and mouse tissue samples in each group is indicated in Figs. 1a and 3b, respectively. **f**, Top 5 GOMF terms of S–PM proteins in the three clusters. *P* values are calculated by hypergeometric distribution. **g**, Validation of TNFRSF11B and NPTX1 in PDAC plasma samples. Human plasma samples from training and validation cohorts were tested by ELISA kits. **h**, Annotation of ligand–receptor pairs in 29 bulk human tumour tissues on the basis of the indicated tumour progression trends. Data are mean ± s.d. All pairs refer to the pairs shown in Extended Data Fig. 3j in which the expression of at least ligand or receptor was significantly changed in human Tumour versus Normal in *N*-glycoproteomic dataset. Box plots are as defined in Fig. 2c (**e**, tissue results of **g**). Box plots of plasma results in **g**: centre line, median; boxes, interquartile range; whiskers, minimum to maximum. *P* values are from two-tailed unpaired Student's *t*-test.

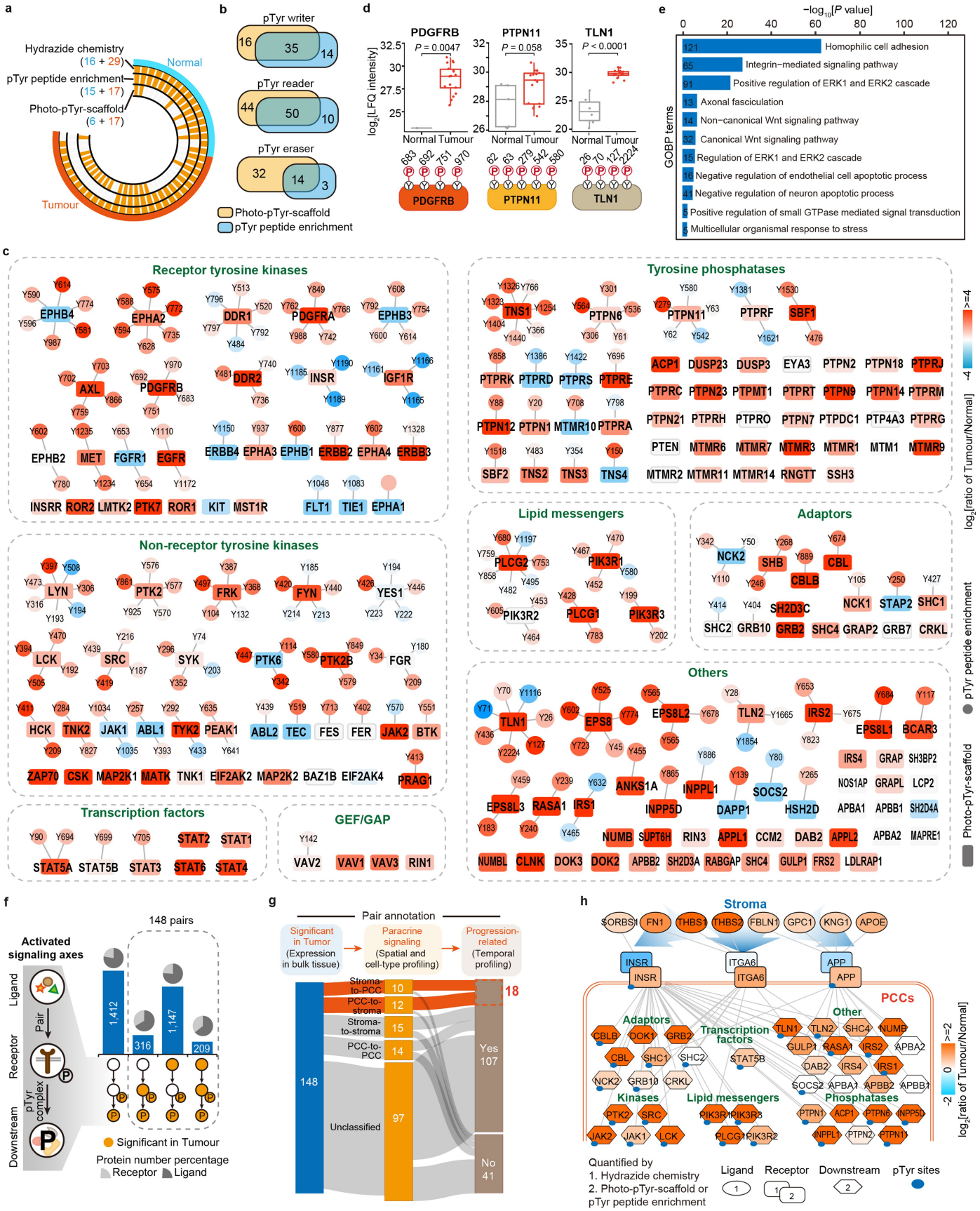

Extended Data Fig. 5 | See next page for caption.

Extended Data Fig. 5 | Extended analysis of pTyr protein complex and pTyr site profiling and integrated analysis of ligand–receptor–downstream signalling axes. a, Clinical tissue samples used for *N*-glycoproteomic analysis, photo-pTyr-scaffold, and pTyr peptide enrichment. **b**, Overlap of pTyr writers, readers, and erasers identified by photo-pTyr-scaffold approach and pTyr peptide enrichment approach. **c**, Summary of all the pTyr writers, readers, and erasers identified by two approaches in Fig. 4b. The rectangle indicates proteins identified by the photo-pTyr-scaffold approach and the circle indicates the pTyr sites identified by pTyr peptide enrichment approach. Proteins are classified according to their molecular functions. **d**, Expression levels and pTyr sites of top ranked pTyr writers, erasers and readers in Fig. 4c. Box plots are as defined in Fig. 2c. *P* values are from two-tailed unpaired Student's *t*-test. **e**, The overlapped GOBP terms of proteins identified by our multidimensional proteomics (S–PM and pTyr machinery proteins identified in tumour tissues by *N*-glycoproteomic profiling and pTyr-mediated complexes profiling) with the core signalling pathways summarized from global genomic analysis of PDAC[77,78]. The core signalling pathways summarized in these two references were combined. *P* values are from hypergeometric distribution. **f**, The four categories of activated ligand–receptor–downstream signalling axes in which the expression of both receptor and downstream protein were significantly changed in tumours in the pTyr signalling dataset (circles labelled with P). **g**, Spatial and temporal annotation of the 148 pairs in Fig. 4d. **h**, The activated paracrine signalling pairs from stromal cells to PCCs in tumour and their downstream proteins screened out from **g**.

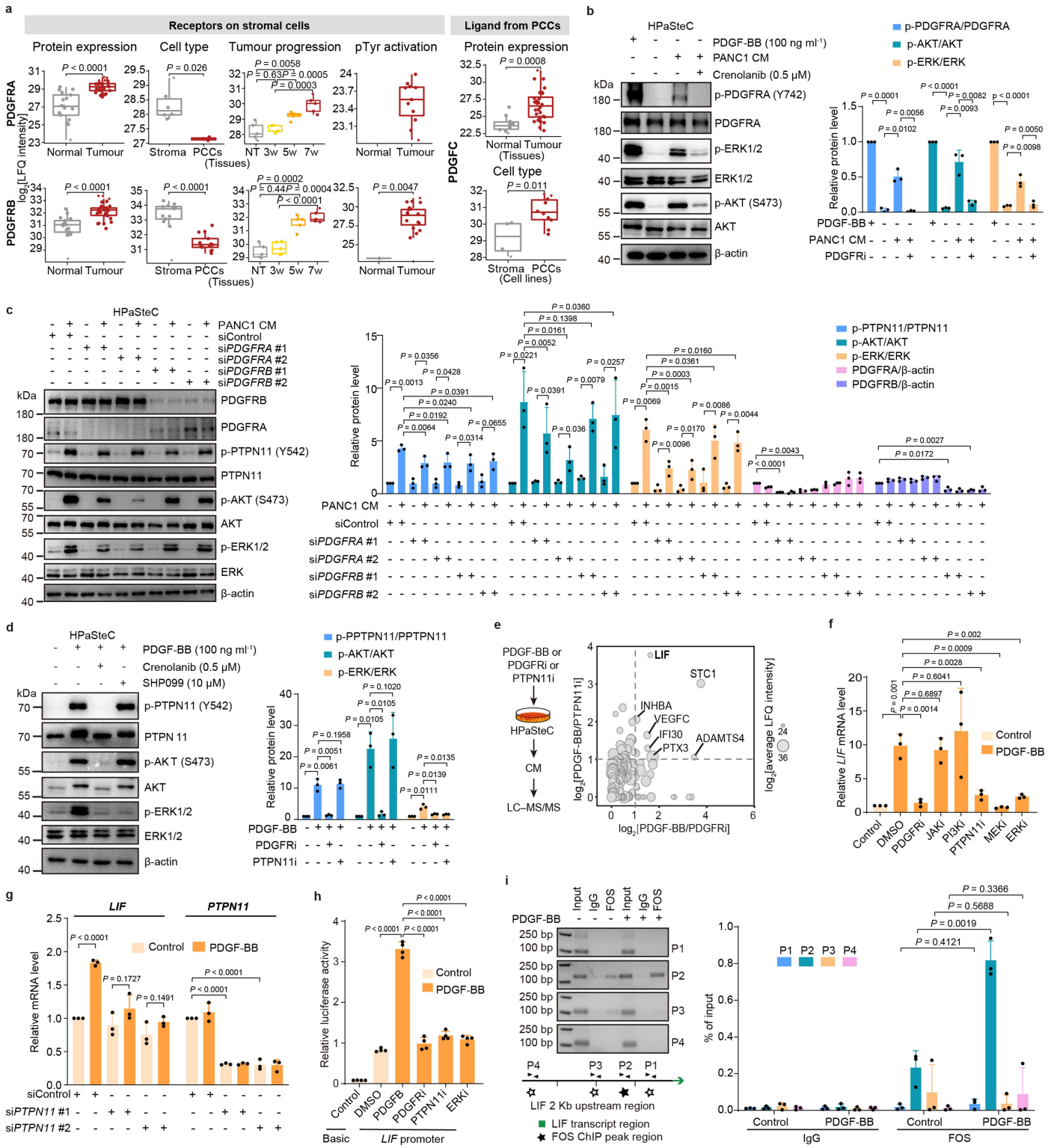

Extended Data Fig. 6 | See next page for caption.

Extended Data Fig. 6 | Functional characterization of reciprocal signalling between stromal cells and PCCs mediated by the PDGFR–PTPN11–FOS signalling axis. a, Expression levels of PDGFRA, PDGFRB, and PDGFC in the multidimensional proteomic datasets shown in Figs. 1–4. The number of samples for protein expression, cell type, tumour progression, and pTyr activation is indicated in Fig. 1a, Fig. 2a, Fig. 3b, and Extended Data Fig. 5a, respectively. Box plots are as defined in Fig. 2c. *P* values are from two-tailed unpaired Student's *t*-test. **b**, Validation of PDGFR activation by PANC1 CM or recombinant PDGF-BB and inhibition by the PDGFR inhibitor crenolanib in HPaSteCs. Cells were starved in FBS-free medium for 12 h with or without PDGFR inhibitor crenolanib, and then stimulated with PDGF-BB or PANC1 CM for 5 min before cell lysis for WB analysis. **c**, Validation of signalling proteins downstream of PDGFRA and PDGFRB. HPaSteCs were transfected with siRNAs targeting *PDGFRA* or *PDGFRB* in normal medium for 24 h, followed by in FBS-free medium for 24 h, and then stimulated with PANC1 CM for 5 min before cell lysis for WB analysis. **d**, Validation of PTPN11 as an upstream regulator of ERK signalling but not AKT signalling. Cells were starved in FBS-free medium for 12 h with or without PDGFR inhibitor crenolanib or PTPN11 inhibitor SHP099 with indicated concentrations, and then stimulated with PDGF-BB for 5 min before cell lysis for WB analysis. **e**, Secretome analysis of HPaSteCs after PDGF-BB stimulation and PDGFR or PTPN11 inhibition ($n = 3$ biological replicates). HPaSteCs were treated with 100 ng ml^{-1} PDGF-BB, 0.5 μM crenolanib or 10 μM SHP099 for 24 h, respectively. **f**, Investigation of the signalling axis regulating LIF expression upon PDGF stimulation. Cells were treated with PDGFR inhibitor crenolanib (0.5 μM), JAK inhibitor ruxolitinib (1 μM), PI3K inhibitor LY294002 (10 μM), PTPN11 inhibitor SHP099 (10 μM), MEK inhibitor mirdametinib (10 μM), or ERK inhibitor ravoxertinib (10 μM) for 24 h before cell lysis for total RNA extraction and measurement of LIF mRNA levels by real-time qPCR. **g**, Effect of *PTPN11* knockdown on LIF protein secretion from HPaSteCs with or without PDGF-BB stimulation. **h**, Effect of inhibitors targeting the PDGFR–PTPN11–ERK signalling axis on *LIF* promoter activity. HPaSteCs were stimulated with PDGF-BB with or without an inhibitor targeting PDGFR, PTPN11 or ERK. *LIF* promoter activity was measured by a dual-luciferase reporter assay system. **i**, Validation of FOS as a *LIF* gene transcription factor after PDGF-BB stimulation (100 ng ml^{-1}, 24 h) as determined by ChIP assay. P1 to P4 indicate four promoter regions of *LIF*, the result shows that P2 region is the binding site of FOS. Due to similar molecular weight of proteins, samples were run on separate gels, with β-actin as sample processing control (**b**–**d**). All the bar graphs are mean ± s.d. of $n = 3$ (**b**–**d**,**f**,**g**,**i**) or $n = 4$ (**h**) biological replicates; *P* values are two-tailed unpaired Student's *t*-test (**a**,**f**–**i**) or one-tailed paired Student's *t*-test (**b**–**d**).

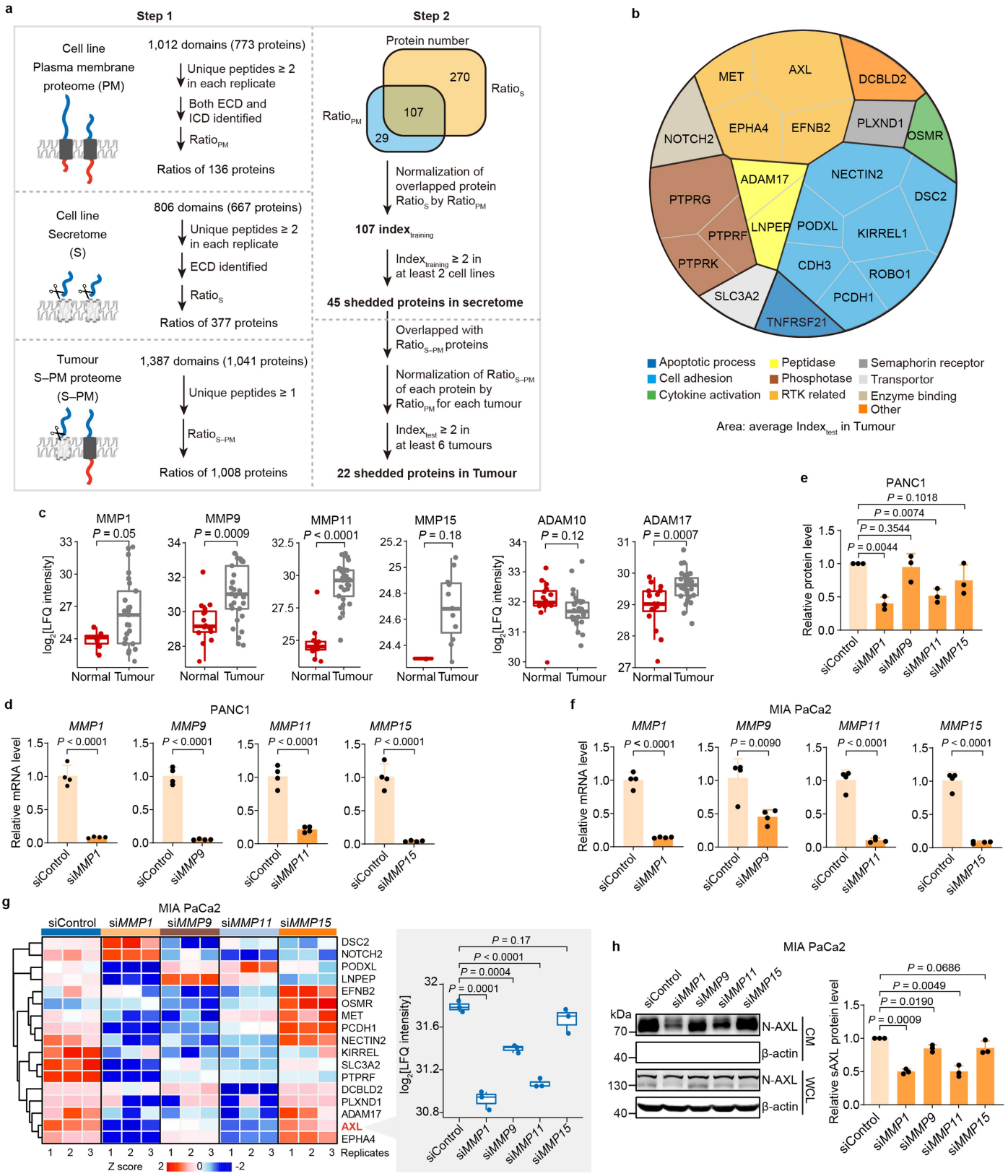

Extended Data Fig. 7 | See next page for caption.

Extended Data Fig. 7 | Workflow for identification of shed PM proteins and extended analysis for validation of MMP-mediated shedding of PM proteins. a, Schematic representation of detail criteria for identification of shed PM proteins in tumours. In step 1, the unique peptide ratio of ECD/ICD for PM proteins ($Ratio_{PM}$) identified in the PM proteome by the *N*-glycoproteomic analysis of cell pellets (data presented in Extended Data Fig. 3c), the same ratio for PM proteins ($Ratio_{S}$) identified by the secretome analysis (data presented in Extended Data Fig. 3c), and the same ratio for PM proteins ($Ratio_{S-PM}$) identified in the S−PM proteome by the *N*-glycoproteomic analysis of 29 PDAC tumour tissues (data presented in Fig. 1b) were calculated after data filtering according to the indicated criteria, respectively. The strict cutoff ensures the reliability and reproducibility of quantification performance in each dataset. In step 2, to avoid false positive calculation of shedding proteins due to the intrinsic difference of sequence length of ECD and ICD, the $Ratio_{S}$ were first normalized to (divided by) their corresponding $Ratio_{PM}$ to generate the $Index_{training}$ values so as to identify shed PM proteins in the secretome of 8 cell lines. Then, 45 shed PM proteins were identified in cell lines. By using the same normalization step and indicated filtering criteria, 22 shed proteins were finally identified and validated in tumour tissues. **b**, Molecular functions of the 22 shed proteins identified in tumour tissues. **c**, Expression level of MMP1, MMP9, MMP11, MMP15, ADAM10, and ADAM17 in tumour and normal tissues by *N*-glycoproteomic profiling. **d**, Knockdown efficiency of each *MMP* by siRNA in PANC1 cells in Fig. 5e. Cells were transfected with siRNAs in normal medium for 24 h, followed by in FBS-free medium for 24 h before that WCLs were collected for total RNA extraction. The mRNA levels of *MMPs* were measured by real-time qRT−PCR. **e**, Statistic analysis of WB result in Fig. 5f, showing sAXL levels in PANC1 CM after knockdown of different *MMPs*. Cells were transfected with siRNA targeting *MMP1*, *MMP9*, *MMP11*, or *MMP15* in normal medium for 24 h, followed by in FBS-free medium for 24 h before that CM and WCL were collected for WB analysis. **f**, Knockdown efficiency of each *MMP* by siRNA in MIA PaCa2 cells. **g**, Global profiling of shedding substrates of MMPs in MIA PaCa2 cells. The heatmap shows shedding level of 17 PM proteins identified as shed proteins in cell lines and tumour tissues. AXL levels are shown as an example. **h**, Validation of AXL shedding upon *MMP* knockdown by siRNAs in MIA PaCa2 cells. Cells were treated with siRNAs by following the same procedure as PANC1. sAXL in CM and WCL was detected by WB, β-actin was run on the same gel as loading control, and the bar graph shows band intensities of sAXL in CM of the WB image. Box plots are as defined in Fig. 2c (**c**,**g**). All the bar graphs are mean ± s.d. of $n = 4$ (**d**,**f**) or $n = 3$ (**e**,**h**) biological replicates. *P* values are from two-tailed unpaired Student's *t*-test (**c**,**d**,**f**,**g**) or one-tailed paired Student's *t*-test (**e**,**h**).

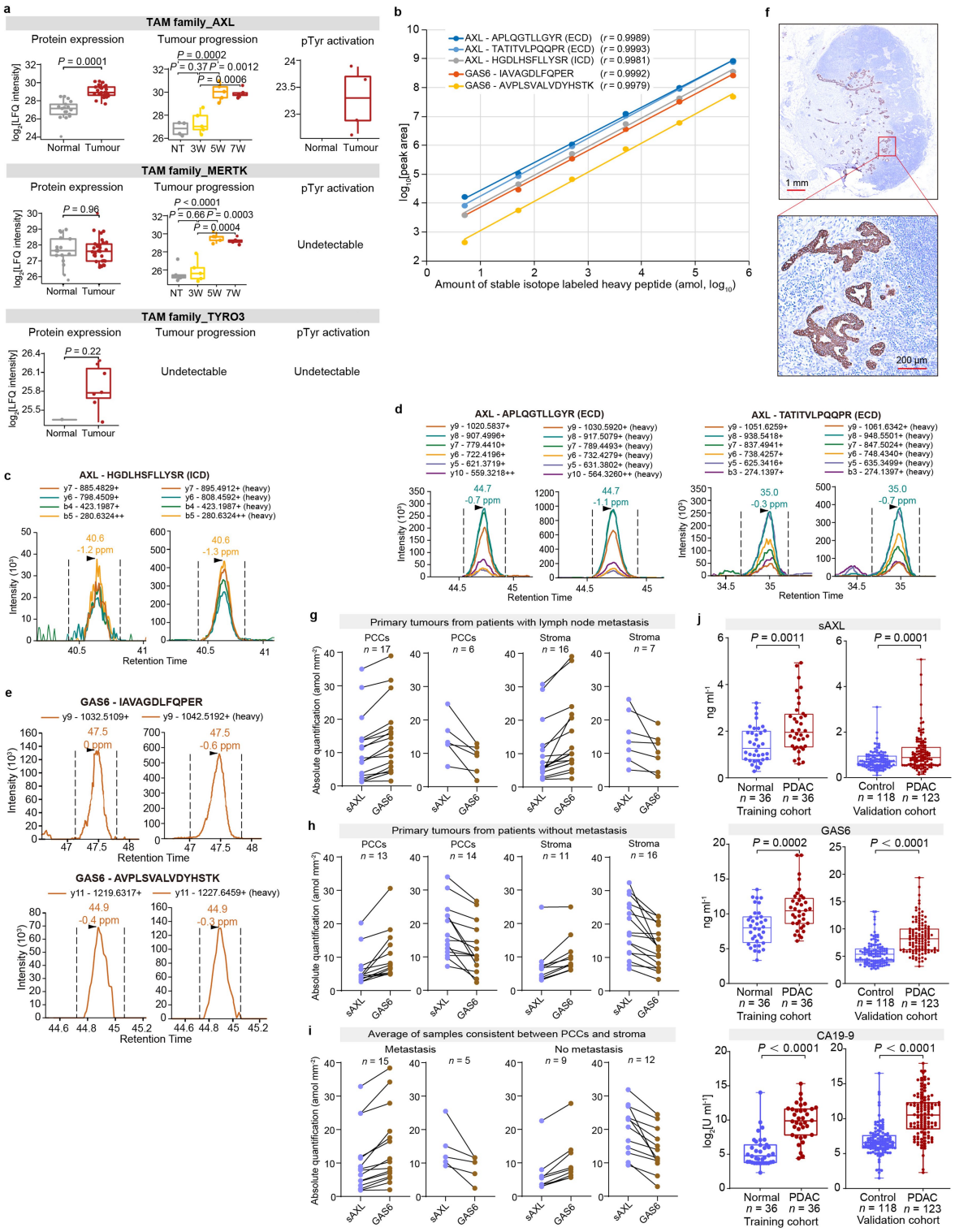

Extended Data Fig. 8 | See next page for caption.

Extended Data Fig. 8 | PRM quantification of AXL shedding in PCC and stromal regions of tumours. a, Expression level of TAM family members AXL, MERTK and TYRO3 in multi-dimensional proteomic datasets. The number of samples for protein expression, tumour progression, and pTyr activation is indicated in Fig. 1a, Fig. 3b, and Extended Data Fig. 5a, respectively. Box plots are as defined in Fig. 2c. *P* values are from two-tailed unpaired Student's *t*-test. **b**, The linearity of PRM quantification for stable isotope labelled heavy peptides of ECD and ICD of AXL, and GAS6. Different amount of heavy peptides were spiked into 100 ng of PANC1 peptides before PRM-MS analysis. **c**-**e**, Representative PRM-MS transition peaks of ICD (**c**) and ECD (**d**) of AXL, and GAS6 (**e**) from tumour samples. The transition peaks of stable isotope labelled heavy peptide spiked into the sample are shown on the right. The dark arrow indicates the retention time and mass error for the highest transition peak. **f**, IHC image of lymph node metastasis. Tumour cells metastasized into the lymph node were marked with IHC staining targeting KRT19. Ten lymph nodes were stained and representative image is presented. **g**–**i**, Classification of tumours according to lymph node metastasis status and relative levels of sAXL and GAS6 in PCC and stroma regions of 50 primary tumour samples (**g**,**h**), and in 41 samples showing consistent trend between PCCs and stroma (namely, the absolute amount of sAXL is higher or lower than GAS6 for both PCC and stromal regions isolated from the same tumour). Displayed are averages of PCC and stromal regions quantified from the same tumour for both sAXL and GAS6 (**i**). **j**, Boxplot of sAXL, GAS6, and CA19-9 levels in human plasma samples from the training cohort and validation cohort of normal controls and PDAC patients. Centre line, median; boxes, interquartile range; whiskers, minimum to maximum. The results from the training cohort and the validation cohort were combined for ROC curve analysis in Fig. 6d.

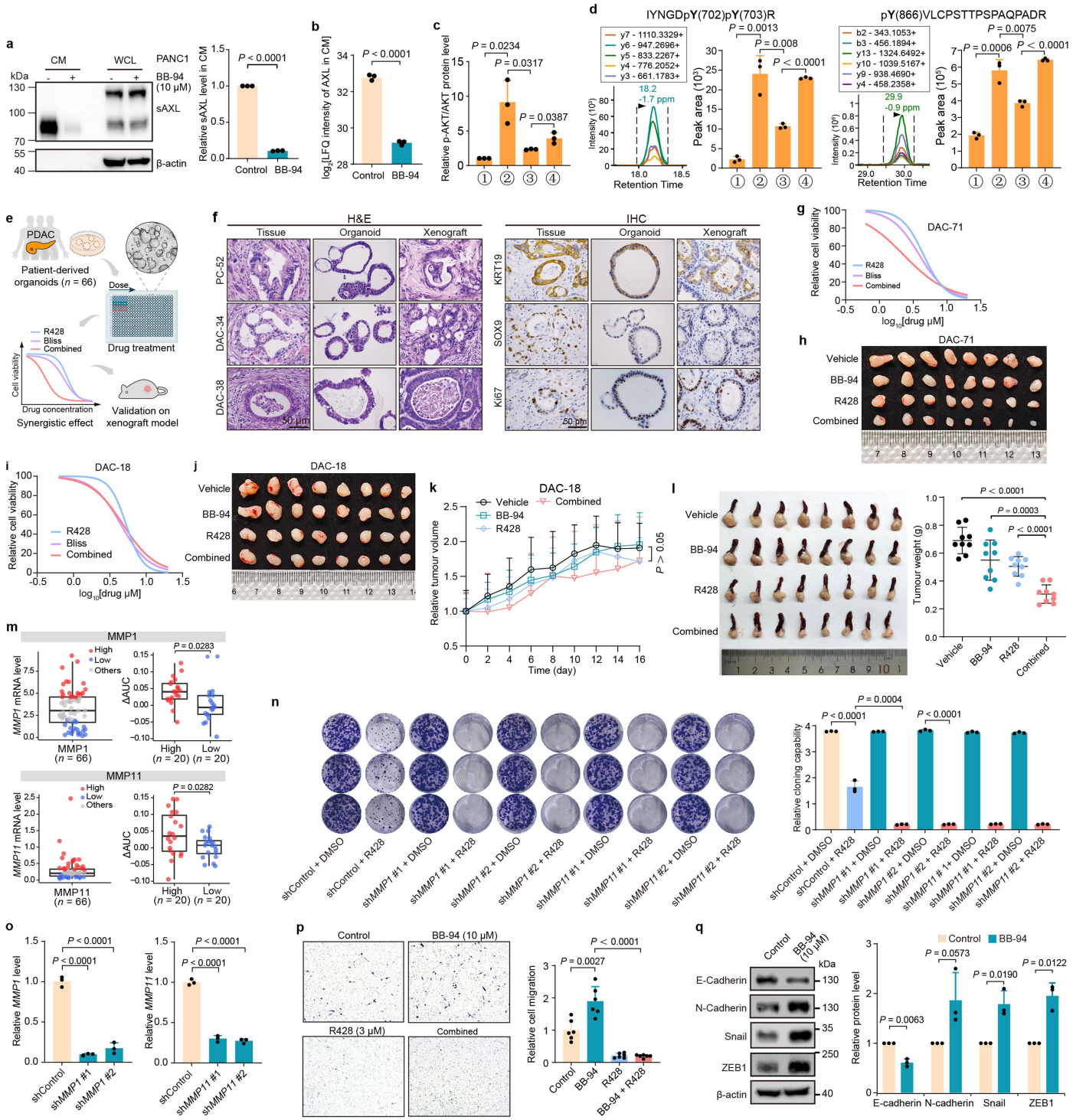

Extended Data Fig. 9 | See next page for caption.

Extended Data Fig. 9 | Combined inhibition of AXL shedding and AXL activity synergistically reduced cancer cell proliferation, migration, and tumour growth. a, Inhibition of AXL shedding by the broad-spectrum MMP inhibitor BB-94. β-actin was run on the same gel as loading control. The bar graph is statistical analysis of sAXL level in PANC1 CM. **b**, Inhibition of AXL shedding in primary KPCP tumour cells by the broad-spectrum MMP inhibitor BB-94. Cells were maintained in FBS-free medium containing 10 μm BB-94 for 24 h, and secretome in CM was profiled by LC-MS/MS analysis. The LFQ intensity of AXL was extracted for comparison between control and BB-94 treatment. **c**, Statistic analysis of the WB results in Fig. 6e, showing relative band intensities of p-AKT after normalization to total AKT. **d**, PRM analysis of two AXL pTyr peptides after enrichment of phosphopeptides. The treatment of PANC1 cells was the same as in Fig. 6e. The left panel of each pTyr peptide is representative transition peaks. The dark arrow indicates the retention time and mass error for the highest transition peak. **e**, Schematic workflow for testing synergistic effect between BB-94 and R428 on PDOs. **f**, Histological characterization of PDAC tumour tissues and corresponding PDOs and PDOs-derived xenografts. PDOs and PDOs-derived xenografts formed typical glandular tubular structures similar to the corresponding patient tumours, and had similar expression levels of the epithelial cell marker KRT19 and SOX9, and cell proliferation marker Ki67. **g**,**h**, Solo or combined drug treatments on xenograft tumours generated by one case of PDO (DAC-71) with significant synergistic response (**g**) between BB-94 and R428 (statistics are presented in Fig. 6g). **i**–**k**, Validation of synergistic effect on xenograft models generated by one case of PDO (DAC-18) with no synergistic response (**i**). Data are mean + s.d. of $n = 8$ xenograft tumours per group (**j**,**k**). **l**, Orthotopic tumours of PDAC under different drug treatment. Orthotopic model was constructed by injecting KPCP primary cancer cells into pancreata of NSG mice. After tumour formation, mice were daily administrated with indicated drugs for 14 days. The dark red tissues were spleens, which were removed before measuring tumour weights. Tumour weights are presented as mean ± s.d. of $n = 9$ mice per condition. **m**, Correlation of *MMP1* and *MMP11* mRNA expression levels in 66 pancreatic PDO lines with drug combination response of BB-94 and R428. Box plots are as defined in Fig. 2c. **n**,**o**, Colony formation assay of MIA PaCa2 cells with stable knockdown of *MMP1* or *MMP11* by shRNAs. Cells were treated with DMSO as control or 0.5 μM R428 for testing of inhibition efficiency (**n**). Knockdown efficiency was measured by real-time qRT–PCR (**o**). **p**, Transwell migration assays of MIA PaCa2 cells under shedding inhibition and/or AXL inhibition. Shown are representative crystal violet-stained images of transwell migration assays of MIA PaCa2 cells under different treatments. Quantification of cell migration determined by counting the number of migratory cells per field and relative numbers of migratory cells were calculated by normalizing to control cells. **q**, Expression of EMT markers in cancer cells upon inhibition of shedding by BB-94. Due to similar molecular weight of proteins, samples were run on separate gels, with β-actin as sample processing control. All the bar graphs are mean ± s.d. of $n = 3$ biological replicates (the data points in **p** are relative cell numbers from 2 random views of each biological replicates). *P* values are from two-tailed unpaired Student's *t*-test (**b**,**d**,**k**,**l**,**m**,**n**,**o**,**p**) or one-tailed paired Student's *t*-test (**a**,**c**,**q**).

nature portfolio

Corresponding author(s): Ruijun Tian, Renyi Qin, Dong Gao, Yu Shi

Last updated by author(s): Sep 2, 2024

Reporting Summary

Nature Portfolio wishes to improve the reproducibility of the work that we publish. This form provides structure for consistency and transparency in reporting. For further information on Nature Portfolio policies, see our Editorial Policies and the Editorial Policy Checklist.

Statistics

For all statistical analyses, confirm that the following items are present in the figure legend, table legend, main text, or Methods section.

n/a	Confirmed
☐	☒ The exact sample size (*n*) for each experimental group/condition, given as a discrete number and unit of measurement
☐	☒ A statement on whether measurements were taken from distinct samples or whether the same sample was measured repeatedly
☐	☒ The statistical test(s) used AND whether they are one- or two-sided *Only common tests should be described solely by name; describe more complex techniques in the Methods section.*
☒	☐ A description of all covariates tested
☐	☒ A description of any assumptions or corrections, such as tests of normality and adjustment for multiple comparisons
☐	☒ A full description of the statistical parameters including central tendency (e.g. means) or other basic estimates (e.g. regression coefficient) AND variation (e.g. standard deviation) or associated estimates of uncertainty (e.g. confidence intervals)
☐	☒ For null hypothesis testing, the test statistic (e.g. *F*, *t*, *r*) with confidence intervals, effect sizes, degrees of freedom and *P* value noted *Give P values as exact values whenever suitable.*
☒	☐ For Bayesian analysis, information on the choice of priors and Markov chain Monte Carlo settings
☒	☐ For hierarchical and complex designs, identification of the appropriate level for tests and full reporting of outcomes
☐	☒ Estimates of effect sizes (e.g. Cohen's *d*, Pearson's *r*), indicating how they were calculated

Our web collection on statistics for biologists contains articles on many of the points above.

Software and code

Policy information about availability of computer code

Data collection	Mass spectrometry data were acquired using Xcalibur software v4.5 (Thermo Scientific). Laser capture microdissection was carried out on a LMD7000 system (Leica). TSA staining images were taken with a SP8 LIGHTNING Confocal Microscope (Leica). Western blot signal was detected using a Tanon 6100C gel imaging system. qRT-PCR was performed with a CFX96 system (Bio-Rad). For ELISA assays, signal acquisition was carried out by a Luminx MAGPIX multiplex immunoassay system (Luminex), or a SR-X system (Quanterix). Luciferase signal was detected using a SpectraMax i3x multi-mode microplate reader (Molecular Devices). NMR spectra were acquired using a Bruker 400 MHz machine.
Data analysis	Database searching for the mass spectrometry raw data were performed using MaxQuant (v1.5.5.1). Extraction of peptide transition peak areas from PRM raw files was performed by Skyline (v20.2.0.286). Bioinformatics and statistical analyses were performed using R (v3.6.1). Normalization of LFQ intensities was performed using R package Limma (v 3.38.3). R packages for visualization and plotting included: ggplot2 (v3.3.5), ggpubr (v0.4.0), pheatmap (v1.0.12), igraph (v1.2.6), RColorBrewer (v1.1-2), reshape2 (v1.4.4), ggrepel (v0.9.1), circlize (v0.4.12), dplyr (v1.0.5), networkD3 (v0.4), voronoiTreemap (v0.2.1), and cytoscape software (v3.8.2). Colocalization analysis of TSA staining results was performed using Colocalization Finder plugin (v1.8) in FIJI. Cell-type deconvolution was performed using CIBERSORTx. Gene ontology enrichments were computed using the 'enrichGO' function from R package 'clusterProfiler (v3.10.1)' . Protein entry was mapped by annotation R package 'org.Hs.eg.db (v3.7.0)'. The tumor progression-related S-PM proteins in the time-resolved proteomic dataset were clustered by applying the fuzzy c-means method from R package 'Mfuzz (v2.50.0)'. The AUC in drug treatment assay on organoids was calculated with the sintegral function in R. The pathway enrichment of ligands, receptors, and pTyr-mediated complexes was analyzed by STRING web-based platform. Other data was analyzed using GraphPad Prism software (v7.0).

For manuscripts utilizing custom algorithms or software that are central to the research but not yet described in published literature, software must be made available to editors and reviewers. We strongly encourage code deposition in a community repository (e.g. GitHub). See the Nature Portfolio guidelines for submitting code & software for further information.

Data

Policy information about availability of data

All manuscripts must include a data availability statement. This statement should provide the following information, where applicable:

- Accession codes, unique identifiers, or web links for publicly available datasets
- A description of any restrictions on data availability
- For clinical datasets or third party data, please ensure that the statement adheres to our policy

In the manuscript, we enclosed a "Data availability" section, stating that "The mass spectrometry proteomics data have been deposited to the ProteomeXchange Consortium via the PRIDE partner repository (https://www.ebi.ac.uk/pride/) with the dataset identifier PXD048644. The UniProt human and mouse proteome databases are available at https://www.uniprot.org/. All other data supporting the findings of this study are available within the article and its Supplemental Information files. Source data are provided with this paper."

Research involving human participants, their data, or biological material

Policy information about studies with human participants or human data. See also policy information about sex, gender (identity/presentation), and sexual orientation and race, ethnicity and racism.

Reporting on sex and gender	We collected and report sex characteristics of patients from whom tumors or plasma were analyzed in the manuscript. Our findings did not investigate sex-based differences. We did not document subjects' gender in this study.
Reporting on race, ethnicity, or other socially relevant groupings	Information on the race, ethnicity, or other socially relevant groupings of human participants was not collected.
Population characteristics	Age, sex, tumor site, tumor size, differentiation, TNM classification, AJCC stage, margins, and levels of tumor markers (CA19-9, CA125, CEA) of PDAC patients enrolled for collection of tissue samples are included in Supplementary Table 1. Age, sex, TNM classification, and AJCC stage of PDAC patients enrolled for collection of plasma samples are included in Supplementary Table 3.
Recruitment	Patients who agreed and signed informed consent were recruited at the Affiliated Tongji Hospital, Tongji Medical College, Huazhong University of Science and Technology. There are no biases on the selection of patients. A total of 122 patients were enrolled in this study for collection of tissue samples, including 78 PDAC patients, 16 other cancer patients diagnosed with tumor sites close (within 5 cm) to pancreas and some part of normal pancreas necessarily resected, and 28 chronic pancreatitis patients. 159 PDAC patients and 154 normal controls were enrolled for collection of plasma samples. Detailed information can be found in the section of "Human samples" in Methods and Supplementary Table 1, 3.
Ethics oversight	The study was approved by the Medical Ethics Committee of Tongji Medical Hospital (# TJDBPS02).

Note that full information on the approval of the study protocol must also be provided in the manuscript.

Field-specific reporting

Please select the one below that is the best fit for your research. If you are not sure, read the appropriate sections before making your selection.

☒ Life sciences ☐ Behavioural & social sciences ☐ Ecological, evolutionary & environmental sciences

For a reference copy of the document with all sections, see nature.com/documents/nr-reporting-summary-flat.pdf

Life sciences study design

All studies must disclose on these points even when the disclosure is negative.

Sample size	For proteomic analysis, the "effect magnitude" was unknown and therefore power was not calculated. Approximated sample sizes were estimated based on the general experiences. For the cell line validation experiments, at least 3 biological replicates were performed. For animal experiments, at least 8 biological replicates were performed. P values were statistically calculated to determine the significance where applicable.
Data exclusions	For the glycoproteomic data of clinical samples, SDS-PAGE was performed to filter the low quality samples with significant protein degradation. No collected data were excluded for other experiments.
Replication	For all the findings reported in the paper, at least three biological replicates were performed with similar results, except for N-glycoproteomic method development experiments, where technical replicates were performed with similar results. Replicates were as noted in figure legends.
Randomization	The tissue and plasma samples from each condition were collected from hospitals and sent for proteomic or ELISA analysis without randomization process. For animal studies, littermates at the same age were randomly enrolled into the cohorts. In all cases, when the treatment started, the mice were all grossly/visually healthy and body weight was not significant different, so randomly assigned into the cohorts of treatments.

Blinding	For MS-based experiments, sample conditions were blinded to investigators during sample processing and decoded for database searching and statistical analysis. For in vivo studies, all the enrolled mice or subsequent samples were labelled only with mouse ID numbers and did not indicate type of treatment. Treatment type was decoded after the data acquisition and quantification analysis were completed. For other experiments, investigators were not blind to group allocation as this information was essential for experiment conducting.

Behavioural & social sciences study design

All studies must disclose on these points even when the disclosure is negative.

Study description	*Briefly describe the study type including whether data are quantitative, qualitative, or mixed-methods (e.g. qualitative cross-sectional, quantitative experimental, mixed-methods case study).*
Research sample	*State the research sample (e.g. Harvard university undergraduates, villagers in rural India) and provide relevant demographic information (e.g. age, sex) and indicate whether the sample is representative. Provide a rationale for the study sample chosen. For studies involving existing datasets, please describe the dataset and source.*
Sampling strategy	*Describe the sampling procedure (e.g. random, snowball, stratified, convenience). Describe the statistical methods that were used to predetermine sample size OR if no sample-size calculation was performed, describe how sample sizes were chosen and provide a rationale for why these sample sizes are sufficient. For qualitative data, please indicate whether data saturation was considered, and what criteria were used to decide that no further sampling was needed.*
Data collection	*Provide details about the data collection procedure, including the instruments or devices used to record the data (e.g. pen and paper, computer, eye tracker, video or audio equipment) whether anyone was present besides the participant(s) and the researcher, and whether the researcher was blind to experimental condition and/or the study hypothesis during data collection.*
Timing	*Indicate the start and stop dates of data collection. If there is a gap between collection periods, state the dates for each sample cohort.*
Data exclusions	*If no data were excluded from the analyses, state so OR if data were excluded, provide the exact number of exclusions and the rationale behind them, indicating whether exclusion criteria were pre-established.*
Non-participation	*State how many participants dropped out/declined participation and the reason(s) given OR provide response rate OR state that no participants dropped out/declined participation.*
Randomization	*If participants were not allocated into experimental groups, state so OR describe how participants were allocated to groups, and if allocation was not random, describe how covariates were controlled.*

Ecological, evolutionary & environmental sciences study design

All studies must disclose on these points even when the disclosure is negative.

Study description	*Briefly describe the study. For quantitative data include treatment factors and interactions, design structure (e.g. factorial, nested, hierarchical), nature and number of experimental units and replicates.*
Research sample	*Describe the research sample (e.g. a group of tagged Passer domesticus, all Stenocereus thurberi within Organ Pipe Cactus National Monument), and provide a rationale for the sample choice. When relevant, describe the organism taxa, source, sex, age range and any manipulations. State what population the sample is meant to represent when applicable. For studies involving existing datasets, describe the data and its source.*
Sampling strategy	*Note the sampling procedure. Describe the statistical methods that were used to predetermine sample size OR if no sample-size calculation was performed, describe how sample sizes were chosen and provide a rationale for why these sample sizes are sufficient.*
Data collection	*Describe the data collection procedure, including who recorded the data and how.*
Timing and spatial scale	*Indicate the start and stop dates of data collection, noting the frequency and periodicity of sampling and providing a rationale for these choices. If there is a gap between collection periods, state the dates for each sample cohort. Specify the spatial scale from which the data are taken*
Data exclusions	*If no data were excluded from the analyses, state so OR if data were excluded, describe the exclusions and the rationale behind them, indicating whether exclusion criteria were pre-established.*
Reproducibility	*Describe the measures taken to verify the reproducibility of experimental findings. For each experiment, note whether any attempts to repeat the experiment failed OR state that all attempts to repeat the experiment were successful.*
Randomization	*Describe how samples/organisms/participants were allocated into groups. If allocation was not random, describe how covariates were controlled. If this is not relevant to your study, explain why.*
Blinding	*Describe the extent of blinding used during data acquisition and analysis. If blinding was not possible, describe why OR explain why blinding was not relevant to your study.*

Did the study involve field work? ☐ Yes ☐ No

Field work, collection and transport

Field conditions	*Describe the study conditions for field work, providing relevant parameters (e.g. temperature, rainfall).*
Location	*State the location of the sampling or experiment, providing relevant parameters (e.g. latitude and longitude, elevation, water depth).*
Access & import/export	*Describe the efforts you have made to access habitats and to collect and import/export your samples in a responsible manner and in compliance with local, national and international laws, noting any permits that were obtained (give the name of the issuing authority, the date of issue, and any identifying information).*
Disturbance	*Describe any disturbance caused by the study and how it was minimized.*

Reporting for specific materials, systems and methods

We require information from authors about some types of materials, experimental systems and methods used in many studies. Here, indicate whether each material, system or method listed is relevant to your study. If you are not sure if a list item applies to your research, read the appropriate section before selecting a response.

Materials & experimental systems

n/a	Involved in the study
☐	☒ Antibodies
☐	☒ Eukaryotic cell lines
☒	☐ Palaeontology and archaeology
☐	☒ Animals and other organisms
☒	☐ Clinical data
☒	☐ Dual use research of concern
☒	☐ Plants

Methods

n/a	Involved in the study
☒	☐ ChIP-seq
☒	☐ Flow cytometry
☒	☐ MRI-based neuroimaging

Antibodies

Antibodies used	These primary antibodies against the indicated proteins were used for western blotting: β-actin (Cell Signaling Technology; clone 8H10D10; cat# 3700; 1:5000), PDGFRA (Cell Signaling Technology; clone D1E1E; cat# 3174S; 1:1000), phospho-PDGFRA-Y742 (Abcam; cat# ab5452; 1:1000), AXL-ectodomain (Abcam; clone EPR19880; cat# ab219651; 1:1000), PDGFRB (Cell Signaling Technology; clone 28E1; cat# 3169S; 1:1000), PTPN11 (Abcam; cat# ab32083; 1:2000), phospho-PTPN11-Y542 (Abcam; clone EP508(2)Y; cat# ab62322; 1:5000), AKT (Cell Signaling Technology; clone D9E; cat# 4060S; 1:2000), phospho-AKT-S473 (Cell Signaling Technology; clone 11E7; cat# 4685S; 1:2000), ERK (Cell Signaling Technology; clone 137F5; cat# 4695; 1:2000), phospho-ERK-T202/Y204 (Cell Signaling Technology; clone D13.14.4E; cat# 4370S; 1:2000), E-Cadherin (Cell Signaling Technology; clone 24E10; cat# 3195; 1:1000), N-Cadherin (Cell Signaling Technology; clone D4R1H; cat# 13116; 1:1000), Snail (Cell Signaling Technology; clone C15D3; cat# 3879; 1:1000), ZEB1 (Cell Signaling Technology; clone D80D3; cat# 3396; 1:1000), HRP-conjugated goat anti-mouse IgG (Beyotime; cat# A0216; 1:1000), HRP-conjugated goat anti-rabbit IgG (Beyotime; cat# A0208; 1:1000). These primary antibodies against the indicated proteins were used for TSA staining: KRT19 (Abcam; clone EP1580Y; cat# ab52625; 1:1000), PDGERB (Cell Signaling Technology, clone 28E1; cat# 3169S; 1:1000), SLC1A3 (Abcam; cat# ab416; 1:200), TRPV4 (Abcam; cat# ab191580; 1:500), PKD1 (Abcam; cat# ab74115; 1:200), CDON (Abcam; cat# ab227056; 1:200), LRIG2 (Abcam; cat# ab157492; 1:100), TMPRSS4 (Abcam; cat# ab150595; 1:200), These primary antibodies against the indicated proteins were used for IHC staining: KRT19 (Cell Signaling Technology; clone D4G2; cat# #12434; 1:500), Ki67 (Abcam; clone SP6; cat# ab16667; 1:500), SOX9 (Cell Signaling Technology; clone D8G8H; cat# #82630; 1:500).
Validation	All antibodies in the study were used according to the user manuals and validation statements can be found on the respective manufacture websites. β-actin (Cell Signaling Technology; clone 8H10D10; cat# 3700): https://www.cellsignal.cn/products/primary-antibodies/b-actin-8h10d10-mouse-mab/3700 PDGFRA (Cell Signaling Technology; clone D1E1E; cat# 3174S): https://www.cellsignal.cn/products/primary-antibodies/pdgf-receptor-a-d1e1e-xp-rabbit-mab/3174 phospho-PDGFRA-Y742 (Abcam; cat# ab5452): https://www.abcam.cn/products/primary-antibodies/pdgfr-alpha-phospho-y742-antibody-ab5452.html AXL-ectodomain (Abcam; clone EPR19880; cat# ab219651): https://www.abcam.cn/products/primary-antibodies/axl-antibody-epr19880-ab219651.html PDGFRB (Cell Signaling Technology; clone 28E1; cat# 3169S): https://www.cellsignal.cn/products/primary-antibodies/pdgf-receptor-b-28e1-rabbit-mab/3169 PTPN11 (Abcam; cat# ab32083): https://www.abcam.cn/products/primary-antibodies/shp2-antibody-y478-ab32083.html

phospho-PTPN11-Y542 (Abcam; clone EP508(2)Y; cat# ab62322):
https://www.abcam.cn/products/primary-antibodies/shp2-phospho-y542-antibody-ep5082y-ab62322.html
AKT (Cell Signaling Technology; clone 11E7; cat# 4685S):
https://www.cellsignal.cn/products/primary-antibodies/akt-pan-11e7-rabbit-mab/4685
phospho-AKT-S473 (Cell Signaling Technology; clone D9E; cat# 4060S):
https://www.cellsignal.cn/products/primary-antibodies/phospho-akt-ser473-d9e-xp-174-rabbit-mab/4060
ERK (Cell Signaling Technology; clone 137F5; cat# 4695):
https://www.cellsignal.com/products/primary-antibodies/p44-42-mapk-erk1-2-137f5-rabbit-mab/4695
phospho-ERK-T202/Y204 (Cell Signaling Technology; clone D13.14.4E; cat# 4370S):
https://www.cellsignal.cn/products/primary-antibodies/phospho-p44-42-mapk-erk1-2-thr202-tyr204-d13-14-4e-xp-174-rabbit-mab/4370
E-Cadherin (Cell Signaling Technology; clone 24E10; cat# 3195): https://www.cellsignal.cn/products/primary-antibodies/e-cadherin-24e10-rabbit-mab/3195
N-Cadherin (Cell Signaling Technology; clone D4R1H; cat# 13116):
https://www.cellsignal.cn/products/primary-antibodies/n-cadherin-d4r1h-xp-rabbit-mab/13116
Snail (Cell Signaling Technology; clone C15D3; cat# 3879):
https://www.cellsignal.cn/products/primary-antibodies/snail-c15d3-rabbit-mab/3879
ZEB1 (Cell Signaling Technology; clone D80D3; cat# 3396):
https://www.cellsignal.cn/products/primary-antibodies/zeb1-d80d3-rabbit-mab/3396
HRP-conjugated goat anti-mouse IgG (Beyotime; cat# A0216):
https://www.beyotime.com/product/A0216.html
HRP-conjugated goat anti-rabbit IgG (Beyotime; cat# A0208):
https://www.beyotime.com/product/A0208.html
KRT19 (Abcam; clone EP1580Y; cat# ab52625):
https://www.abcam.cn/products/primary-antibodies/cytokeratin-19-antibody-ep1580y-cytoskeleton-marker-ab52625.html
PDGERB (Cell Signaling Technology, clone 28E1; cat# 3169S):
https://www.cellsignal.cn/products/primary-antibodies/pdgf-receptor-b-28e1-rabbit-mab/3169
SLC1A3 (Abcam; cat# ab416):
https://www.abcam.cn/products/primary-antibodies/eaat1-antibody-ab416.html
TRPV4 (Abcam; cat# ab191580):
https://www.abcam.cn/products/primary-antibodies/trpv4-antibody-ab191580.html
PKD1 (Abcam; clone 7e12; cat# ab74115):
https://www.abcam.cn/products/primary-antibodies/polycystin-1pc1-antibody-7e12-ab74115.html
CDON (Abcam; cat# ab227056):
https://www.abcam.cn/products/primary-antibodies/cdon--cdo-antibody-n-terminal-ab227056.html
LRIG2 (Abcam; cat# ab157492):
https://www.abcam.cn/products/primary-antibodies/lrig2-antibody-ab157492.html
TMPRSS4 (Abcam; cat# ab150595):
https://www.abcam.cn/products/primary-antibodies/tmprss4-antibody-ab150595.html
KRT19 (Cell Signaling Technology; clone D4G2; cat# #12434)
https://www.cellsignal.cn/products/primary-antibodies/keratin-17-19-d4g2-xp-174-rabbit-mab/12434
Ki67 (Abcam; clone SP6; cat# ab16667)
https://www.abcam.cn/products/primary-antibodies/ki67-antibody-sp6-ab16667.html
SOX9 (Cell Signaling Technology; clone D8G8H; cat# #82630)
https://www.cellsignal.cn/products/primary-antibodies/sox9-d8g8h-rabbit-mab/82630

Eukaryotic cell lines

Policy information about cell lines and Sex and Gender in Research

Cell line source(s)	The human pancreatic cancer cell lines PANC1 (CRL-1469), AsPC1 (CRL-1682), MIA PaCa2 (CRL-1420), KP4 (JCRB0182), SU.86.86 (CRL-1837) and SW 1990 (CRL-2172), and the human embryonic kidney cell line HER293T (CRL-11268) were acquired from ATCC. The spontaneously immortalized pancreatic stellate cell line hPSC, which was isolated and established from a pancreatic cancer patient (PMID: 21558392), was provided by Evans group (Salk). The human pancreatic stellate cell line HPaSteC was purchased from ScienCell. KPCP cancer cells were primarily established in the lab.
Authentication	All the cell lines from ATCC were authenticated by STR profiling by ATCC. Other cell lines were not authenticated.
Mycoplasma contamination	Cell lines were tested for mycoplasma contamination every month. The mycoplasma contamination test results were negative.
Commonly misidentified lines (See ICLAC register)	none.

Palaeontology and Archaeology

Specimen provenance	*Provide provenance information for specimens and describe permits that were obtained for the work (including the name of the issuing authority, the date of issue, and any identifying information). Permits should encompass collection and, where applicable, export.*
Specimen deposition	*Indicate where the specimens have been deposited to permit free access by other researchers.*

Dating methods	*If new dates are provided, describe how they were obtained (e.g. collection, storage, sample pretreatment and measurement), where they were obtained (i.e. lab name), the calibration program and the protocol for quality assurance OR state that no new dates are provided.*

☐ Tick this box to confirm that the raw and calibrated dates are available in the paper or in Supplementary Information.

Ethics oversight	*Identify the organization(s) that approved or provided guidance on the study protocol, OR state that no ethical approval or guidance was required and explain why not.*

Note that full information on the approval of the study protocol must also be provided in the manuscript.

Animals and other research organisms

Policy information about studies involving animals; ARRIVE guidelines recommended for reporting animal research, and Sex and Gender in Research

Laboratory animals	Three-, five-, and seven-week-old transgenic KPC (KrasLSL-G12D/+; Trp53flox/flox; Pdx1-Cre) mice were kindly provided by Yu Shi from Salk institute. Five-week-old NSG mice were purchased from Shanghai Model Organisms Center and used for generating orthotopic PDAC model. Six-week-old SCID mice were purchased from Biocytogen Pharmaceuticals (Beijing) Co., Ltd. and used for generating organoid-derived xenograft model. Mice were housed in standard closed plastic cages supplied with bedding, food and water. The specific pathogen free room is maintained at temperature of 20-26 ℃℃℃degrees Celsius, humidity of 40-70%, and 12h/12h lighting cycle (on from 7:00-19:00).
Wild animals	none.
Reporting on sex	Sex was not considered in the study design.
Field-collected samples	none.
Ethics oversight	All animal studies were performed in accordance with the guidelines and regulations, and ethical approval was received from the Institutional Animal Care and Use Committee (IACUC) at Southern University of Science and Technology (experiments using orthotopic mouse models), or from IACUC at Center for Excellence in Molecular Cell Science (experiments using xenograft mouse models).

Note that full information on the approval of the study protocol must also be provided in the manuscript.

Clinical data

Policy information about clinical studies

All manuscripts should comply with the ICMJE guidelines for publication of clinical research and a completed CONSORT checklist must be included with all submissions.

Clinical trial registration	none.
Study protocol	*Note where the full trial protocol can be accessed OR if not available, explain why.*
Data collection	*Describe the settings and locales of data collection, noting the time periods of recruitment and data collection.*
Outcomes	*Describe how you pre-defined primary and secondary outcome measures and how you assessed these measures.*

Dual use research of concern

Policy information about dual use research of concern

Hazards

Could the accidental, deliberate or reckless misuse of agents or technologies generated in the work, or the application of information presented in the manuscript, pose a threat to:

No	Yes	
☐	☐	Public health
☐	☐	National security
☐	☐	Crops and/or livestock
☐	☐	Ecosystems
☐	☐	Any other significant area

Experiments of concern

Does the work involve any of these experiments of concern:

No	Yes	
☐	☐	Demonstrate how to render a vaccine ineffective
☐	☐	Confer resistance to therapeutically useful antibiotics or antiviral agents
☐	☐	Enhance the virulence of a pathogen or render a nonpathogen virulent
☐	☐	Increase transmissibility of a pathogen
☐	☐	Alter the host range of a pathogen
☐	☐	Enable evasion of diagnostic/detection modalities
☐	☐	Enable the weaponization of a biological agent or toxin
☐	☐	Any other potentially harmful combination of experiments and agents

Plants

Seed stocks

Report on the source of all seed stocks or other plant material used. If applicable, state the seed stock centre and catalogue number. If plant specimens were collected from the field, describe the collection location, date and sampling procedures.

Novel plant genotypes

Describe the methods by which all novel plant genotypes were produced. This includes those generated by transgenic approaches, gene editing, chemical/radiation-based mutagenesis and hybridization. For transgenic lines, describe the transformation method, the number of independent lines analyzed and the generation upon which experiments were performed. For gene-edited lines, describe the editor used, the endogenous sequence targeted for editing, the targeting guide RNA sequence (if applicable) and how the editor was applied.

Authentication

Describe any authentication procedures for each seed stock used or novel genotype generated. Describe any experiments used to assess the effect of a mutation and, where applicable, how potential secondary effects (e.g. second site T-DNA insertions, mosiacism, off-target gene editing) were examined.

ChIP-seq

Data deposition

☐ Confirm that both raw and final processed data have been deposited in a public database such as GEO.

☐ Confirm that you have deposited or provided access to graph files (e.g. BED files) for the called peaks.

Data access links
May remain private before publication.

For "Initial submission" or "Revised version" documents, provide reviewer access links. For your "Final submission" document, provide a link to the deposited data.

Files in database submission

Provide a list of all files available in the database submission.

Genome browser session
(e.g. UCSC)

Provide a link to an anonymized genome browser session for "Initial submission" and "Revised version" documents only, to enable peer review. Write "no longer applicable" for "Final submission" documents.

Methodology

Replicates

Describe the experimental replicates, specifying number, type and replicate agreement.

Sequencing depth

Describe the sequencing depth for each experiment, providing the total number of reads, uniquely mapped reads, length of reads and whether they were paired- or single-end.

Antibodies

Describe the antibodies used for the ChIP-seq experiments; as applicable, provide supplier name, catalog number, clone name, and lot number.

Peak calling parameters

Specify the command line program and parameters used for read mapping and peak calling, including the ChIP, control and index files used.

Data quality

Describe the methods used to ensure data quality in full detail, including how many peaks are at FDR 5% and above 5-fold enrichment.

Software

Describe the software used to collect and analyze the ChIP-seq data. For custom code that has been deposited into a community repository, provide accession details.

Flow Cytometry

Plots

Confirm that:

☐ The axis labels state the marker and fluorochrome used (e.g. CD4-FITC).

☐ The axis scales are clearly visible. Include numbers along axes only for bottom left plot of group (a 'group' is an analysis of identical markers).

☐ All plots are contour plots with outliers or pseudocolor plots.

☐ A numerical value for number of cells or percentage (with statistics) is provided.

Methodology

Sample preparation	*Describe the sample preparation, detailing the biological source of the cells and any tissue processing steps used.*
Instrument	*Identify the instrument used for data collection, specifying make and model number.*
Software	*Describe the software used to collect and analyze the flow cytometry data. For custom code that has been deposited into a community repository, provide accession details.*
Cell population abundance	*Describe the abundance of the relevant cell populations within post-sort fractions, providing details on the purity of the samples and how it was determined.*
Gating strategy	*Describe the gating strategy used for all relevant experiments, specifying the preliminary FSC/SSC gates of the starting cell population, indicating where boundaries between "positive" and "negative" staining cell populations are defined.*

☐ Tick this box to confirm that a figure exemplifying the gating strategy is provided in the Supplementary Information.

Magnetic resonance imaging

Experimental design

Design type	*Indicate task or resting state; event-related or block design.*
Design specifications	*Specify the number of blocks, trials or experimental units per session and/or subject, and specify the length of each trial or block (if trials are blocked) and interval between trials.*
Behavioral performance measures	*State number and/or type of variables recorded (e.g. correct button press, response time) and what statistics were used to establish that the subjects were performing the task as expected (e.g. mean, range, and/or standard deviation across subjects).*

Acquisition

Imaging type(s)	*Specify: functional, structural, diffusion, perfusion.*
Field strength	*Specify in Tesla*
Sequence & imaging parameters	*Specify the pulse sequence type (gradient echo, spin echo, etc.), imaging type (EPI, spiral, etc.), field of view, matrix size, slice thickness, orientation and TE/TR/flip angle.*
Area of acquisition	*State whether a whole brain scan was used OR define the area of acquisition, describing how the region was determined.*

Diffusion MRI ☐ Used ☐ Not used

Preprocessing

Preprocessing software	*Provide detail on software version and revision number and on specific parameters (model/functions, brain extraction, segmentation, smoothing kernel size, etc.).*
Normalization	*If data were normalized/standardized, describe the approach(es): specify linear or non-linear and define image types used for transformation OR indicate that data were not normalized and explain rationale for lack of normalization.*
Normalization template	*Describe the template used for normalization/transformation, specifying subject space or group standardized space (e.g. original Talairach, MNI305, ICBM152) OR indicate that the data were not normalized.*
Noise and artifact removal	*Describe your procedure(s) for artifact and structured noise removal, specifying motion parameters, tissue signals and physiological signals (heart rate, respiration).*

Volume censoring

Define your software and/or method and criteria for volume censoring, and state the extent of such censoring.

Statistical modeling & inference

Model type and settings

Specify type (mass univariate, multivariate, RSA, predictive, etc.) and describe essential details of the model at the first and second levels (e.g. fixed, random or mixed effects; drift or auto-correlation).

Effect(s) tested

Define precise effect in terms of the task or stimulus conditions instead of psychological concepts and indicate whether ANOVA or factorial designs were used.

Specify type of analysis: ☐ Whole brain ☐ ROI-based ☐ Both

Statistic type for inference

Specify voxel-wise or cluster-wise and report all relevant parameters for cluster-wise methods.

(See Eklund et al. 2016)

Correction

Describe the type of correction and how it is obtained for multiple comparisons (e.g. FWE, FDR, permutation or Monte Carlo).

Models & analysis

n/a	Involved in the study
☐	☐ Functional and/or effective connectivity
☐	☐ Graph analysis
☐	☐ Multivariate modeling or predictive analysis

Functional and/or effective connectivity

Report the measures of dependence used and the model details (e.g. Pearson correlation, partial correlation, mutual information).

Graph analysis

Report the dependent variable and connectivity measure, specifying weighted graph or binarized graph, subject- or group-level, and the global and/or node summaries used (e.g. clustering coefficient, efficiency, etc.).

Multivariate modeling and predictive analysis

Specify independent variables, features extraction and dimension reduction, model, training and evaluation metrics.